Mechanisms of Charge Injection and Transport in Trischelated Ruthenium(II) Complexes for Light-Emitting Device Applications

by

Erika Diane Abbas

B.A., Physics, 1994
Wellesley College, Wellesley MA

Submitted to
the Department of Materials Science and Engineering
in Partial Fulfilment of the Requirements for the Degree of

Doctor of Philosophy in Electronic Materials

at the

Massachusetts Institute of Technology

June 1999

Author .....
Materials Science and Engineering
April 30, 1999

Certified by .....
Michael F. Rubner
TDK Professor of Materials Science and Engineering
Thesis Advisor

Accepted by .....
Linn W. Hobbs
John F. Elliott Professor of Materials
Chairman, Departmental Committee on Graduate Students

Mechanisms of Charge Injection and Transport in Trischelated Ruthenium(II) Complexes for Light-Emitting Device Applications

by
Erika Diane Abbas

Submitted to the Department of Materials Science and Engineering
on April 30, 1999 in Partial Fulfillment of the Requirements for the Degree of
Doctor of Philosophy in Electronic Materials

ABSTRACT

In this work, observations of the light-emitting device behavior of several trischelated ruthenium(II) systems are unified into one mechanistic picture. The systems ranged in size and mobility from a small trisbipyridyl ruthenium(II) diol to an ionically crosslinked trisbipyridyl ruthenium(II) polyester in a polyelectrolyte complex. Current and light were monitored as functions of voltage, time, temperature, and frequency. Although this testing resulted in a large range of device behaviors, results could be assigned to two general cases.

For the highest brightness devices, the ruthenium(II) complexes behave in a traditional electrochemical mode. Ionic mobility at the metal/organic interface is required to form a double layer to aid in charge injection. Additionally, counterion motion is required within the bulk of the film to allow the transition from a fully 2+ insulating state to a conducting gradient of 3+/2+ or 2+/1+ redox couples. The process of this insulator/conductor transition has an exponential dependence on applied voltage as predicted by redox switching theory. Once the mixed valence states are in place, charge transport by electron hopping is very fast, with device operation possible above 20 kHz. This electron hopping is an activated process between clusters of ruthenium species that follows distributed transport theory. The diffusion constants have an arrhenius dependence with temperature, yielding activation energies in the range of 1 to 20 kJ. Light emission is consistent with the bimolecular reaction of 3+ and 1+ states to form the excited 2+ state which then relaxes and yields a photon.

Under conditions where ionic response is slow on the time scale of the measurement, either due to depressed mobility at low temperatures or rapid voltage sweeps at room temperature, a secondary method of charge injection is observed. In this case, current flows without producing any light; we infer that only one charge, likely the electron, is being injected. When hole-transport material is added to form a heterostructure, light emission is possible, and the slow electrochemical charging process does not occur. These observations support the hypothesis of fast electron-transport that is no longer dependent on ionic movement. This mode of transport is a small fraction of the total current possible in the electrochemically active process, and therefore the total light is much lower in these faster responding devices.

Thesis Supervisor: Michael F. Rubner
Title: TDK Professor of Materials Science and Engineering

TABLE OF CONTENTS

List of Figures

CHAPTER THREE

CHAPTER FOUR

CHAPTER FIVE

CHAPTER SIX

CHAPTER SEVEN

List of Tables

Acknowledgments

I have grown and changed in more ways than I can count during my five years here at MIT and even through the process of writing this document. I am certain that I could never have done it alone, and so I would like to acknowledge the role that these people have played in bringing me to this place and time.

The members of my committee:
Prof. Harry Tuller for keeping me grounded in Electronic Materials
Prof. Craig Carter for stepping in at the last minute and wonderful writing advice
Prof. Michael Rubner for being my advisor in every sense of the word,
for providing an excellent role model of a happy and successful balance between the crazy world of academic science and the rest of life,
and for knowing me better than I sometimes would have liked

The members of the Rubner Group past, present, and future:

Augustine Fou, Mary Ferreira, Osamu Onitsuka, Doug Howie, Bill Stockton, Ken Zemach, Cormac Lyons, Dongsik Yoo, Jeff Baur, Sara O'Connor, Aiping Wu, Seimei (Akira) Shiratori, Jason Pinto, Tom Wang, Peter Wan, Jonas Mendelsohn, JeriAnn King, Jeeyoung Choi, Aaron Raphel, Amlan Pal

for each teaching me something different about lab and life

Mike Durstock for sharing this adventure with me from first class to final defense
(cue "Mission Impossible" theme music)
Erik Handy for teaching this physicist all she knows about chemistry
(and the international symbol for waveguiding, among other things)
Erik for playing "Name that Tune" and Mike for naming it
Hartmut Rudmann for jumping into the fray with both feet--this project is in good hands
Stephanie Hansen for keeping us well fed, well supplied, and well organized
for holding the group together and calling me "Pumpkin"

The members of my study group:
Jason, Ken, Larry, and Lynne for getting me through the first year
and especially Lynne for being an anchor for the remaining four,
and an inspiration in the final approach to the finish--Jer. 29:11

The members and guest stars of the Slack Train, both in its 11:30, 2:00 version and in the extended combination run:

Nat and Tracey for parties where no one goes home hungry (or sober--unless they're driving) and for letting me choose to just not go home
Doug for long drives to nowhere and advice on everything from junkyards to jelly rolls
("Everybody needs a Doug")
Arun for Fridays at the Muddy and LSC classics
Eric "the Pickle Guy" for Howard Stern and weight room quotes
Aaron for stupid guy-movies, trips in the "Charm-mobile," and Mother Goose
Srikar's mom for fabulous Indian food and Srikar for always inviting me
Erin for Sunday Brunches, phenomenal wedding cakes, jogs around the Charles,
latenight IHOP runs, and countless adventures in Helga
and for being there for me, always

The greater MIT community:

Cecil for dealing with my trash--physically and emotionally
Jon and Mike for humor in the halls
Heidi for her Tweety Birds
Sally and Sanjay for cooking and Pictionary

Kari for the summer of Christina's and the 1369
Debbie for spontaneous cooking sessions and the Blue Baby
Amie for scones, Animaniacs, and lots of plants
Bats for 11pm apple pies and washing all the dishes

Eric for the lending library and Berkshires hikes
Greg for reminding me to think

Mike for reminding me what to think and picking up where Doug left off
Annie for being cool and for the awesome Provincetown souvenir
Debbie for Midwest chats, invitations to Park Street, and real corn

The Tech Jazz Singers (especially Adam, Rose, Sol, Matt, and Josh)
and Healthworks Advanced Boxing class for helping me to blow off steam

Josh for introducing me to this other part of my brain and teaching me to,
in the words of Mel Brooks, "Now myself"

Beni for being an instant friend before any of this started, a super officemate, a wonderful housemate, and a saint for not killing me long ago. She gives new meaning to the saying, "A friend is someone who knows everything about you and still loves you."

and my family:

Geoff for helping me to figure out Mom and Dad and for not pummeling me now that he's big enough to do so
Kristen for being a cool addition to the family, keeping Geoff pulled together, and dealing with the rest of us with much humor and love
Mom for being a wonderful role model of a strong woman who is not afraid to speak her mind--I am not afraid to be turning into my mother
Dad for always really answering why--in detail--and instilling in me the love of science that started this whole journey

Finally, I would like to thank the folks around me who have lived their lives in such a way as to remind me of my true source of Life:
"I can do all things through God who strengthens me."

1. Introduction and Background

1. 1 Objective

The objective of this thesis was to develop an overarching mechanistic theory to describe the charge injection and transport in the trischelated ruthenium(II) systems studied by the Rubner group. This task required assembling all previous observations on each of the systems, studying the current literature on redox active molecules, and developing a theory based on the literature that was consistent with all of the systems under all conditions. To evaluate the hypotheses, I gathered additional data on every system described here, reanalyzed existing data looking for previously hidden trends, and designed new experiments to extract the materials constants relevant to the suggested theories.

The final goal was twofold. First, a consistent picture of the movement of charge through our devices was needed to determine the best approach for continuing to improve the engineering performance. We wanted to improve the light output, stability, and, most importantly to this thesis, the on/off switching time of our devices. Secondly, although the trisbipyridyl ruthenium(II) molecule has been studied extensively in the solution state, only recently has it been used in the solid state. Furthermore, recent studies of redox-active molecules in solid films have approximated the solution state as closely as possible, involving complicated devices with solvent and electrolyte contact and elaborate pre-conditioning routines before the samples are tested. However, for practical device application, a completely solventless system is needed. Therefore, I took the first steps to describe the behavior of these ruthenium(II) based materials in the absence of any external solvent or electrolyte as they transition from insulators at equilibrium to light-emitting conductors under the influence of an applied field.

1. 2 Organic Light Emitting Devices

Chemiluminescence and electroluminescence in small organic molecules has been known for some time.[1] However, most of this luminescent behavior was observed in solution and was not practical for making devices. When used in the solid state, these small chromophores often crystallized, causing quenching of the luminescence and instability in the device performance.[2] When conjugated polymers were observed to be effective in light-emitting devices,[3] there was much hope in the polymer community that the macromolecular nature of the polymer would resist the crystallization and quenching of

the luminescence that plagued small molecule devices. These polymers have proven to be capable of producing enough light for standard computer displays and can be easily patterned into flexible diode arrays.[4] Several new companies have been incorporated to develop and market these polymer devices.[5]

Organic materials have some advantages over traditional inorganic semiconductors. They are processed under much less extreme conditions (generally under 300°C and at ambient pressure or low vacuum), and involve relatively nontoxic materials when compared with the reagent gases used in CVD processes. They also are mechanically flexible, allowing for novel device structures and flexible diodes. Because the band gap of these materials is determined by their molecular configuration, not by a well defined crystal structure, the emission wavelength can be tuned by modification of groups pendant from the polymer backbone. Consequently, blue light emission is achieved fairly readily in organic materials; full color displays and white light emission are available through use of these materials.[6]

Although these materials seem very promising and much engineering of devices has been successfully accomplished using organics, many aspects of the basic device mechanisms are unknown. Unlike traditional semiconductors, for which the crystal structure and electronic band structures have been established, these devices are amorphous and therefore do not have strictly defined conduction and valence bands. In addition, the nature of carrier motion, carrier injection, and carrier recombination in these materials is still under debate. Many models have been put forward but none is yet conclusive.[7, 8] In the next sections, I will present the most commonly described device picture.

Another difficulty with organic devices is with device stability. Although the use of macromolecules in addition to, or instead of, small molecules has served to increase device lifetimes, the stability is still nowhere near that of inorganic devices. Many of the difficulties lie in the low quantum efficiency of these materials; excess charge passing through the device can cause resistive heating and degradation of the polymer/metal interface. Also, many of these organics are electrochemiluminescent, meaning that they generate light from the relaxation of charge injected in an electrochemical oxidation or reduction process. These electrochemically active materials require the movement of small ions to maintain charge neutrality. The ions can migrate under load and short out weak areas in the device. We hope that, with a better understanding of the charge injection and transport mechanisms, the relative rates of charge injection can be balanced such that device efficiencies and therefore device stability will be improved.

1.2.1 Carrier Transport and Recombination in Organic Devices

The first demonstrated light emitting polymer devices were fabricated from poly(para-phenylenevinylene) in 1990.[3] Since then many groups have used PPV and similar aromatic derivatives as the emitting layers in thin film device structures. Devices made from PPV have shown reasonable light output and stability and are the most widely used in this field. Therefore, we will be using them as a benchmark against which we can compare the performance of the ruthenium(II) systems. The structure of PPV is given in Figure 1-1. It is highly intractable in its final conjugated form, and therefore is generally processed as a precursor. It is then heated to eliminate the leaving groups and form carbon-carbon double bonds in the backbone of the polymer that can overlap and allow for electronic conduction.

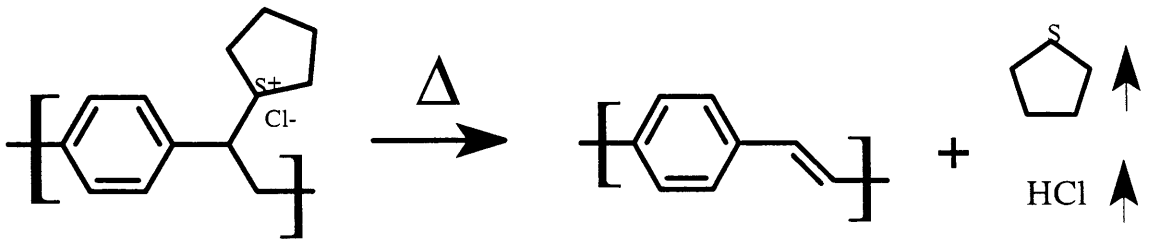

Figure 1-1. The structure of the PPV sulfonium precursor and the reaction to create its final conjugated form.

The method of carrier motion in PPV is considered to be due to the formation and migration of polarons or bipolarons.[9] These bond alternation defects were discovered primarily through the study of solitons in poly(acetylene), one of the earliest identified conducting polymers. In conjugated systems, the p_z orbitals along the backbone can overlap, allowing delocalization of the π^* orbitals and formation of a conduction-band-like series of energy levels. These energy levels can accept the addition of a charge delocalized over a few phenyl units, forming a polaron, or two charges, forming a bipolaron (shown in Figure 1-2 for the related PPP material). This structure can also support a neutral electron-hole pair called a polaron-exciton. It is believed that the nature of the radiative recombination in PPV is through the decay of polaron-excitons formed when oppositely charged polarons come together. The emission is centered around 530 nm, which is in the yellow-green portion of the spectrum.[3]

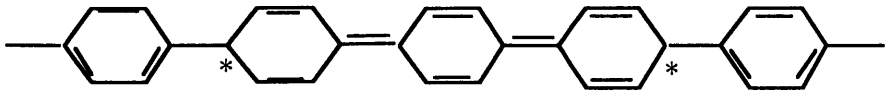

Figure 1-2. Schematic of a bipolaron or polaron-exciton on a poly(para-phenylene) chain. The * may be positive or negative charges or unpaired electrons.

1.2.2 Carrier Injection in Organic Devices

In the standard architecture of a solid-state organic device, the active light emitting material is contacted on one side by a high work function metal to serve as an anode and on the other by a low work function metal as a cathode. These metals are chosen to match the energy levels of the active material, as shown in Figure 1-3.

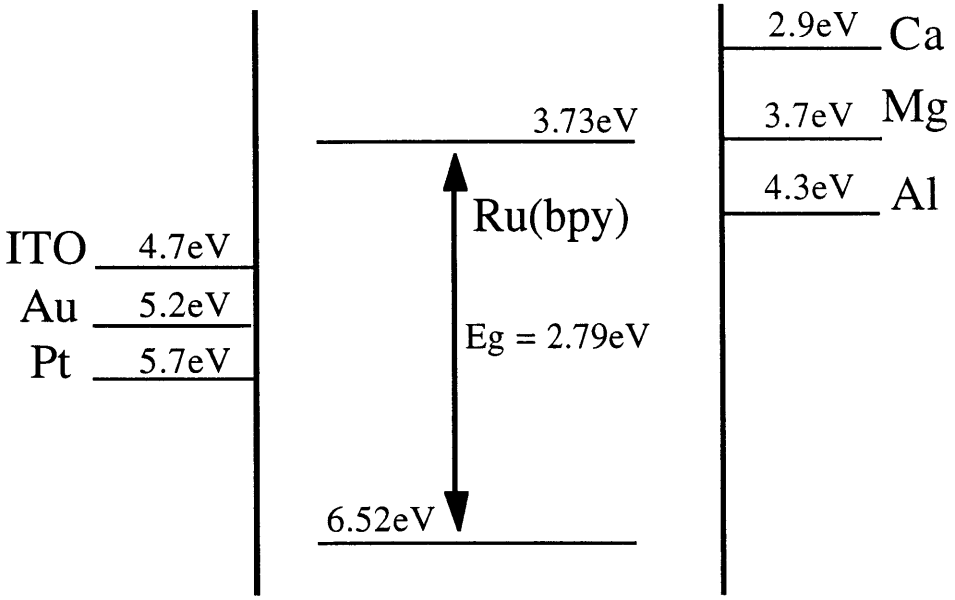

Figure 1-3. The relative energy levels for materials used in light-emitting devices. Common anode materials are on the left; cathode materials are on the right. Lower work function metals, such as calcium, provide easy electron injection into the conduction band of the active material. High work function metals, such as gold, are better matched to the valence band and are used to inject holes. The energy levels for the oxidation and reduction of ruthenium(II) trisbipyridyl are included for reference. (calculated via equation in [10])

The anode is commonly indium tin oxide (ITO) because it is transparent and allows for the escape of any light produced by the device. Although the cathode is generally magnesium or calcium,[8, 11] we have used aluminum because it is considerably more stable.

When the materials are brought into contact, the Fermi energies of the electrons must equilibrate. Electrons flow from the high energy metal to the low energy one until the electric field generated within the material becomes large enough to balance the energy differential. If the material does not have many mobile ions (a good approximation for many organics such as PPV), the electric field remains constant across the entire device with no band bending as shown in Figure 1-4A.

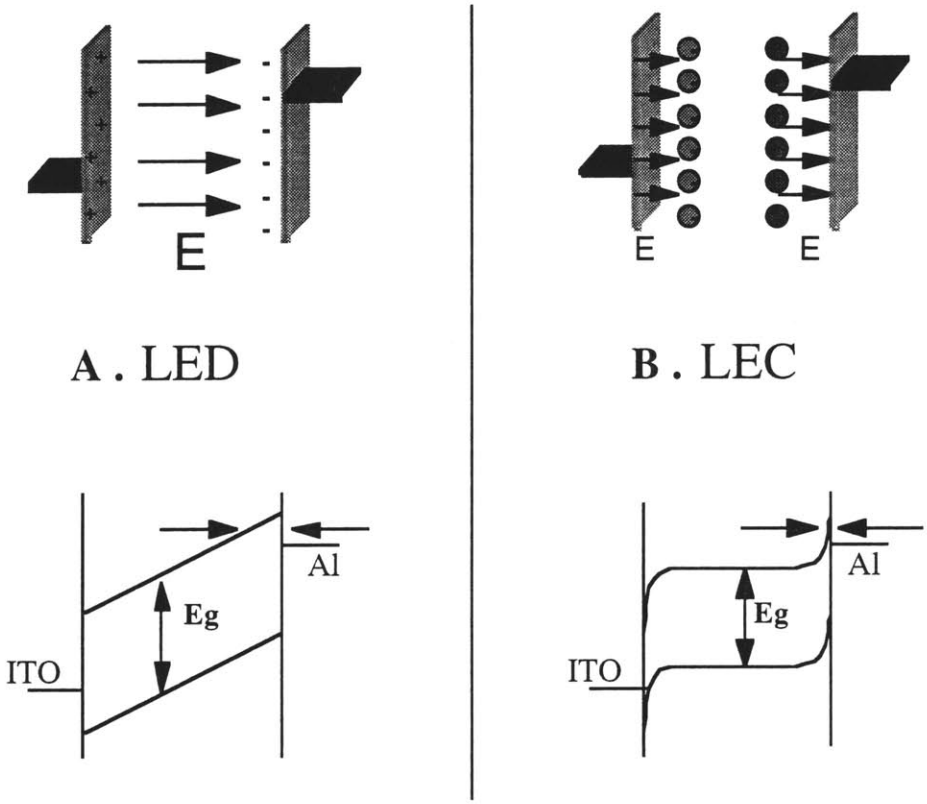

Figure 1-4A and B. The physical picture and resulting band structure of a device under forward bias. In an LED, (A), the material does not polarize and the resulting bands are rigid and have a large energy barrier to electron injection. In an LEC, (B), the ions move and polarize the material so the resulting bands bend considerably and maintain a constant energy level in the bulk of the device. Most devices operate somewhere between these two extreme pictures.

This picture represents the case for an organic light emitting diode, or LED. When an external voltage is applied, the gradient of the energy difference across the device increases until the barrier to electron injection is thin enough for electrons to tunnel through. This model has been elaborated by Parker.[8] In this case, device performance is highly dependent upon both the work function of the electrode and the electric field across the

device because both factors determine the width of the barrier seen by the electrons (or holes).

1.2.3 Carrier Injection in Organic Devices with Added Salt

Very recently, a new device structure has been studied in which mobile ions are intentionally added during the processing of the PPV sample by mixing some salt into the solution. These structures have been dubbed light emitting electrochemical cells, or LEC's.[12] Here, as the electric field develops across the device, the ions migrate and create an internal field that partially cancels the effects of the electron migration that was caused by the equilibration of the Fermi energies. This ion movement increases under an applied bias, as in Figure 1-4B. In the extreme case, the ionic space charge field completely cancels the electric field in the center of the device, and any further applied field drops only across the interfaces. This phenomenon is related to the double layer that builds up in a traditional electrochemical cell as ions migrate through the solution to the electrodes until equilibrium is reached.[13]

When a voltage is applied across the device, tunneling across the thin barrier into the material can begin as soon as the lowest unoccupied molecular orbital (LUMO) energy level is reached. The LUMO energy is generally the same as the reduction potential of the isolated molecule in solution and is the equivalent of the conduction band for a more extended crystalline material. Although the exact nature of charge transfer from the electrode is somewhat different, using a band model for approximation of the injection into the LUMO levels is convenient and consistent with the general device results. For these devices, as long as the ionic content is sufficient to form the double layer at the interface, the performance is independent of the electrode chosen. In addition, the barrier is not dependent upon the electric field but rather upon the voltage applied.

Because this barrier to injection has been thinned, much lower voltages are required for device operation. The turn-on voltage is no longer dependent upon the electric field across the device and is therefore independent of device thickness. Also, because the character of the electrode is no longer critical for charge injection, devices have similar performance regardless of whether the aluminum or ITO is used to inject electrons, and the resulting current-voltage curve is symmetric with respect to applied bias. Finally, these LEC's show a large time dependence in the current and light output, because relatively slow-moving ions are involved in the process. These characteristics are hallmarks of

electrochemical behavior and will become critical in describing the ruthenium(II) systems studied in this thesis.

1.2.4 Transition to Redox-Active Systems

The addition of small mobile ions to the PPV materials improved device performance in many ways but complicated the processing, because the salts tended to phase separate and form clusters.[14, 15] Also, the true role of the ions in these PPV films has been hotly contested. One group, represented by deMello and Friend, claim that the role of the ions is purely to thin the barriers to injection as described above.[16] A second faction, represented by Smith and Heeger, claim that true electrochemical doping occurs in the PPV, creating highly conductive regions at the interfaces.[17] The regions then extend into the bulk of the PPV, creating p-type and n-type regions within the device followed by the formation of a p-n junction in the center where the electrons and holes recombine. The outstanding question is whether these PPV films behave like traditional electrochemically active materials or whether the ability of charges to delocalize as polarons (described in section 1.2.1) rather than remaining localized on a single molecule lends unique properties to this system.

About the same time, our group was beginning to look at the feasibility of using traditionally solution-state electrochemically active species in solid-state cells. Fortuitously, the charged nature of these systems means that small mobile counterions are already present in abundance and are necessarily homogeneously mixed with the chromophores. Also, although it is convenient to describe the charge injection in these systems in terms of bands in analogy to more traditional semiconductors, these redox active ruthenium systems have no known "band-like" character to their electronic conduction. Reports in the literature are consistently of activated electron-hopping between individual molecules.[18] We felt that these systems would be good to compare with the recent reports on PPV-based LEC's to determine which device properties are unique to PPV and which are common to electrochemically active systems in general. However, before this comparison could take place, I needed to formulate a coherent picture of the important mechanisms in trischelated ruthenium(II) and the behavior under a wide variety of testing conditions.

Because the trischelated ruthenium(II) complexes have small counterions, they will naturally fall near to the LEC version of charge injection as pictured in Figure 1-4B. However, as the relative concentration and mobility of the ions within a device are varied, the response to the applied field can move along the continuum from band bending of high

curvature to completely rigid bands as in Figure 1-4A. Under conditions of low ionic mobility, whether due to lowered temperature or to physical constraints, it could be possible for more LED-like charge injection to occur in the ruthenium materials. This transition would cause devices to go from being independent of the electrode choice to being very dependent on the work function of the metal used to inject charge. I investigate this phenomenon in Chapter 4.

A final interesting case happens when partial compensation of the ions at the interface of an LEC occurs as charge is injected into the device. If charge transport is the rate limiting step, injected species will build up near the electrodes. These charges counterbalance the ions and the barrier to injection begins to increase, as in Figure 1-5. This process insures that the rate of charge injection at steady state does not exceed the rate of charge transport.[17] Under steady-state DC bias, if charge injection happens faster than transport, these ruthenium(II) complexes will show this increase in the barrier to injection. This case is investigated in Chapter 5.

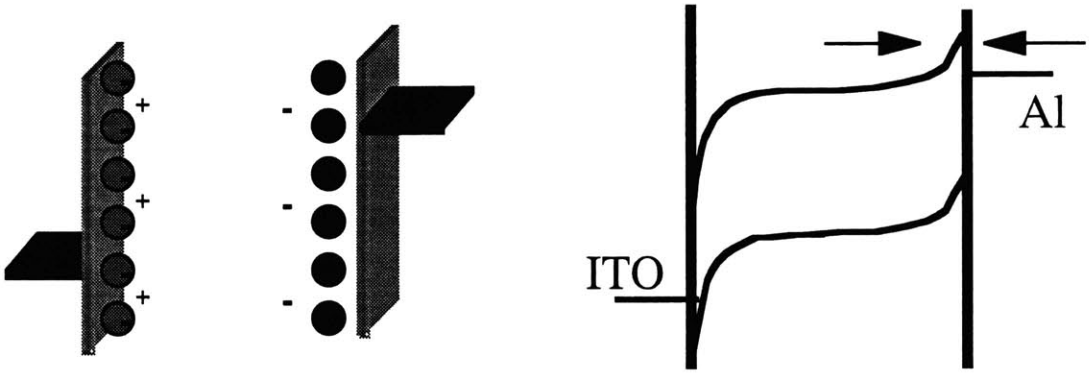

Figure 1-5. Partial compensation of the space charge layer in a material by injected charges. The physical picture at left results in a spreading of the band curvature and an increase in the energy barrier to charge injection as shown at right.

1.2.5 Carrier Transport and Recombination in Ruthenium(II) Complexes

The carrier transport mechanisms in the ruthenium materials are much different from those of PPV. Here, molecules undergo a complete charge transfer and become oxidized or reduced by the electrodes, forming 1+ and 3+ states respectively. These oxidation states must be stabilized by the movement of counterions through the system as

the charged states diffuse away from the electrodes. A schematic of this concept is given in Figure 1-6:

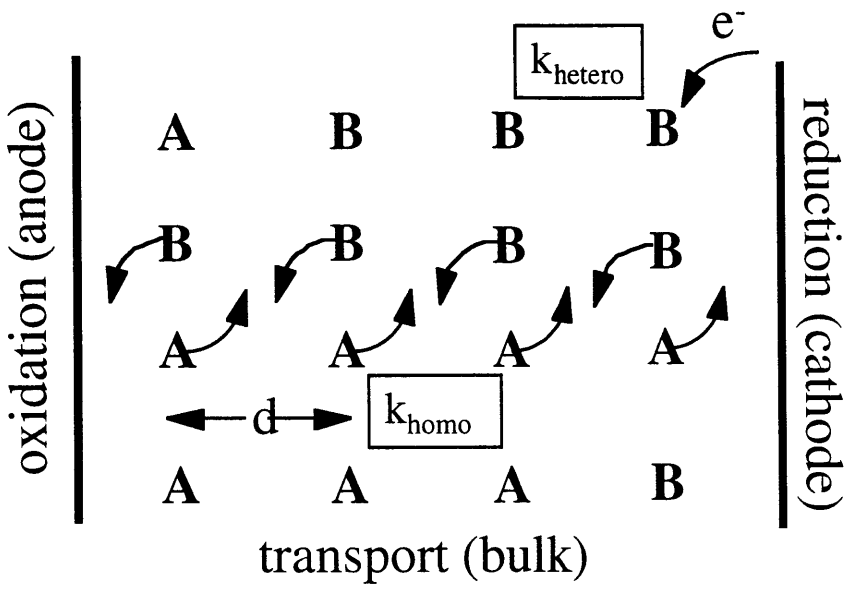

Figure 1-6. Schematic of the bimolecular hopping. A and B are the oxidized and reduced forms, respectively, of the species in question. In our case they would represent Ru(2+) and Ru(1+) or, alternatively, Ru(3+) and Ru(2+). For light emission we require both sets of redox couples, i.e. the addition of a species C.

In general, the charge transfer rate is dependent upon the relative ratios of 3+ to 2+ states or 2+ to 1+ states, with the highest rate of reaction occurring at a 50/50 blend. The hopping rate is also dependent upon the average distance between redox centers in the film, or more specifically, their relative separation when the charge transfer event occurs. The final equation is given by:

$$J = D_{conc}\frac{\partial B}{\partial x} + D_{elec}\left(\frac{AB}{A+B}\right)\left(\frac{\partial \theta}{\partial x}\right)$$

$$D_{conc} = k_{homo,conc}(A+B)d^2$$
$$D_{elec} = k_{homo,elec}(A+B)d^2$$

where A and B are the concentration of oxidized and reduced species, θ is the applied potential, k is the homogeneous charge transfer rate constant for hopping (driven either by a concentration or a voltage gradient), and d is the distance between species at the time of electron transfer.

Once charge has been injected, the redox centers will form a concentration gradient with the maximum number of charged species allowed by the injection equilibrium at the electrode, decaying to zero as the charges diffuse away. For light emission, two concentration gradients must be formed and meet within the device, one of the 3+/2+ redox couple and the other of the 2+/1+ couple, so that the 3+ and 1+ species are both present in the device. When the 1+ and 3+ meet, they undergo another charge transfer, creating 2+ and 2+*, where the * indicates an electron in an excited state. It is the relaxation of the 2+* species which causes the radiative behavior in this ruthenium complex.[19] The emission occurs near 630 nm, which is red light.

Results generated by many groups, most prominently that of Murray and co-workers, have been fairly consistent with this theoretical description.[20-22] However, some of the current-voltage data could not be fit with this simple picture and required some modifications to the theory.[23, 24] These modifications state that redox hopping through the film is a gated process such that the rate-limiting step is actually jumps between clusters of centers and not between individual species. Therefore the appropriate charge transfer distance to use in the equation is not one discrete value, but actually a distribution of distances. This distributed transport theory was originally described by Scher and Montroll and elaborated by Pfister [25, 26] and will be used in my analysis of data in Chapter 4.

1. 3 Evolution of a Thesis

The beginning of this thesis project came out of an effort to improve the efficiency of the light-emitting devices currently produced in the Rubner lab. Films of PPV gave luminances around 10-50 cd/m^2. Literature reviews indicate that PPV is primarily a hole conductor, so we reasoned that the efficiency would be improved if we added an electron transport material.[7] Preliminary work was being done on a ruthenium(II) trisphenanthroline complex that seemed to be a likely electron transport candidate. Small molecules were expected to crystallize, so large bulky phenyl rings were attached to the phenanthroline moiety during synthesis. Layer-by-layer processing was a promising film deposition technique, so the phenyl rings were additionally sulfonated to provide extra charges to use in that process. The resulting molecule was spun onto a PPV layer-by-layer film to yield the now infamous device curve given in Figure 1-7. The heterostructure device gave much higher light and efficiency than the PPV devices made at the time.

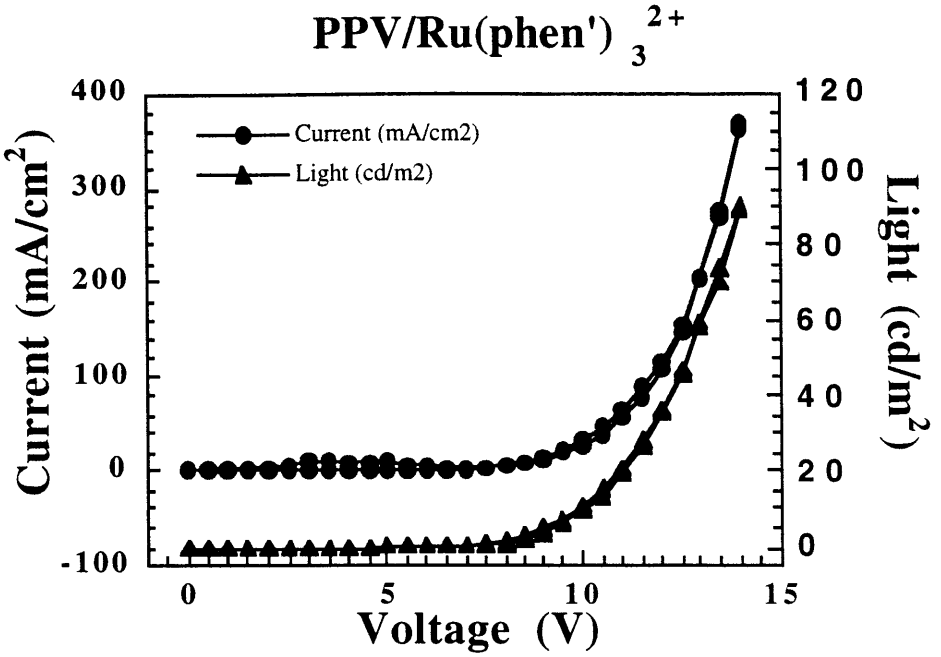

Figure 1-7. The original heterostructure device curve measured by E. S. Handy. PPV devices at the time generally gave around 10-50 cd/m2.[27]

However, devices of this ruthenium material alone gave quite high luminescence compared to that seen from PPV. Current-voltage curves for phenanthroline only devices showed an interesting positive hysteresis loop. Further study showed that, when held at a constant voltage, the current and light increased slowly with time until they reached a maximum and then began to slowly decline. The turn-on voltage, or first appreciable increase in current and light, was very close to the redox potential of the ruthenium(II) complex in solution. In addition, unlike PPV devices, the turn-on voltage did not appear to be dependent on the electrode used or the thickness of the film. These characteristics seemed to point to an electrochemical mode of operation for these solid-state films similar to the behavior of the molecule in the solution state.[28] This mode of operation is described in the previous sections of this chapter.

However, several details of the device performance were not typical of solution electrochemistry. Limiting current behavior was never reached in these films. Current was symmetric in most cases but light was not. The addition of an ion-transport polymer, PEO, improved device stability but did not appreciably affect charging time. Additional small

mobile ions dissolved into the processing solution also did not speed up the light emission process. The heterostructures of these materials with PPV did not show the hysteresis that was characteristic of the films of the phenanthroline complex by itself.[27, 28] These exceptions to the expected electrochemical behavior needed to be included in the final explanation of device mechanisms and performance.

Therefore, this thesis proposed to outline the mechanisms of device behavior in these heterostructure devices and to unify these observations into one overarching theory. As more materials systems have been synthesized and tested, the picture has become more complicated. However, the device properties have become considerably better, with the current maximum light output around 1000 cd/m^2, the best efficiency at 3%, the best lifetime at over 8 days, and stable operation in air.[29] The challenge becomes the determination of the rate limiting step for current transport in each material for a variety of testing conditions. The effect of this limiting mechanism on the final light output can then be evaluated so the next round of devices can be improved.

The biggest challenge in evaluating these films is the separation of many competing effects that occur simultaneously. Traditional methods for distinguishing mechanistic regimes such as temperature dependence, short time transient measurements and capacitance have been used to test these devices during the course of this thesis. However, many of the characteristic physical constants, such as the activation energies for electron hopping and ion diffusion, have similar orders of magnitude making the determination of different mechanisms difficult. In addition multiple driving forces are often present, making the interpretation of rate constants, etc., ambiguous. Fortunately, through testing a wide variety of related systems, from relatively mobile small molecules to highly immobile polyelectrolyte salt complexes, I have been able to interpret the relative importance of materials constants when absolute values might be questionable. The end result is a general picture of the performance of trischelated ruthenium(II) molecules in the solid state and some discussion of conditions under which they may be able to violate the general rule.

1. 4 Introduction of Ruthenium Compounds

Each of the ruthenium complexes studied during the course of this work provides different opportunities for probing the overall device mechanism. Changes in structure, counterion size, chromophore density, and mobility will all have varying impacts on the final electronic performance of the material. This section will outline some of the points common to all of the molecules and will highlight their important differences. It will also

review some of the important observations made on the device performance of these systems prior to and during the early stages of my involvement with the project. Particular attention will be focused on the factors that could not be explained at the time.

Common to all of these materials is the fact that they have a formal 2+ charge on the ruthenium center. This charge must be balanced by the presence of a counterion to maintain electroneutrality. In most cases the counterion is a small molecule, such as Cl- or PF_6-, although the layer-by-layer processed polymers have predominantly polymeric counterions. In addition, all of the ruthenium(II) complexes have conjugated ligand groups that support higher energy electrons in their overlapping π^* orbitals, allowing stable reduction. Electrons can also be withdrawn from the d-orbital of the ruthenium metal center to allow stable oxidation. Typical cyclic voltammetric curves can be produced from all of the materials, yielding values for the oxidation and reduction (redox) potentials not far from the well-known redox potentials of trisbipyridyl ruthenium(II) in solution.[27, 30] . These common characteristics incline all of these materials to be electrochemically active under standard conditions, i.e. at room temperature and in solution. In the following sections, I note these common responses and point out the unique constraints for each system which may alter this behavior under certain conditions.

1.4.1 Trisbipyridyl Ruthenium(II) Diol ($Ru(bpy)_3$ diol)

This small molecule system was synthesized by Erik Handy as an intermediary step to the polymers introduced in the next sections. We were planning to do the polymer synthesis because most literature reviews indicated that small molecules had trouble with crystallization and quenching. However, when controls were made of the diol alone to compare with the polymer performance, surprisingly good films with excellent device properties were formed. The structure of the diol is given in Figure 1-8. The diol formed slightly better films than the commercially available $Ru(bpy)_3$ without the alcohol groups pendent to the ligands, presumably due to additional hydrogen bonding in the diol. The counterion was almost always PF_6- to allow for dissolution in organic solvents such as pyridine.

Because the diol is accompanied by two counterions per molecule, a high concentration of ions are available to stabilize any electrochemistry done in the film. In addition, the small molecule nature allows for relatively high rotational mobility of the matrix. The combination of both of these factors should result in reasonable ionic conductivity at room temperature, and this system was expected to be the most idealized

one that I studied. Under most conditions, it served as a standard for the "typical" device behavior in a solid-state electrochemically active system. Because the ligands on this diol are the smallest that I studied, it was also expected to pack the most tightly and to have the highest electronic conductivity as well. As a neat film, with no other material included to interfere with charge transport, it has the highest density of chromophores and the smallest distance required for electron hopping. This high density may contribute to self-quenching of the light emission however.

Current-voltage plots showed large positive hysteresis loops with significantly more current and light on the return sweep. Current-time plots at constant voltage reflected this behavior as a slow rise in current. This rise was determined to be related to the ions in some way, by Handy who investigated the effects of the size of the counterions on the device charging time.[31] However, the specific reason for this effect was unknown. Another question was the lack of light in reverse bias. For an electrochemically active system, we expected the device performance to be independent of bias direction. Plenty of current passed through the device in reverse bias, but it was not accompanied by the expected light emission which was not understood. The origin of both of these effects will be discussed in this thesis.

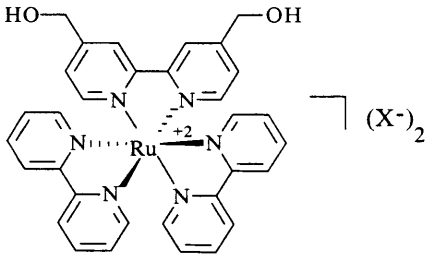

Figure 1-8. Trisbipyridyl ruthenium(II) diol. The related $Ru(bpy)_3$ without the alcohols attached to the ligand is commercially available and was used in some comparison studies. The counterion (indicated in the figure by an X-) was generally PF_6-.

1.4.2 Sulfonated Trisphenanthroline Ruthenium(II)

This sulfonated trisphenanthroline ruthenium(II) compound was the first material that was studied by our group; the structure is given in Figure 1-9. Throughout this work, it will be designated as the phenanthroline complex or $Ru(phen')_3$. A non-sulfonated analog was later synthesized, but the performance of that compound is not included in this thesis. The phenanthroline ligand was chosen by Jin-Kyu Lee because solution state data indicated that the photoluminescence efficiency was higher, likely due to the extra link

between the conjugated rings that reduced the amount of oscillation about the central bond and therefore the quenching of emission by vibrational nonradiative pathways. As noted in section 1.3, this compound was synthetically designed with large phenyl rings to prevent crystallization and quenching in the solid state. In addition, sulfonate groups were covalently attached to each phenyl ring to provide more charged groups to allow the material to be used in the layer-by-layer deposition process described in the next chapter.[30] The resulting ligand group is quite bulky, and therefore does not allow the packing of these chromophores to be as dense as the diol case. The rotational mobility of the ruthenium centers is also reduced because of these large groups. These two factors should increase the chromophore separation and decrease the rate of electron hopping. The counterion used to neutralize the ruthenium center was chosen to be the chloride ion to allow for aqueous processing.

When current-voltage and current-light plots were taken by Dongsik Yoo, device performance was similar to the diol, with symmetric current, asymmetric light, and charging times on the order of 2 to 3 minutes.[27] Although this molecule had much higher photoluminescent efficiency in solution than the diol, the external quantum efficiency of the electroluminescence was much lower. This result was completely counter to what we had expected. In addition, when Cormac Lyons included the molecule in a polyethylene oxide blend, we expected an increase in the rate at which the system reached maximum light and current, because PEO is a known ion conductor. The blend with PEO allowed slightly more uniform films to be made, but little change in the charging time was seen; the addition of excess salt also did not affect this process.[28] This result was unexpected because the addition of an ion conductor or more free ions was thought to aid in the charging rate.

When I spoke with other researchers in the field at conferences, questions were raised about the nature of the counterions present in the final material. Some evidence is available based on crystallization studies of related molecules that the chloride ions actually complex with two of the sodium ions from the sulfonate groups leaving the final compound with two negatively charged sulfonate groups to counterbalance the ruthenium charge.[32] Elemental analysis confirmed this suspicion, showing many fewer chlorine atoms present than expected.[31] In addition, because chlorine is an electrochemically active species itself, the remaining chlorine ions in the film likely cause side reactions at the electrodes and are not the best choice for an ECL system. Because of these complications, this system

was our most difficult to understand. However, these considerations can be included in the final device picture that I describe in this thesis.

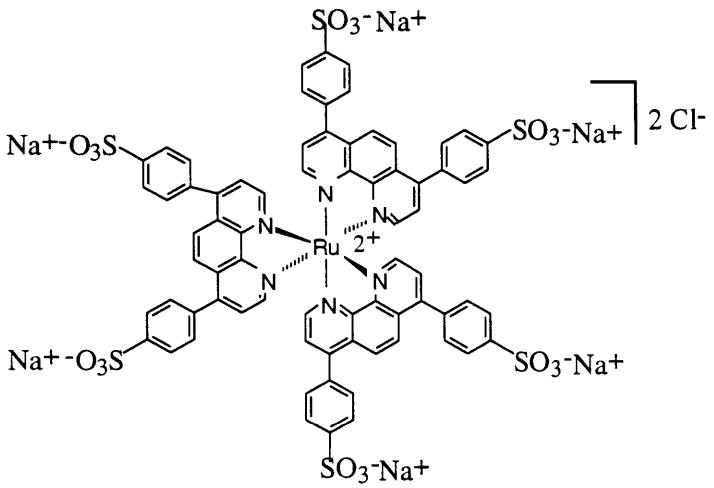

Figure 1-9. Sulfonated trisphenanthroline ruthenium(II). Although a non-sulfonated version of this molecule was also synthesized in our group, all of the work in this thesis was done with the sulfonated form of the complex.

1.4.3 Trisbipyridyl Ruthenium(II) Polyurethane

The diol described in section 1.4.2 was a precursor in Handy's synthesis of a polyurethane with approximately 10 molecular repeat units per chain.[31] The version of the polyurethane investigated in my thesis contained a 12-carbon spacer, similar to the polyester described next. The structure of this molecule is given in Figure 1-10. In most cases the counterion was a PF_6- molecule, but for the layer-by-layer deposition described in the experimental chapter a chloride ion was used.

Films of this material had a lower chromophore density than the pure diol samples due to the extra dilution by the hydrocarbon spacers. This separation causes a larger distance between redox centers for electron hopping. In addition, the ionic conductivity and molecular mobility is expected to be drastically reduced due to the covalent bonds restricting the degrees of freedom of the chromophores and increasing the rigidity of the matrix. Hydrogen bonding from the urethane linkages will also contribute to lowered mobility. This material is expected to be slower responding than the diol system, but the essential electrochemistry should not be significantly different because the type of ligand and counterion has not changed dramatically.

Films of this material showed very high turn-on voltages when tested.[31] In contrast to the 3V evidenced by the diol, the polyurethane generally required up to 8V on the first application of bias. When the device was repeatedly cycled, the turn-on voltage would slowly decrease to 3V. Current-time measurements of these films were qualitatively similar to those of the diol; however the charging time for the trisbipyridyl ruthenium(II) polyurethane was now on the order of 20 to 30 minutes rather than 2 to 3 as for the diol. The effect of the slower ionic conductivity on the slower device response will be discussed in this thesis.

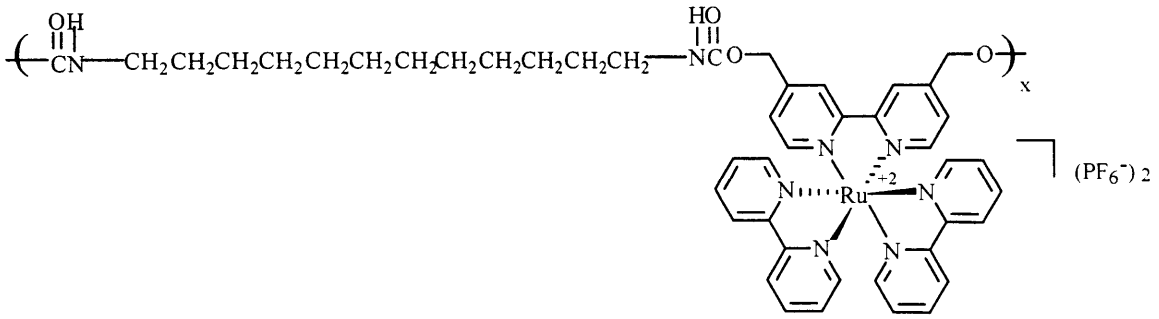

Figure 1-10. Trisbipyridyl ruthenium(II) polyurethane. The counterion (PF_6- in the figure) was PF_6- for all spincoated samples and was Cl- for the few layer-by-layer samples made with this material. The resulting polymer contained approximately 10 repeat units (x=10).

1.4.4 Layer-by-layer Films of Trisbipyridyl Ruthenium(II) Polyester

This polyester is very similar to its polyurethane analog described in the previous section. Its structure is given in Figure 1-11. The primary difference between these samples and those of the polyurethane is the use of this material in the layer-by-layer electrostatic assembly process, which results in the shedding of most small counterions and their replacement with polyions. Details on the nature of the film fabrication process will be given in Chapter 3; however, this assembly makes use of the ruthenium sites as positively charged centers to build-up multiple layers of material by alternation with a negatively charged polymer. The resulting film is a molecular-level blend of the two polyelectrolytes, so the matrix is ionically cross-linked. The final material should have the lowest ionic conductivity of any I studied because of the loss of small ions and the crosslinking of the matrix. This low conductivity is very important in the device behavior of these films.

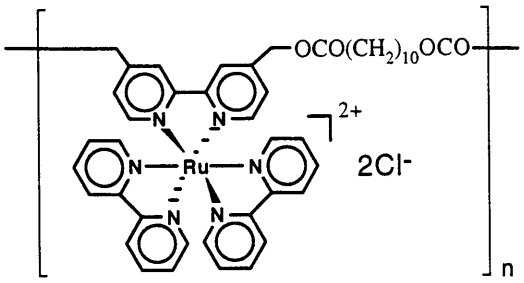

Figure 1-11. Trisbipyridyl ruthenium(II) polyester. The final oligimer contained 5 to 7 repeat units (n=5 to 7).

Studies of this system by Aiping Wu showed a large dependence of the device performance on the nature of the counter-polymer used in the deposition process. Current-voltage plots ranged from completely symmetric, as in all the cases described above, to completely rectifying. The light emission characteristics also changed, with reverse bias light emission now evident in some cases. In no case did the turn-on voltage drop as low as 3V, but remnant positive hysteresis loops were often seen.[33, 34] All of these observations had to be reconciled with each other and with the observations on the other systems described above. This thesis provides that final consistent picture.

1. 5 Outline of the Present Work

The next chapter outlines in detail some of the recent literature on redox active systems, ruthenium-based light emitters, and electrochemically active devices with specific attention to the role this background knowledge plays in the understanding of our devices. Chapter Three presents the experimental procedures, with explanation of the layer-by-layer processing technique which allowed detailed probes of molecular environment and device interfaces. Possible mechanisms of charge injection are discussed in Chapter Four with respect to the variety of ruthenium-based light emitting compounds that have been introduced during the duration of this work. Chapter Five introduces charge transport mechanisms in relation to data obtained on these films, and some of the relevant physical constants are calculated for these materials. Special considerations for device performance due to the thin film nature of our samples are presented in Chapter Six, and the unique characteristics of heterostructure devices are revisited in Chapter Seven. Finally, a summary of the current understanding for the performance of each ruthenium(II) system is presented in Chapter Eight, along with suggestions of areas for future study.

2. Background Literature

This chapter is intended to provide a general overview of some of the relevant literature from the past 25 years for the interested reader. In large part, it is an expansion with further detail on the basic theories presented in Chapter 1. The older papers regarding solution-state serve as a frame of reference so that the evolution of thought on these redox active molecules can be understood. Later solid-state experiments build on these earlier notions, particularly within the context of kinetics issues such as ionic mobility and charge transfer rates. These later papers also introduce additional complications present in the solid-state that were not influential factors in the earlier studies but will be important in the study of our current systems.

2.1 Electrogenerated Chemiluminescence in Solution

The first reports of electrogenerated chemiluminescence from chelated ruthenium(II) complexes came from Tokel and Bard in 1972.[1] This work was an extension of standard cyclic voltammetry by which the oxidation and reduction potentials of a molecule can be determined in dilute solution. They reported visible light emission from an acetonitrile solution of $Ru(bpy)_3$ when a platinum electrode was cycled between the oxidation and the first reduction potential of the molecule at (+1.70V) and (-1.09V) respectively versus Ag wire reference. Interestingly, more intense light was seen when the second or third reduction potentials, at (-1.27V) and (-1.53V) corresponding to Ru (0) and Ru (-1), were used.

Bard and coworkers established that the mechanism of electrogenerated chemiluminescence in this system follows the reaction mechanism:

$$Ru^{3+} + Ru^{1+} \rightarrow Ru^{2+*} + Ru^{2+}$$
$$Ru^{2+*} \rightarrow Ru^{2+} + h\nu$$

This direct annihilation scheme in other light-emitting redox species is generally due to a singlet-singlet recombination such that the resulting energetic species is energy-sufficient for light emission. $Ru(bpy)_3$ is an unusual system in that the 3+ and 1+ are in fact triplet states that generally require more energy during recombination than singlet states, but the final reaction product retains enough energy to form the 2+* state. The $Ru(bpy)_3$ triplet has an unusually short lifetime, so that non-radiative reactions become less likely and high efficiency results.[2] The $Ru(bpy)_3$ system generally has an ECL quantum efficiency of around 5%. For the related $Ru(phen')_3$ system, that value can reach 24%,[3] and low temperature measurements have increased the maximum efficiency to 33%.[4]

In these systems, the 3+ charge is centered on the d-orbital of the ruthenium center while the 1+ charge is distributed on the ligand. As a consequence of this difference, the 1+ charge tends to move faster through materials (have a relatively larger diffusion constant) but is much more sensitive to the environment of the complex.[5] In fact the formal oxidation potential of the complex can change substantially, based on the type of chelating ligand and its solvating environment.[6, 7] These differences are also reflected in the color of the light emission that can vary over 50 nm from red to red-orange.[8]

Generally, ECL experiments are done in an AC configuration whereby both charge species are produced at the same electrode. The resulting concentration profile of reactants follows a standard Fickian diffusion for the first charge; however, due to conproportionation reactions when 3+ and 1+ meet, they annihilate each other and the profile of the second species becomes more complicated. The distance of the light emission zone from the electrode depends upon the diffusion rates of the molecules and the AC oscillation frequency. As long as the complexes near the electrodes can be reversibly oxidized and reduced, the cycle will continue. However, common side reactions with higher oxidation state products often produce non-emitting species.[9] In addition, electrolysis of the solvent can cause a buildup of contaminants near the electrode.

In order to monitor steady-state ECL, the two species must be produced at separate electrodes. A very common experimental setup is the rotating ring-disk electrode system, where the spinning of the disk disperses the molecules in solution, allowing fresh redox complexes to flow from solution perpendicular to the electrodes.[10] Other more complicated systems have been devised, including flow systems so that a fresh supply of redox active molecules is always present.[11-13] The simplest DC setup, and the one closest to our solid-state devices, is the thin layer cell. In this case, two parallel electrodes are held a fixed distance apart while a DC current is passed through the solution between them. This setup has the advantage of simplicity of construction, and the modeling of the emission front is also much more straight forward. However, the operating lifetimes of these cells are typically only a few hours.[9] Interestingly, the best lifetime performance is in cells without added supporting electrolyte.[14]

These basic mechanisms of light emission and charge transfer are consistent with everything that we have seen in our systems; however, a few important distinctions need to be made. The mechanism of charge transport in solution is generally translational motion of the redox molecules that we do not expect to occur in the solid state. Therefore, the diffusion equations must be modified. Also, the kinetics of electron transfer from the electrode is assumed to be generally fast relative to the diffusion such that the interface is at equilibrium. This assumption may not hold in our films. In addition, the high efficiency

of the phenanthroline system in solution-state is not reflected in our solid-state films. Some of these complications are addressed in the following literature.

2.2 Electrochemistry of Molecules at Electrodes

The advantages of solution cell approaches are certainly the high ionic conductivity available in the solution state and the direct application of solution electrochemistry measurement techniques. However, for many applications, the immobilization of the redox species is crucial, such as in biological tagging or chemical sensing. Effects of redox site distance can be studied in a controlled fashion by controlling the amount of diluting material. In addition, low temperature or low pressure experiments can be performed if no solvents are present that can freeze or evaporate during the measurement process. For these reasons, research in the field turned to the incorporation of $Ru(bpy)_3$ molecules into solid-state films.

One of the most common approaches is the use of Nafion, a perfluorinated ion-exchange polymer, as a macromolecular solvent for the individual $Ru(bpy)_3$ molecules. The Nafion is deposited onto an electrode, and the film is dipped into a solution of $Ru(bpy)_3$ molecules. The redox species then ion exchanges with the small ions in the polymer and is held in place by the Nafion matrix.[15-17] A second approach is the incorporation of the redox species directly into a polymer which is then electropolymerized onto the electrodes. This approach has been used extensively by Murray's group for various redox active complexes, including a $Ru(bpy)_3$ derivative.[18-23] Both approaches allow for the localization of the redox sites. However, most research still relies on solvent contact to provide the necessary ionic conductivity in the system.

The electrochemical properties of redox complexes sequestered at electrodes vary somewhat from the dilute solution case. Although swelling of the polymer by solvent helps to increase mobility, ionic conductivity is generally much lower in these systems due to physical barriers in the polymer film as well as ion-polymer interactions that increase with the higher concentrations of ions and chromophores present in a solid film.[15, 24, 25] This slower diffusion creates a characteristic signal in the CV curves, a broadening and separation of the oxidation and reduction peaks, indicating quasi-reversible behavior. Heterogeneous charge transfer at the interface between the electrode and the polymer can be slower.[26, 27] Charge transfer within the film can also be slower, as redox sites become dependent upon polymer segment motion to bring them close enough to support electron transfer.[28, 29] All of these points have been extensively studied in the presence of an external solvent/electrolyte system and will be a useful starting place from which to examine our films.

Another difference between solution ECL and adsorbed molecule ECL is the proximity of the emitting species to the electrode interface. Extensive studies of the influence of the electrode material on the emission of $Ru(bpy)_3$ have shown that although partial quenching of the excited state by the metal does occur, the two reactions are competitive.[30] Quenching was least noticeable on tin oxide electrodes as compared to platinum or gold, but in all cases visible light emission was still observed.[31] Increased concentration of redox species allows for self-quenching effects as well.[17] A distribution of redox sites may also be present in these solid-state films due to phase separation effects of the polymers.[26] Redox species in different regions of the film may see different environments for charge and ion transport, resulting in a distribution of diffusion rates and reaction times.[32] This non-ideality turns up in prefactors required in the modeling of the charge transport that will be discussed in Chapter 5.[33, 34] Additional complications, such as interactions between the ions and the polymer matrix and ion-ion interactions due to increased ion concentration, require additional corrections to the theory but will not be discussed in detail here.[24, 35]

In a few cases, processes to adsorb the small $Ru(bpy)_3$ molecule directly onto an electrode without intervening polymeric material have been explored.[36, 37] This approach avoids many of the complications imposed by the inert polymer matrix but still relies on solvent contact for ionic conductivity. Some difficulties are seen in retaining the molecules on the surface during multiple oxidation/reduction cycles. In addition, the high concentration of $Ru(bpy)_3$ molecules can exacerbate quenching effects seen between the excited 2+* and 3+ species.[16] These results should help to explain some of our results for similar $Ru(bpy)_3$ molecules deposited directly onto electrodes.

2.3 Solid-State Electrochemistry

All of these previously mentioned reports have involved investigations of the redox species in contact with a solvent and supporting electrolyte. However, to understand our films, we must consider what happens without the aid of an ion-conducting solvent. The first report of what is termed "solid-state voltammetry" was from Jernigan et al. in 1985 when they described measurements on osmium-containing films in the absence of an electrolyte solution. These researchers coined the term "ion budget" to emphasize the fact that oxidation and reduction of species within the film were now limited by the quantity of ions already present in the material. For considerations of electroneutrality, the number of species oxidized at one electrode must be equal to the number of species reduced at the other. This produces a set of redox couple concentration gradients as the concentration of ions also varies throughout the film. Figure 2-1 shows the representation of this concept as

per [5]. This picture also considers the resulting gradients when more than one reduction state is reached, i.e. Ru 0 as well as Ru 1+, although little discussion of this case occurs in later papers.

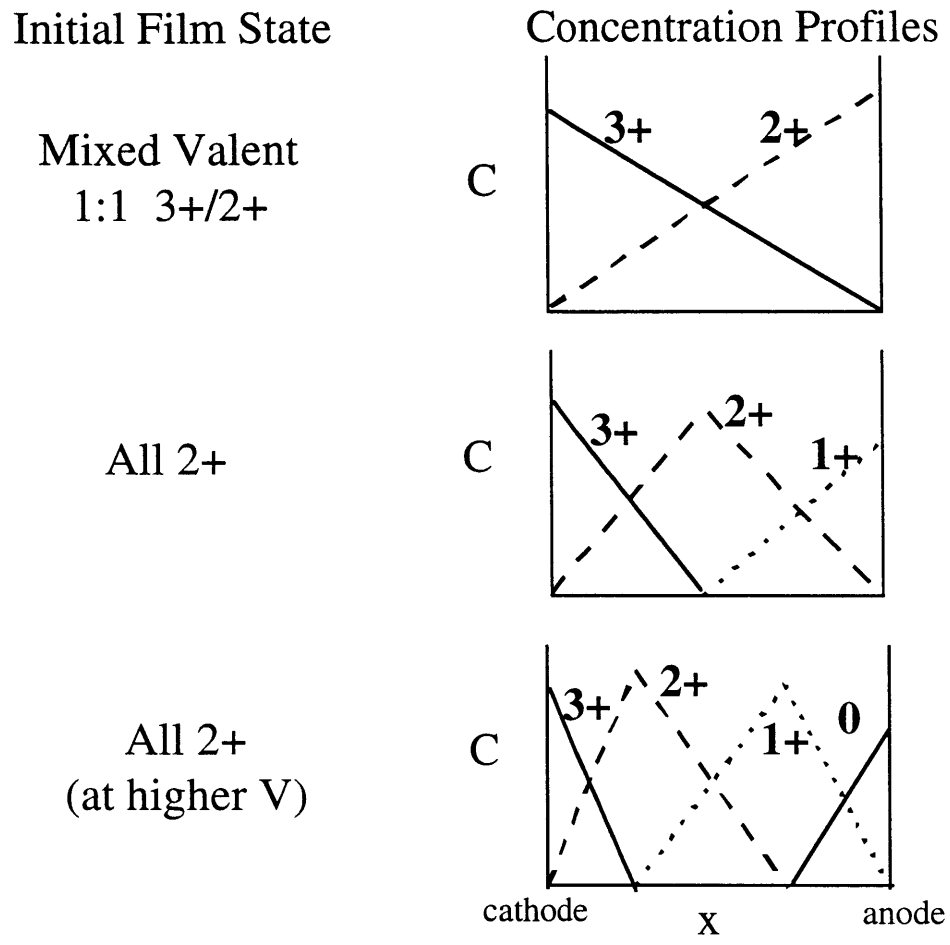

Figure 2-1. Representations of concentration gradients resulting in a redox active film. The initial state of the film is determined by the state of the sample after being removed from contact with solvent and supporting electrolyte. After Jernigan et al.[5].

In these investigations, the concentration-gradient driven electron hopping rates were measured in a series of environments, from solvent contact to dry nitrogen. Interestingly, although the rate of hopping for the 3+/2+ couple slowed when the films were dried, as would be expected for a reduction in mobility, the rate of hopping for the 2+/1+ couple actually increased. The explanation forwarded by the authors argues that the distance between redox centers decreases in the dried film, thereby increasing the ligand overlap and therefore the diffusion rate for the 1+ state centered on the ligands. They infer that electron transfer in this system requires very little if any counterion displacement once

the redox couples have been formed.[5] This reasoning will be explored in Chapter 5 in our discussions of charge transport in our films.

These reports were followed by several others from Murray's group investigating the details of electron exchange in these solid-state systems.[18, 21, 22, 33, 34, 38] Dalton et al. gives a good review of the understandings of the group through 1990. The most dramatic report in Dalton's paper was that the electron exchange constants for concentration-gradient driven transport and for voltage-gradient driven transport were equal within experimental error. Therefore, the basic mode of electron exchange is independent of the driving force, and we must consider the effects of both on our device performance. Note that for the voltage-gradient driven mode of transport, a mixed valent state was imposed on the material in the presence of excess electrolyte so that concentration-gradient effects would not interfere in the measurement. This separation of driving forces is not possible in our "ion-budgeted" case. Verification of the presence or absence of a voltage gradient in the films was accomplished via a four-point-probe type measurement in which three similar devices were connected. Voltage was then applied across the outer leads, and the potential measured across the inner leads. In this way, Jernigan et al. were able to determine when ionic rearrangements in the film played an important role in device operation.[39]

The following papers primarily added subtleties to the theory and included more complicated reactions such as those considered theoretically by Andrieux and Saveant.[24, 40, 41] They verified the bimolecular rate law for a variety of ratios of oxidized to reduced centers and showed that maximum conduction occurred at a 1 to 1 ratio of the mixed valent species. They also examined the dependence on redox center separation in detail. Sosnoff et al. compares hopping rates based on Marcus theory with dispersive transport considered by Scher and Montroll and elaborated by Pfister.[42, 43] This dispersive transport theory describes a case in which the rate of transport is not limited by site to site hopping but by transport between clusters of sites. The concept translates theoretically into the existence of a distributed diffusion packet by which the fastest carriers traverse the film much more quickly than the average. This mathematical model becomes reflected later in the analysis of our films in Chapter 5.

2.4 Solid-State Electrochemistry with Light Emission

Two papers by Maness et al. in 1996 and 1997 returned to the concept of ion-budgeted films with a ruthenium polymer system that was now capable of light emission.[21, 44] In addition, rather than creating only one redox couple (either 3+/2+ or 2+/1+), they created both mixed valence gradients so that the final 3+/1+ reaction would be

possible and light emission could be observed. This study is the closest approximation available in the literature to the device structures I have studied. It serves, along with the 1985 paper by Jernigan et al., as a primary supplement to the data I have taken. Their results must be included in my final description of all of these ruthenium(II) systems.

In these experiments, they formed concentration gradients of redox couples in the presence of a solvent system to allow for the redistribution of counterions that preserve charge neutrality. At room temperature they observed the characteristic transient capacitive charging of the device as the ionic double layer is set up, followed by a rise in current to a plateau, reminiscent of our device behavior. Light emission was delayed by up to 12 seconds, consistent with a certain transit time for species to cross the 2 micron thick device. They calculate diffusion constants for the redox couples of 1.1×10^{-9} cm^2 /s for the 3+/2+ couple and 5.0×10^{-10} cm^2 /s for the 2+/1+ couple. However, although the diffusion rates are different for electrons and holes, the emission zone should be confined to the center of the device due to the constraints of limited ions in the film. This "ion budget" requires that the total number of oxidized species equal the reduced species, as emphasized in calculations by Elliot and coworkers[45], if the assumption of local electroneutrality is valid.

These devices were then cooled below the glass transition of the polymer with the bias in place so that the ionic gradients would be kinetically locked. The resulting structures showed rectification ratios of approximately 100:1, presumably due to the inability of the electronic charges to diffuse opposite to the concentration gradients of the redox couples when the reverse bias was applied. They did however see a low level of back current which gave some evidence of charge injection at the interfaces. This injection was counter to the redox gradient and occurred even in the absence of ionic movement. They comment that in their case the voltage across the film is not sufficient to cause disproportionation (creation of 3+ and 1+ species) in the center of the film; however, at sufficient voltages (or for sufficiently thin films) this reaction is a possible mechanism for reverse bias operation. This comment will become important to our thin film devices. Also, at low temperatures, ions cannot move to counter the applied field, so the constraints of electroneutrality may be violated and the electric field across the device could become non-zero. In this way, a voltage-gradient driven mode of operation could allow for the transport of charge even though the concentration-gradient driving force opposes the motion. This contribution from the voltage-gradient as a primary driving force will be used extensively to monitor current in our films.

A related paper from Murray's group using viologens as the redox active species contributes several other interesting observations.[34] Terrill et al. confirm the bimolecular

dependence of the current on the product of the concentrations of 2+/1+ species such that a 1:1 ratio gave the highest conductivity. Again, Terrill does not see significant current in films that are of all one valence state, but his films are also 2 microns thick. The most important results were the high variability in the current responses from a concentration gradient containing film as compared with a uniform mixed valent film. Indeed, these films show substantial reverse bias current, which is opposite the direction of the pre-formed concentration gradient. The authors explain these observations as being due to the extremely high electric fields that these gradients set up at the film interfaces. The interfaces are also highly resistive due to the imbalance of redox states (recall that the most conductive film occurred at a ratio of 1:1, therefore straying from this ratio causes an increase in the film resistance). Calculations by the authors of the potential across the film reveal very steep gradients within approximately 100 nm of each interface. They claim that this gradient can cause a significant enhancement in the oxidation rate, which consumes approximately 5% of a monolayer per second even in the non-mixed valent film and presumably more in the presence of a higher electric field gradient. Assuming similar rates of back reaction for our system, the process that they can ignore in their devices would consume our entire device within the space of 16 minutes. The significance of this difference between their film thickness and ours will be explored in detail in later chapters.

2.5 PPV-based Electrochemically Active Devices

Quite recently, Richter et al demonstrated a poly-para-phenylene vinylene device containing both excess salt and an ion-conducting material (PEO).[46] This group found that, in comparison with traditional PPV devices, this new structure exhibited a lower turn-on voltage, symmetric current and light behavior, and increased light output. They attributed this behavior to the electrochemical doping of the polymer followed by the in-situ formation of a p-n junction. The high doping caused ohmic contacts with the electrodes, thus eliminating the work function dependence of the charge injection, and the highly defined recombination zone increased the probability of electron-hole capture and therefore increased light emission.

This first observation has been followed with extensive experimental and theoretical debate over the mechanisms of device operation.[44, 47-53] Smith calculates the potential distribution and concentration of carriers (both electronic and ionic) through the bulk of the film based upon Heeger's model of device operation.[48] In this model, the excess ions in the film segregate to the edges of the device under low applied bias serving to thin the barriers to charge injection. Below the onset of junction formation, the electric field within the device is zero, except for a thin space charge region at each electrode. After the p-n

junction forms, the concentration of injected carriers becomes larger than the concentration of ions in the film. At this point the electric field can no longer remain zero and a field develops in the center of the film. This field differs from that of a traditional p-n junction in that the voltage drop is a consequence of excess carriers, not of charged dopant molecules left behind in the film. In his paper, Smith gives no rationalization for why such a voltage drop should occur in the center of the film rather than distributed evenly across the bulk of the device. He does however calculate all of the relevant equations and predicts the distributions of potential and carriers based on assumptions for various materials parameters.

A second model for device performance has been developed by deMello et al.[47] In this paper, they assert that the primary purpose of the ions in the PPV device is to thin the barrier to electron injection and to preserve local electroneutrality but that no electrochemical doping takes place. In this view, the ions segregate at the interfaces, forming an ionic space charge layer reminiscent of the double layer in a traditional electrochemical cell. This layer of ions shields the device from feeling the effects of the differences in work function of the various metal electrodes. In addition, the material becomes polarized during device operation as ions migrate to counteract the applied electric field. The carriers injected into the device are transported via diffusion along a concentration gradient rather than migration driven by a voltage gradient. In this way, electron injection is enhanced by the local field which increases the final light emission. The high-field case in which the injected carriers exceed the concentration of ions is not treated by deMello in terms of mathematical calculations. However, they do comment that for this regime, they expect that the barrier to current injection should first increase due to compensation of ions in the vicinity of the interface. Eventually the space charge regime should start to spread throughout the bulk of the device until the bias no longer remains zero at the center.

The primary experimental evidence disputed by the two papers is the significance of an experiment performed by Dick et al. [52] in which the electric field across a PPV device was measured via optical beam induced current experiments. The difficulties lie in the fact that a definite electric field was found in the center of the device, counter to the explanations of deMello et al. However, the width of this region was significantly larger than the thickness of a typical PPV device, due to the changes in geometry required for the OBIC measurements (IDA versus sandwich electrodes). In addition, deMello et al. argue that as the device is quenched in order to perform the OBIC experiment, non-equilibrium distributions of ions occur because the ionic mobility is less than the electronic mobility.

Although the deMello theoretical arguments are compelling, conclusive experimental evidence is currently lacking.

A recent contribution to this discussion has been made by Riess,[53] building on his earlier work in the area of mixed ionic electronic conductors (MIEC's).[54-56] In this paper, he calculates the electron, hole, and ion distribution in the film assuming local electroneutrality. Significantly, the assumption of no internal field within the device seemed to hold true when these equations were applied to Heeger's data. This result supports the idea that under standard conditions the space charge drops mainly at the interfaces so the remnant voltage within the device is quite small. I will make use of his criteria for the validity of local electroneutrality in Chapter 4 when discussing the field in our devices.

The most recent input in this debate is a following paper from Smith and Heeger in which electroabsorption measurements and capacitance measurements were made on operating cells to measure the internal electric field and p-n junction width. According to these experiments, the electric field rises dramatically in the device after the turn-on voltage is reached. This rise is accompanied by an increase in the capacitance. The authors argue that the capacitance shows a narrowing of the separation of charges due to the formation of an internal junction in the device. Friend and coworkers have not yet had an opportunity to respond, and they have not yet treated the case for high injection levels. In their brief comment they report that the electric field would then increase within the device when injected charge begins to compensate ions in the film. It seems that the most definitive experiment would be one in which the resolution would be sufficiently large to localize the electric field within the device and to determine whether it its centered in the middle or falls as a gradient over the entire film.

The point of significance relative to this current work for all of these papers is the distinction (or lack thereof) between the operation of PPV devices and the more traditional electrochemical cells, such as the ones I have studied. If the mechanisms are sufficiently similar, the body of theoretical work on charge and potential distribution in the solid state can be applied to ruthenium systems as well as semiconducting polymers. According to statements by Murray and Bard,[44] a similar origin of device operation seems likely. However, the additional band-like component to the electronic conductivity of PPV does seem to cause some differences in device behavior. It is my hope that this work will serve to help bridge the gap between the understanding of charge transport in redox active polymers and the mechanisms of thin film electrochemically active light-emitting devices.

3. Thin Film Processing and Experimental Procedures

This chapter outlines the processes I used to make the samples tested for this thesis work, giving particular attention to a relatively new approach developed in our group involving the layer-by-layer adsorption of polyelectrolytes. A brief description of the testing protocol is given for the various characterization methods I used to test the devices. All of these measurements were acquired using automated data collection software that I wrote or substantially modified in the process of this work.

3.1 Device Fabrication

3.1.1 Typical Device Architecture

The standard devices fabricated for this thesis were simple sandwich structures consisting of 3 mm lines of ITO patterned onto a glass substrate, a film of one of the ruthenium complexes, and a 2 mm wide top electrode, generally aluminum. The active area of the sample was defined by the intersection of the two electrodes. A schematic of this structure is given in Figure 3-1:

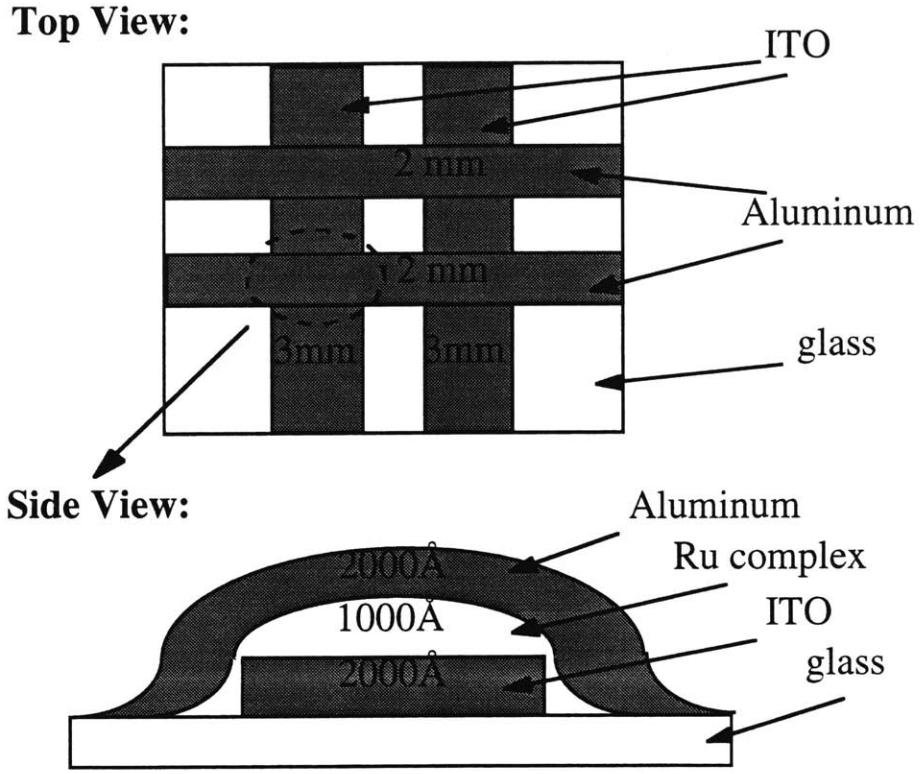

Figure 3-1. Schematic of basic device architecture. The ruthenium complex is deposited either via spin-coating from solution or by the layer-by-layer deposition of polyelectrolytes. Typical dimensions for each component are given in the figure.

Other electroactive materials were used to modify either the ITO or aluminum interface in some studies. In general, however, the total electroactive material between the two electrodes was between 1000Å and 2000Å thick.

3.1.2 Materials

All of the redox active materials examined in this thesis were synthesized by either Jin-Kyu Lee or Erik Handy in our group. Details of the synthetic procedure have been outlined elsewhere.[1-4] In general, they are analogs of the ruthenium(II) trisbipyridine compound studied in such great detail in the literature (see references in Chapters 1 and 2). The synthetic modifications have focused on additions to the ligands to allow for the formation of polymers with the ruthenium centers in the backbone. All of the ruthenium(II) materials are salts, with a native 2+ charge on the ruthenium atom at the center. To satisfy the charge, various counterions have been used, primarily Cl- for the aqueous solutions, and PF_6- for the organic solutions.

The structures of some of these materials are given in the following figures. These complexes include: a trisbipyridine ruthenium(II) with diols pendent to one of the three bipyridyl groups (A); a trisphenanthroline ruthenium(II) with phenyl rings and sulfonate groups pendent to all three ligands (B); a polyester with the diol reacted with an olefinic diacid to form an oligomer of 5 to 7 repeat units per chain (C); and a polyurethane with a higher molecular weight of approximately 10 repeat units (D). Many other analogs were synthesized in the course of research by Handy, but the resulting device performance is not summarized here.

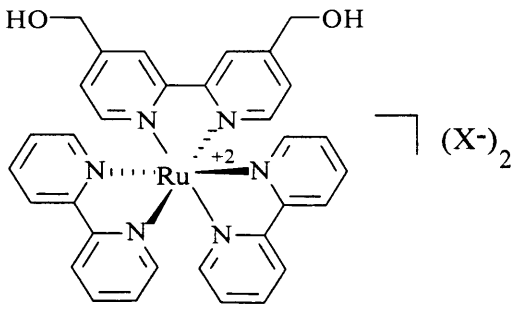

A.

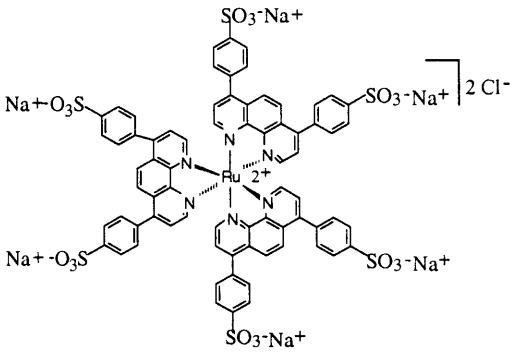

B.

C.

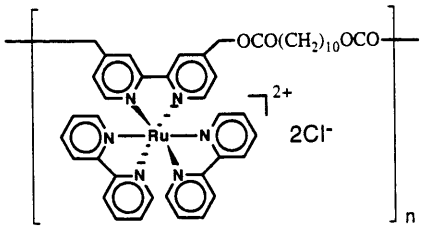

D.

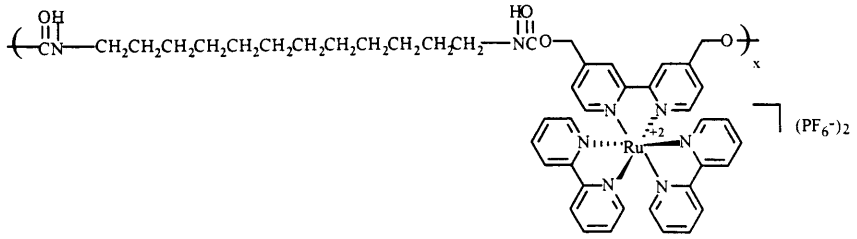

Figure 3-2. The four ruthenium-based complexes used in this thesis. A. Trisbipyridyl ruthenium(II) diol. B. Sulfonated trisphenanthroline ruthenium(II) C. Trisbipyridyl ruthenium(II) polyester. D. Trisbipyridyl ruthenium(II) polyurethane.

For the layer-by-layer deposition process described in the next section, polyanionic materials were required. The two materials most commonly used were poly(acrylic acid), a weak acid, and sulfonated poly(styrene), a strong acid. Early work for this thesis was done with poly(methacrylic acid) but the results were similar to those of PAA, and PAA gave more reproducible results. To increase film adhesion to the substrate, a single layer of poly(ethylene imine) or a bilayer of poly(allyl imine hydrochloric acid) with PAA was sometimes deposited. The SPS, PAH, and PEO polymers were purchased from Aldrich, and the PAA, PMA, and PEI polymers were purchased from Polysciences. All were used without further purification.

Sulfonated Poly(Styrene) [SPS]

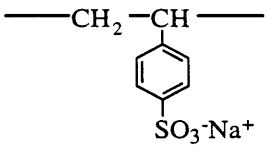

Poly(Acrylic Acid) [PAA]

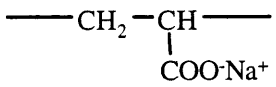

Poly(Ethylene Imine) [PEI]

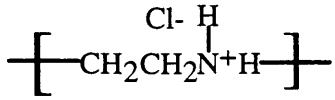

Poly(Allylamine Hydrochloride) [PAH]

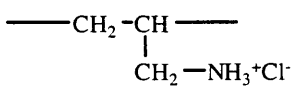

Figure 3-3. Insulating polymers used in the film deposition of the ruthenium complex films or to aid in film adhesion to the substrate.

In the electrode modification studies, a variety of conducting and semiconducting polymers were used. These polymers included poly(para-phenylene)+, poly(para-phenylene)-, poly(aniline), poly(pyrrole), and poly(para-phenylene vinylene). The PPP polymers were obtained through a collaboration with John Reynolds at the University of Florida. The polyaniline was synthesized in house by Jeff Baur. The patterned poly(pyrrole) electrodes were furnished by Dr. Shashidar at the Naval Research Laboratory in Washington, D.C. The PPV solutions were purchased from Lark, although early work was done with PPV from a collaboration with Bing Hsieh at Xerox.

Poly(Aniline) [PAni]

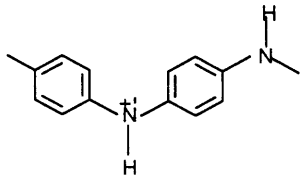

Poly(p-Phenylene Vinylene) precursor[pPPV]

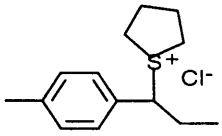

Poly(p-Phenylene) [PPP+, PPP-]

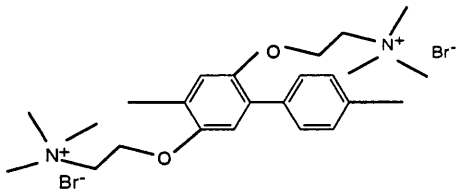

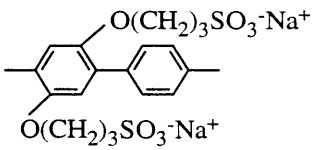

Figure 3-4. The semiconducting or conducting polymers used for studies of charge injection or heterostructure formation.

Solvents used for the spin coating of the ruthenium molecules were primarily 2-methoxyethanol for the Cl salts and pyridine for the PF_6 salts. The 2-methoxyethanol was purchased from Aldrich; the pyridine was purchased from Mallinckrodt. Both were used without further purification. The ultrapure water used in the layer-by-layer dipping process was purified with a Milli-Q filtration system to 18 Mohms resistance. The pH of the solutions was adjusted using either a 1M HCl solution, diluted with Milli-Q water from concentrated HCl from Mallinckrodt, or NaOH from Mallinckrodt.

3.1.3 General Principles of Layer-by-layer Deposition

Some of the samples studied in this thesis were prepared by a novel process consisting of the sequential adsorption of polyelectrolytes. This process was proposed by Decher [5-7] and investigated in depth by our group.[4, 8-12] In this procedure, a charged substrate is dipped into an aqueous solution containing a polyelectrolyte of opposite charge.

The polymer spontaneously adsorbs onto the substrate due to the Coulombic attraction of the opposite charges. Due to the high entropy of the polymer chain, some of the charges along the backbone will bind to the substrate, but some will also be present at the surface and effectively change the charge on the substrate. The substrate can then be rinsed vigorously to remove any polymer that is only physically entangled, and the remaining sample will then retain one layer of polymer ionically bound to the surface. The sample can then be dipped into a polyelectrolyte solution of opposite charge and the entire process repeated. According to studies done in our group, the adsorption process is self-limiting over time. After approximately 10 minutes in the solution, equilibrium is reached and no further buildup is observed.

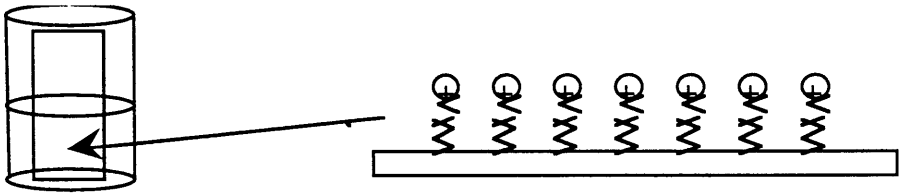

1. Substrate Pretreatment

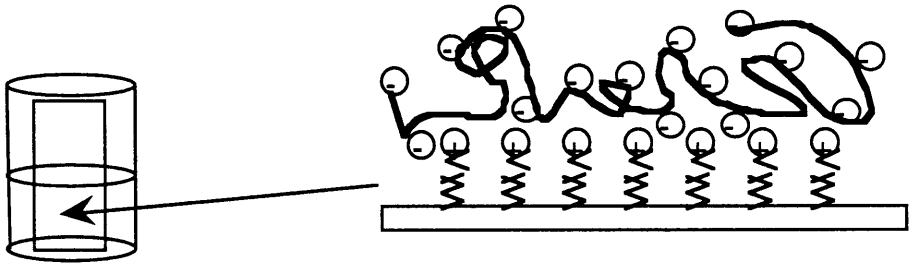

2. Adsorption of Polyanion

3. Rinse

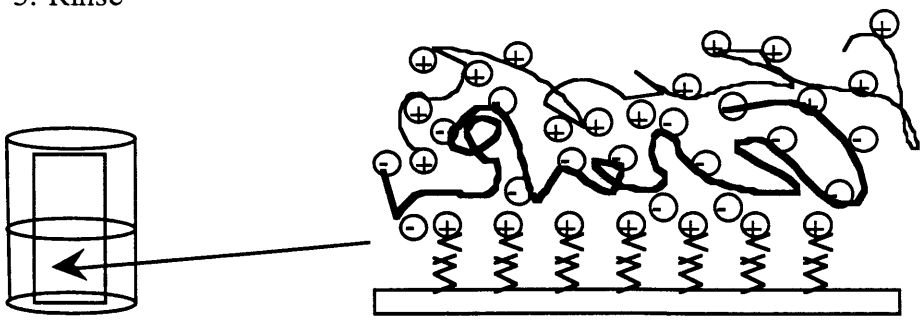

4. Adsorption of Polycation

5. Rinse

Figure 3-5. Steps for the absorption of polyions onto a substrate.

The thickness of the polymer layers can be controlled through adjusting the pH and the ionic strength of the polyelectrolyte solutions. This process can be understood through charge shielding effects. The pH of the solution is a measure of the equilibrium constant between charged ionic groups on the polymer and associated salts. With a high density of charge along the backbone, the charges along the polymer repel each other and tend to force the polymer into a more extended configuration. This condition will create a very flat, thin polymer layer that will mix closely with the next layer. If more of the functional groups on the backbone are in their neutral form, the polymer takes on a more coiled configuration due to entropic considerations. The resulting layer will be thicker and have many loops and tails extending into the solution that can still intermingle with the next polymer layer that is deposited.

Similar effects occur due to the ionic strength of the solution. When the polymer is surrounded by a large number of mobile ions (such as Na+ or Cl-) the small ions serve to shield the charges on the polymer backbone from each other and the chain contracts. However, with fewer ions present in the solution, the chain will again extend. These factors effect the overall thickness of a monolayer. A typical bilayer system (one polyanionic and one polycationic layer) can range in thickness from 5Å to as many as 100Å per bilayer, depending upon the amount of salt in the system and the pHs of the different solutions. None of the films considered in this thesis contained excess salt beyond that required to adjust the pH of the polymer solutions.

In addition to the thickness of the layers, the relative interpenetration of one layer with another can also be varied with solution parameters. In general, the polymers will attempt to maximize the number of polymer-polymer contact ion pairs such that all of the small counterions present in the solution (Na+ and Cl-) will be displaced. Ionic conductivity measurements of around 10^{-11} to 10^{-12} S/cm^2 confirm a very low level of residual ions in the multilayer films.[11] The high level of polymeric mixing is extremely important in determining the percolation pathway for charges through these films. Through varying the relative thickness of each layer, the average site-to-site distance between redox species can be changed on the angstrom level.

3.1.4 Demonstration of Sequential Adsorption in Redox Active Polymers

The sequential adsorption of the electroactive polyelectrolytes used in this thesis has been previously demonstrated by other researchers in our group,[8, 10, 13] excepting only the ruthenium(II) bipyridyl polyurethane. The growth of this polyurethane material has been monitored for this thesis work by UV-visible absorption, and it displays a linear

increase of the absorption peak with the number of deposited bilayers. The data, given in Figure 3-6, is very similar to the resulting curves from all of the other polyelectrolytes studied by our group and demonstrates that an equivalent amount of material is deposited with each completed bilayer. Occasionally the first few bilayers are thinner due to substrate effects, but after separation from the surface, the growth is very reproducible.

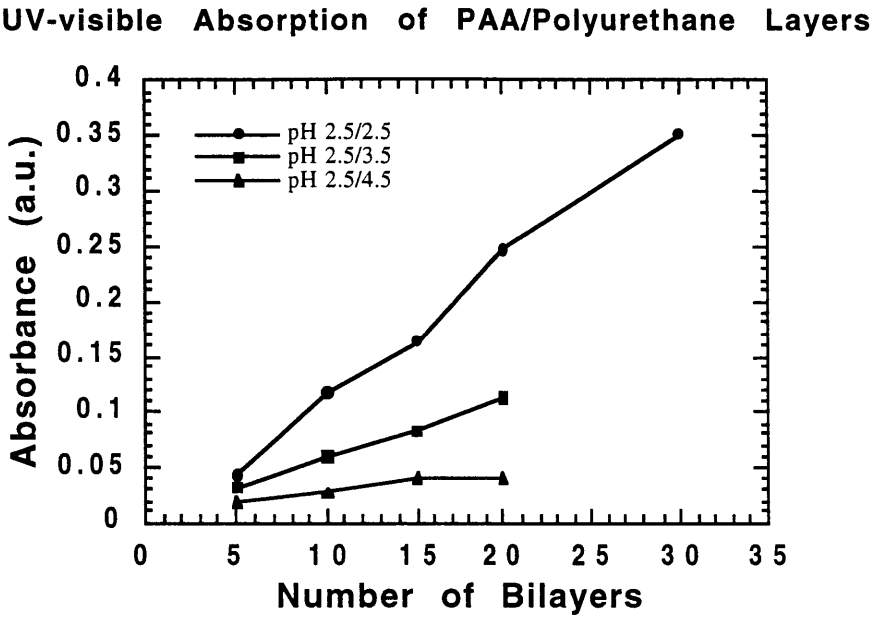

Figure 3-6. The increase of UV-visible absorption with number of sequentially adsorbed layers of the ruthenium(II) bipyridyl polyurethane with PAA.

The growth of the polyurethane with PAA was monitored at pH of 2.5, 3.5, and 4.5 of the PAA solution. As expected, the thickest layers are achieved at a pH of 2.5 where the PAA is less fully charged. This growth is demonstrated in Figure 3-7 where actual thickness data was measured via profilometry. The films deposited at pH 4.5 were extremely thin so that reliable thickness measurements were difficult to obtain. However, the samples at pH 2.5 gave around 90Å per bilayer, and those deposited at pH 3.5 were about 20 Å per bilayer. Some difficulties were encountered in making good quality films of this material. These problems were attributed to incomplete removal of the PF_6- counterions during the metathesis reaction from the as-synthesized polymer to the chloride version. When a version of the polymer was synthesized with initial chloride ions, the material formed very uniform films.

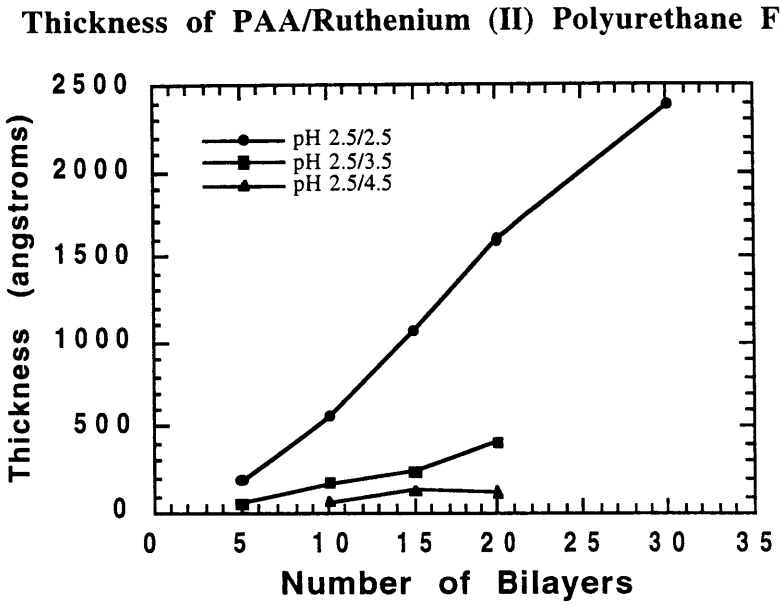

Figure 3-7. Thickness of ruthenium(II) polyurethane layers sequentially adsorbed with PAA. The pH of the PAA solutions were changed; the polyurethane pH was held constant at 2.5. Thicknesses were measured via profilometry; the 5 bilayer film at pH 4.5 was too thin to yield reliable thickness measurements.

Solution parameters for the other materials in this thesis were based on optimized films from other research in our group.[8, 11-13] The summary of the solution conditions are given in Table 3-1. For polyester films, one preparation layer of PAH/PAA was required to get good adhesion to the underlying glass substrate.

	dilution	pH	filter size
PPV	1/500	~5.5	2 μm
PPP+	10-3M	3.5	1 μm
PPP-	10-3M	3.5	1 μm
PAni	10-2M	2.5	0.45 μm
SPS	10-2M	3.5	2 μm
PAA	10-2M	3.5	1 μm
PMA	10-2M	3.5	2 μm
PEI	1%	3.5	1 μm
PAH	10-2M	3.5	1 μm
polyester	10-3M	3.5	0.45 μm
polyurethane	10-2M	2.5-4.5	0.45 μm

Table 3-1. Dipping parameters for the various polymers used in the fabrication of samples tested for this thesis. The effects of these polymer layers are presented in Chapter 7.

3.1.5 Spin Coating

Although some work has been done using the small ruthenium compounds for self assembly, it is difficult to form good films with these small molecules. These chromophores do not have sufficient charges per molecule to ensure adequate anchoring to the substrate. In general, solid-state films of the small molecules have been formed by traditional spin casting of the material from 2-methoxyethanol for the chloride salts and pyridine for the PF_6- salts. Other solvents have been investigated; however, these two solvents gave the most uniform films. The 2-methoxyethanol was supplied by Aldrich; the pyridine was supplied by Mallinckrodt. All solvents were used without further purification or drying. A blend of the small molecule with polyethylene oxide improved the film quality for the phenanthroline complex but did not significantly improve device performance for the diol. Thickness control in this case is determined by both the concentration of the solution and the speed with which the substrate is spun. The samples are then subjected to an annealing step under dynamic vacuum to help solvent evaporation and to achieve better film stability.

The spin coater used was a Headway photoresist spinner. Most films were spun from 4 or 5 wt % solution at 2000 rpm for 50 seconds. The rate of acceleration was not controlled. This combination yields devices between 800 and 1000Å thick. Film thickness was measured on a Tencor P10 surface profiler. Films were annealed for two hours at 110°C which is sufficiently above the boiling point of water to ensure that excess moisture from the atmosphere would be driven out of the film during annealing. Films were then transferred immediately to the thermal evaporator for vacuum deposition of aluminum.

3.1.6 Substrate and Cathode Preparation

The standard substrate cleaning protocol consisted of a one minute etch in 1M hydrochloric acid followed by 15 minute sonication steps in each of the following solutions: 1:3 mixture of Lysol:water, pure Milli-Q water (twice), 111-trichloroethane, acetone, and methanol. The acetone and methanol were purchased sometimes from Mallinckrodt and sometimes from EM Sciences. The 111-trichloroethane was purchased from the Package Chemical Company. All were used without further purification. The substrates were rinsed with pure water between each step and were dried thoroughly before the 111-trichloroethane bath because residual water forms an emulsion in that solvent. Substrates were then air-dried briefly just before film deposition.

Cathode materials were almost exclusively aluminum for the devices tested. Aluminum films were thermally evaporated under a minimum vacuum of 10^{-6} torr. Early samples were formed with a resistive tungsten wire heated with an applied voltage of 110

volts for 10 seconds. The majority of samples used a newer evaporator with a tungsten boat and a controlled deposition rate of approximately 10Å per second. These later samples showed none of the scorching occasionally exhibited by the first deposition process. In addition, a quartz crystal monitor allowed for reproducible electrode thicknesses of approximately 2000Å, rather than the less precise time and voltage dependent technique.

Platinum was deposited via electron-beam sputtering. In this process, a plasma of hot electrons impinges a platinum target and forcibly ejects platinum atoms from the surface. Deposition occurred at a vacuum level of 8×10^{-7} torr with an argon transport gas at 5 mtorr. The e-beam was at a bias of 1.8 kV for a power of 200W. The deposition was run for 5 minutes.

3.2 Testing Protocols

3.2.1 Current and Light versus Voltage and Time

Room temperature device measurements were carried out in a dry box under a nitrogen atmosphere. Current-voltage, light-voltage, current-time and light-time characteristics were measured using a Hewlett-Packard variable voltage source with a Keithley digital multimeter and a Newport Optics silicon photodiode calibrated to a center wavelength of either 530 nm for PPV (green light) or 630 nm for the ruthenium compounds and heterostructures (red light). Low temperature measurements were done by attaching the sample to a liquid nitrogen coldfinger inside an evacuated Janis cryostat with the photodiode mounted to the exterior window. Temperature was regulated via a resistance heating unit mounted on the coldfinger and connected to a thermocouple feedback loop.

External quantum efficiencies were calculated[11] based upon the amount of light the photodiode captures from the front face of a device using the assumption that the emission is Lambertian. According to calculations by Greenham et al. [14] the total flux leaving a device that is not waveguided, F_{ext}, at a distance L_0 from the detector is:

$$F_{ext} = \int_0^{\pi/2} 2\pi L_0 \cos(\theta)\sin(\theta)d\theta = \pi L_0$$

In our case, the light collected by the photodiode, F_1, is only within the emission angles $\theta = 0$ to 21°, so we integrate only over those limits and obtain $F_1/F_{ext} = 0.1284$. We then divide our measured power output by this factor and use the corrected power, P, in the following formula:

$$\eta_{ext}(\%) = \frac{P/h\nu}{I/e}$$

where h is Planck's constant, ν is the center frequency of the emitted radiation, I is the current, and e is the elementary charge.

3.2.2 Capacitance, Conductivity, and Dielectric Constants

The basic C_p-R_p plots used to determine ionic conductivity and dielectric constants were performed on an HP meter 4284A. Cole-Cole plots were generated, and the diameter of the semicircle was evaluated to determine the resistance of the films at various applied voltages. The instantaneous values for the dielectric constant were calculated using an Excel spreadsheet using the impedance values, Z, and the relation:

$$\varepsilon = \frac{1}{i\omega C_0 Z}$$

where i is the square root of -1, ω is the frequency of the applied oscillation, and C_o is the geometric capacitance of the cell.

Capacitance versus time plots were generated using the same equipment. The HP does not come with a time sweep function. However, by sweeping over a small change in frequency using many points, an effective time axis can be created. The frequency was scanned from 10 kHz to 10,010 Hz in 0.01Hz steps with a time delay between each step. In general, a square wave DC pulse was applied across the sample and a 100 mV AC oscillation was superimposed. Capacitance was observed to decrease immediately upon application of the new voltage, in part due to injection of charge at the interface, and perhaps in part due to the slow polarization response of the material. After the voltage pulse was relaxed, the transient capacitance could be monitored to measure the characteristic time constant for the movement of ions in the films.

3.2.3 High Frequency and Transient Responses

High frequency light measurements were taken using two different experimental setups. To monitor light as perceived by the eye, samples were measured using the Newport Optical silicon photodiode as described above. This photodiode averages over several cycles so the average light intensity is reported. The bias was applied using the HP 4284A meter with an offset DC bias so that the films did not experience a negative bias but were oscillated from 0V to some positive value. The frequency of the voltage could then be scanned using the frequency sweep function on the impedance analyzer.

Short time light transients could be measured with a photomultiplier tube. The signal was obtained by applying a square wave pulse from the HP 3245A function

generator. The output of the photomultiplier was recorded by an HP 54616B digital oscilloscope and downloaded onto the computer for later analysis. Again, devices were not subjected to reverse bias pulses when the high frequency data was being taken.

3.2.4 Automated Data Collection

All of the measurement equipment used in this thesis was computer controlled for data collection. The data collection software was written for these specific applications using the LabView instrumentation language. The preliminary current-voltage and light-voltage control program was written by Augustine Fou in our group. The control panel for the main capacitance testing was written by Michael Durstock. Major modifications to both programs were made as part of this thesis work. In addition, a new program for downloading data from the digital oscilloscope was written and the square wave pulse capacitance protocol was implemented.

4. Charge Injection in Unconditioned Devices

The first step in the process of electrochemiluminescence is the injection of charges into the material which can then be transported to the place where they recombine to create light. As described in the introduction, the general behavior for a light-emitting electrochemical cell, or LEC, requires the movement of free ions to the electrode interface to thin the barrier for injection. Charge transfer then occurs from the metal to the organic molecule. Finally, the electrons or holes must hop away from the electrode to create the mixed valence states in the bulk that allow for further electronic conduction. The limiting steps for each of these processes will be examined using examples from the ruthenium(II) systems that I studied, noting both the general case and exceptions that occur when the material is under additional constraints.

4.1 Charging of the Double Layer

All of the materials examined in this thesis, with the exception of the sequentially adsorbed structures, contain mobile counterions of chloride (Cl-) or phosphorus hexafluoride (PF_6-), which can migrate in the device. Capacitance data was taken in collaboration with Erik Handy on all of these systems and I calculated the dielectric constant and ionic conductivity based upon the magnitude and phase lag of the response of the device to an applied AC voltage. The dielectric constant and the ionic conductivity of these materials are given in Table 4-1 and descriptions of the calculations are given in the experimental section. Conductivities were calculated based upon the resistance of the devices as determined from the diameter of a Cole-Cole plot at zero DC applied bias. The ionic mobilities were calculated based on the assumption of approximately 10^{20} /cm^3 for the ion density. This value was calculated by assuming a radius of the chromophore of approximately 10Å and assigning two ions per chromophore. I also estimated the

	dielectric constant	ionic conductivity	ionic mobility
diol	4.5	1.6 x 10-8	1.04 x 10-9
phenanthroline	2.75	6.8 x 10-9	4.25 x 10-10**
polyester	4.4	4.9 x 10-9	3.06 x 10-10
polyurethane	3.5	2.0 x 10-9	1.25 x 10-10
SA polyester	8.5	8.7 x 10-12	5.4 x 10-13 **

Table 4-1. Values of the dielectric constant and ionic conductivity at 0V applied bias for various ruthenium complexes. See text for details of measurement procedure. Ionic mobility was calculated assuming an ionic density of approximately 10^{20} /cm^3. **This value is a lower limit for the mobility of ions because these films are expected to have many fewer carriers to contribute to the conductivity.

chromophore concentration by assuming a density of 1 g/cm^3, dividing by the molecular weight of the repeat unit, and taking the inverse. For a first order approximation, all of these values of the chromophore concentration were the same order of magnitude.

For devices of these materials, the ionic content should be sufficient to form a reasonable double layer at the interface. If we calculate the required screening length according to Riess, the assumption of local electroneutrality should be valid for ionic concentrations greater than 10^{16} /cm^3, which is well below our concentration.[1] Additionally, based upon calculations done by deMello [2] and Smith [3] for PPV, the double layer should only be between 10 and 50 angstroms thick. This value is dependent upon the ionic concentration in the film, 10^{20} /cm^3 for these films, and is also dependent upon the binding energy between the ions, in our case the small anions and the more immobile ruthenium centers. Assuming the ionic conductivity of the system is representative of the ability of the interface to be polarized, the double layer should form in less than a millisecond when an external bias is applied.

In the sequentially adsorbed systems, we expect that most of the small ions that are present in solution have been displaced by polyion contact pairs.[4] Particularly in the case of the strong acids, such as SPS, very little mobility of the ions should be possible. In the case of the weak polyacids, such as PAA, however, there are situations where some free acid groups remain in the structure. Other groups have demonstrated measurable protonic conduction in PAA films.[5] In addition, recent measurements on PAA and SPS films fabricated with insulating poly(allyl imine hydrochloric acid) have shown that the ionic conductivity with PAA is much higher than that with SPS, so that more small ions may be trapped in the PAA films than in the similar SPS structures.[6] If these mechanisms are active in our films, some of the double layer could be created even in the sequentially adsorbed structures.

4.1.1 Support of Double Layer Formation

Now that the assertion has been made that these films should have well defined ionic double layers, the device dependence on electrode and electric field will be examined. As demonstrated in Figure 4-1 for the ruthenium(II) phenanthroline system, these materials exhibit current-voltage behavior that is generally symmetric both in magnitude and in turn-on voltage. This symmetry indicates that the injection electrode is not important in this regime. The turn-on voltage does not change as device thickness is varied, at least for films thinner than 2000Å; therefore, charge injection is independent of electric field. Alternate electrodes, such as platinum and gold, have been applied and have yielded similar

characteristics. All of these observations are consistent with a traditional electrochemical mechanism of injection as described in the introduction.

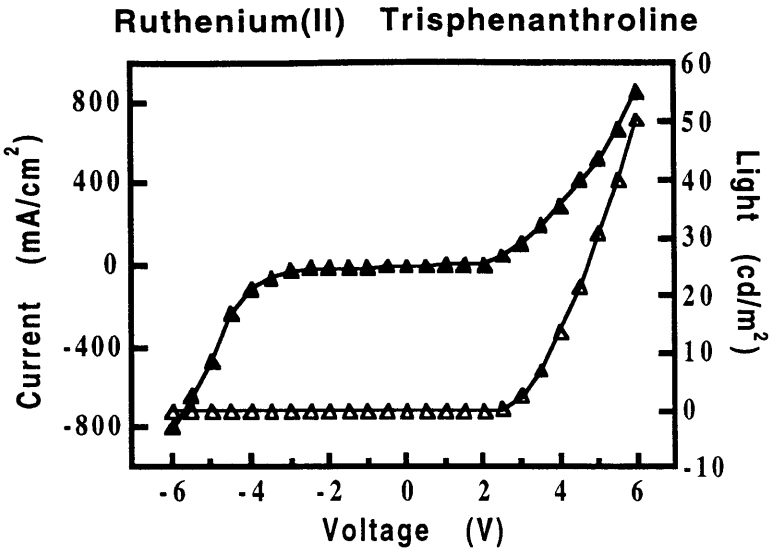

Figure 4-1. A room temperature current-voltage (closed symbols) and light-voltage (open symbols) plot for the ruthenium(II) trisphenanthroline system. The shape of this curve is general for all of the spin-coated ruthenium systems after some preconditioning to bring them to their steady-state behavior. The polymers have a slightly higher initial turn-on voltage.

4.1.2 Complications with the Double Layer

An interesting exception to the observations described in the previous section is the performance of some of the layer-by-layer assembled films. The films composed of large amounts of poly(acrylic acid) (around 50% per bilayer) are consistent with the other materials that I studied and give symmetric device performance as expected from electrochemical cells. The plot in Figure 4-2 B shows fairly ideal electrochemical behavior, with light and current showing symmetric turn-on voltages and similar magnitudes in both forward and reverse bias. These films are expected to have a large number of mobile protons which can contribute to the formation of a double layer.

For the structure assembled with sulfonated poly(styrene), given in Figure 4-2 A, devices show completely rectifying behavior until much higher voltages are reached. This rectification in the current was quite surprising because all of the other ruthenium systems had shown consistently symmetric current. One explanation was that the local environment of the ruthenium centers in the presence of SPS had changed, altering the redox potential

dramatically. The forward bias behavior however was similar to the PAA case, so a change in the injection properties was proposed. This system containing SPS showed a difference in device performance between electron injection from aluminum and that from ITO, so the electrode interface properties were studied.

To test this hypothesis, I fabricated two other device structures with RuP/SPS alternately at the ITO or the Al interfaces, shown in Figure 4-2 C and D. As few as 3 bilayers of the Ru/SPS material at the Al interface cause rectifying device behavior even in a bulk Ru/PAA film that normally allows for symmetric performance. This behavior is consistent with a substantial reduction in the ions available for forming a double layer at the interface of the aluminum, causing a dramatic increase in the barrier to charge injection. The same layers at the ITO interface do not seem to interfere as substantially with charge injection, perhaps because the barrier to injection of electrons from ITO, around 1 eV, is much smaller than the barrier for holes from Al, approximately 2.2 eV (see Figure 1-4).

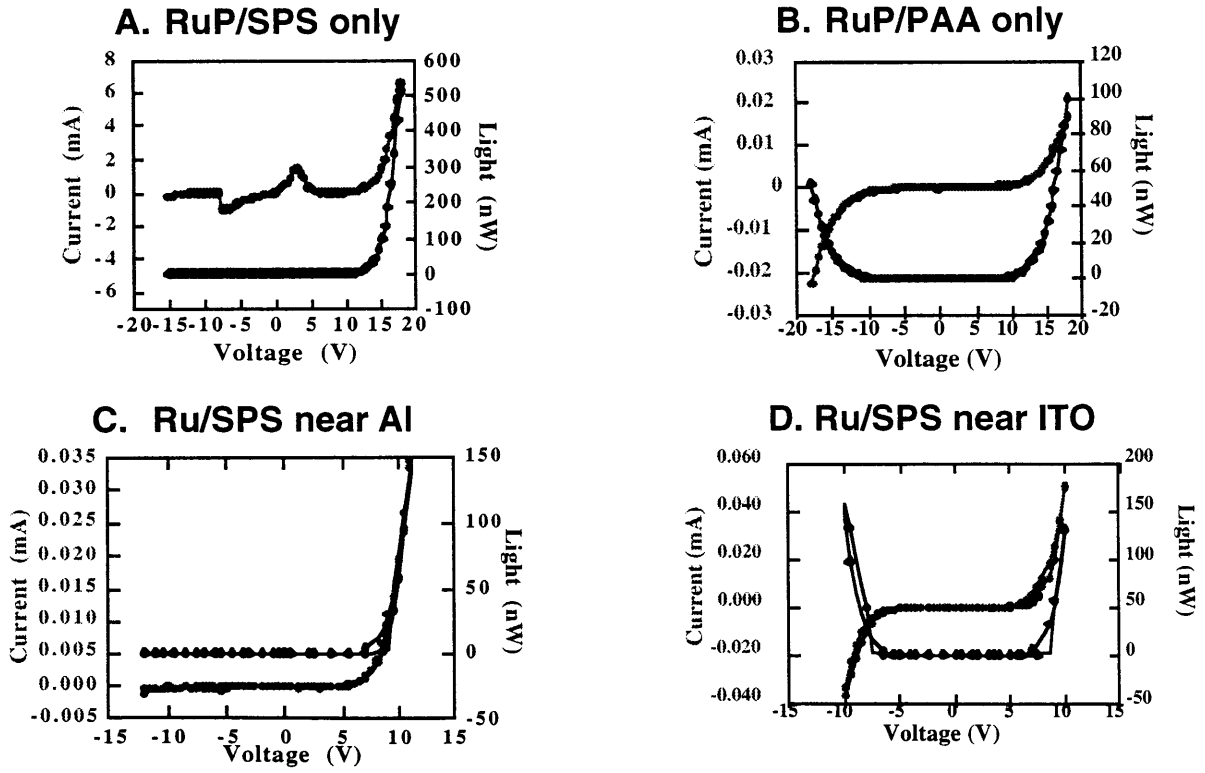

Figure 4-2. The current-voltage and light-voltage plots for layer-by-layer films of the ruthenium polyester (Ru) and poly(acrylic acid) or sulfonated poly(styrene) (SPS). All devices are approximately 1100Å thick. For films C. and D., 5 bilayers of the Ru/SPS system were deposited with 18 bilayers of the Ru/PAA system to probe whether the difference is an interface or a bulk effect.

The creation of rectifying devices by the use of sequentially adsorbed films has also been noted by Neher and coworkers. They ascribe the rectifying behavior to a low concentration of mobile anions in the device compensated by cationic groups immobilized on a polymer. The anions can move to one interface and form a narrow space charge region and a thin barrier to injection; however, the cations cannot move and the space charge at the opposite electrode must then be distributed over a larger area of the film and create a larger tunneling barrier.[7] An analogous process could be happening in our films to break the symmetry of the device structure.

In general the layer-by-layer devices have much higher turn-on voltages than are seen for the same materials in a spin-cast film. According to our band energy picture, this required overpotential indicates less efficient formation of the double layer and therefore a higher barrier to injection at the interface. A higher barrier is also expected for electron hopping in the bulk of the film due to increased separation of the redox centers which would cause a higher potential necessary for conduction. However, the measured current is too low to get a reliable activation energy for these films. Therefore, another way to determine the limitation must be determined. This analysis is given in section 4.2.2.

4.2 Charge Transfer from Electrodes

For standard electrochemical devices, we expect charge injection according to Butler-Volmer theory. Following the notation used by Bard and Faulkner,[8] the appropriate equations are:

$$i = nFA[k_f C_O - k_b C_R]$$
$$k_f = k_0 \exp\{-\alpha nf(E - E^0)\}$$
$$k_b = k_0 \exp\{(1-\alpha)nf(E - E^0)\}$$

where n is the amount of charge transferred in one oxidation or reduction step, F is the Faraday constant, A is the area of the electrode, C_o is the concentration of oxidized and C_R the concentration of reduced species, f is defined as F/RT where R is the universal gas constant and T is the temperature in Kelvin, E_0 is the formal potential of the redox couple. The equations contain two adjustable parameters: k_0 is known as the standard rate constant and α is the transfer coefficient. Note also that this formulation also takes into account the back reaction of charge from the material to the electrode. Back reactions will be particularly strong when charge transport rates are slow; however, they can be negligible for reactions that are injection limited or for large applied electric fields.

In the solution state, the Nernst relation can be used to solve for the concentration of charged species at a given potential:

$$E = E^0 + \frac{RT}{nF} \ln \frac{C_o^*}{C_R^*}$$

where C_o * and C_R * are the concentrations in the bulk of the solution. In the solid state, the concentration of species at the electrode interface will follow this equilibrium for an ideal electrode so that we can substitute the Nernst equation into the previous description of the current. However, for an overpotential, we will get additional charge at the interface above the equilibrium value. The final equation becomes:

$$i = i_0[\exp(-\alpha nf\eta) - \exp((1-\alpha)nf\eta)]$$
$$i_0 = nFAk^0 C_O^{*(1-\alpha)} C_R^{*\alpha}$$
$$\eta = E - E_{Eq}$$

where E_{eq} takes on the value of E in the Nernst equation at equilibrium.[8] p103. In this picture, the rate of injection has an exponential dependence on the applied voltage, or overpotential, and also on the transfer coefficient which describes the symmetry between the forward and back reaction. It is also linearly related to the standard rate constant, which Bard describes as the "idle speed" for the rate of electron hopping back and forth between the electrode and the material.[8] p104.

The current-voltage relationship described by this equation rises exponentially at positive values of the overpotential and falls exponentially at negative values of the overpotential. The value of α determines whether the current will increase at the same rate for positive and negative overpotential, with the perfectly symmetric case falling at α equal to 0.5. This formulation is very specific to only one redox couple so that the potential drives the concentrations of oxidized and reduced species away from the equilibrium values with an increase in one relative to the other. However, until an overpotential is reached, no current should flow because injection cannot occur.

4.2.1 Analysis of Charge Transfer Limited Current in the Polyurethane

The polyurethane system is a good system in which to look for charge transfer limited behavior. When the material first experiences a voltage bias, an overpotential of 7V is required for injection, resulting in a turn-on voltage of approximately 10V. This unconditioned device seems to be limited by injection of current from the electrodes. A good method of determining the extent of injection limitation on device performance is the use of a Tafel plot. The mathematics involved are the same as the Butler-Volmer equation presented above, however, the form of the graph is such that the logarithm of the current is plotted versus the overpotential. At large values of the overpotential, one of the terms (either the forward or back reaction) can be neglected and the equation becomes:

$$\log i = \log i_o - \frac{\alpha nF\eta}{2.3RT} \quad \text{or}$$

$$\log i = \log i_o - \frac{(1-\alpha)nF\eta}{2.3RT}$$

Each of these equations will produce their own lines on the plot and can be extrapolated to zero overpotential, or the equilibrium potential. The intercept of this plot gives the logarithm of the exchange current, i_o, and the slope gives the value of the charge transfer coefficient if the value of the overpotential is known.[8] p106.

In the case of the polyurethane devices, this method is particularly valuable because the exact value of the overpotential is not certain (the formal potential of the polyurethane device is not available for the solid state). In addition, the current is a combination of the forward and back reactions of two separate redox couples, each with their own value of the overpotential. However, if the data is plotted with respect to the applied voltage, the equilibrium potential can be estimated from the crossing point of the two branches of the Tafel plot. The value of the redox potential serves only to shift the values of the x-axis and does not interfere with the determination of the charge transfer constant from the slope of the curve. This type of graph is shown in Figure 4-3.

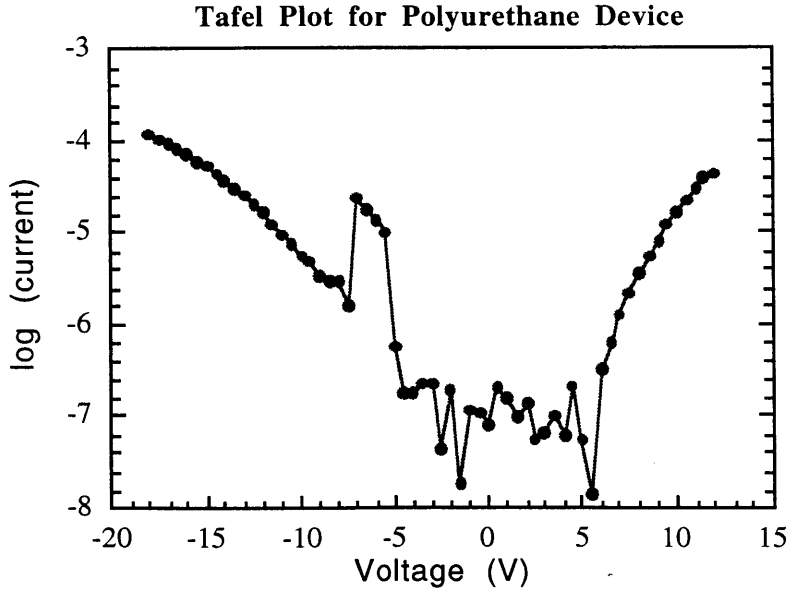

Figure 4-3. Tafel plot for a polyurethane device measured at room temperature with a linear sweep. The random noise in the data between -5V and 5V indicate that back reactions are significant in that regime. The slopes at large overpotential (>5V) are used to calculate the charge transfer constants for this system.

Because these data can be fit to a Tafel plot with a distinct turn-on voltage in forward and reverse bias, injection limitations can be investigated. Each branch of the plot can be analyzed separately and fit to a straight line. The charge transfer numbers are then calculated from the slope of this line, following the equation given above. The transfer constant accounts for the fact that the current does not increase as quickly as expected for an ideal redox process. The numbers for the polyurethane system are exceptionally small, generally less than 0.01 on a scale of 0 to 1, where 0.5 would be a perfectly symmetric reaction. This very small value of the charge transfer number indicates that back reactions to the electrode are quite strong so that even higher overpotentials are required to drive the forward reaction away from the metal electrode. Therefore, the system does not appear to be limited by charge transfer from the electrodes. The transport of charge away from the interface is not fast enough to prevent significant back reactions from occurring.

4.2.2 Charge Transfer in the Layer-by-Layer Polyester

When the same analysis is applied to the layer-by-layer system, the results are similar to the polyurethane case. Almost no current is seen until extremely high overpotentials, even after several voltage sweeps. The Tafel plot for the polyester is given in Figure 4-4. Unlike the polyurethane, the layer-by-layer films never succeed in charging sufficiently that the voltage drops close to the redox potential. The increased distance for electron hopping due to further dilution by the insulating PAA is expected to contribute to this overpotential. This hypothesis is supported by the very small charge transfer number obtained from the Tafel plot. As in the case of the polyurethane, back reactions are very strong, and therefore the high barrier to charge transport impedes the injection of charge into the device.

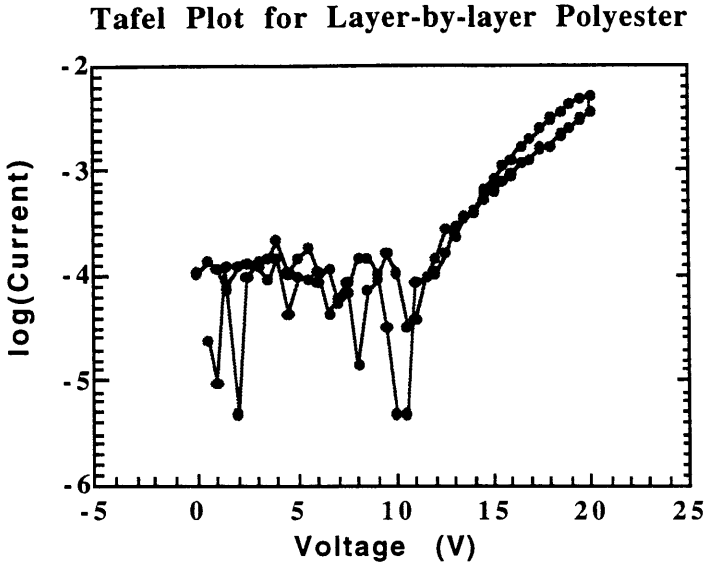

Figure 4-4. Tafel plot for the layer-by-layer polyester film fabricated with PAA. Back reactions are clearly important until very high potentials, around 12 V. This system is severely injection limited, especially on the first measurement sweep, represented by this curve.

4.2.3 Charge Transfer in Other Systems

Analysis of our current data from other systems using the Butler-Volmer equation is difficult because our values are the combination of injection from two interfaces and the equilibrium between two separate redox couples. In addition we do not use a reference electrode, so the potential drop at each interface is not controlled. These factors make the determination of the value of the overpotential difficult. If a Tafel plot is created, plotting the logarithm of current versus applied voltage, current is seen to rise immediately upon application of any bias, meaning that no overpotential is necessary. In addition, a secondary turn-on occurs that is finally accompanied by light emission. This type of voltage response is not predicted by injection-limited behavior and requires a more complicated analysis than the one considered here. Another complication is that even when the first current is ignored and the second part of the current analyzed, the value of alpha must be made extremely large or small to fit the data. These constants are no longer physically meaningful, and therefore must not be adequately describing the behavior for these other systems.

4.3 Insulator/Conductor Transition

The next step in the development of light and current in these films is the transition from a fully 2+ insulating state to a mixture of 3+/2+ and 2+/1+ redox couples. This process is highly time dependent and causes a slow rise in current and light over time, also known as "charging." This charging causes the current-voltage curves to exhibit large hysteresis, particularly during the first several scans. A typical current-time and light-time plot for device operation close to the redox potential is given in Figure 4-5. The current increases over several minutes, then decreases again. Light then increases slowly, reaching a maximum after approximately 10 minutes, accompanied by a second increase in the current. The characteristic times required to reach maximum light and current vary with the precise material and the applied voltage, but all systems exhibit this type of slow light and current rise. In general, increase in current is a result of either an increase in the flux of charges through the device or an increase in the area available for conduction at a constant flux. We note that devices often exhibit a speckled appearance so that the light emission is not completely uniform, consistent with an increase in the area of conducting material with time. The increase in conduction is characteristic of the formation and growth of percolation pathways in the device.

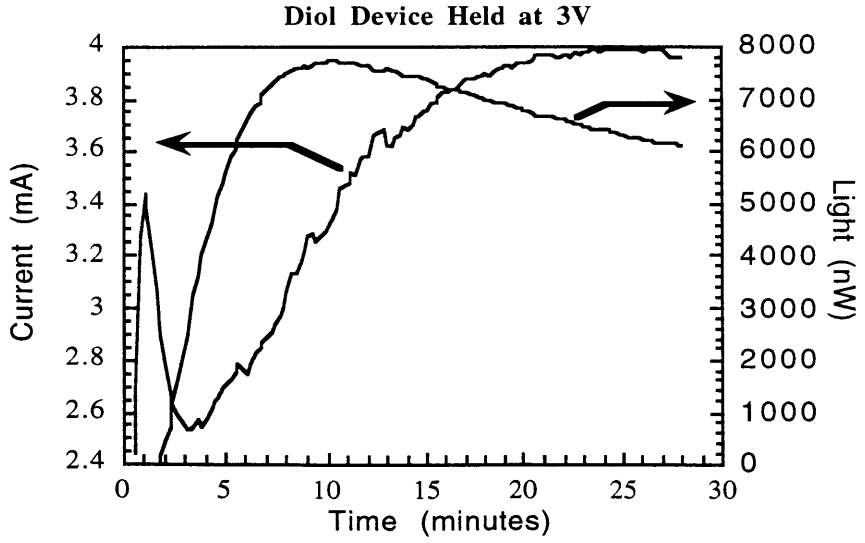

Figure 4-5. The current-time and light-time behavior of a diol device ramped to 3V and held. The slow rise to maximum brightness is characteristic of these films, although the time required varies with the system and with the applied voltage. The double peak in the current is particular to the diol system at low voltages.

4.3.1 Redox Switching

The nucleation of preferential charge transport pathways has been seen in conducting polymers such as poly(aniline) and poly(pyrrole) that become electrochemically doped under applied bias. In a mechanism known as "redox switching", the material reversibly converts from an insulating material to a conducting one. Aoki et al have studied this process in depth and have suggested the following theoretical framework.[9, 10] Due to the high electric field at the interface, a shallow interfacial layer of material becomes oxidized (or reduced). Small inhomogeneities within the film then cause nucleation of percolation pathways that also become oxidized. Because of the conducting nature of these regions, they no longer support a voltage drop, and the electric field at the end of the pathway becomes much larger. This increased electric field becomes a driving force for growth of the conducting region until it reaches the other electrode. The further oxidation of material is then perpendicular to the axis of the conducting fibril until the fibrils connect.

The end result of this physical picture is a curve reminiscent of the one given in Figure 4-5. Applying the Aoki theory, we can interpret it in the following manner. If the initial charge transport is fairly slow as the pathways are being generated, the concentration gradient of redox species at the interface will be very steep. Because the charge flux is directly proportional to the concentration gradient, the current will also be very large. As the pathways connect through, the transport becomes much faster, and the concentration gradient will decrease again causing a concomitant drop in current. The entire process is dependent upon the applied voltage because a higher voltage will cause a higher driving force for the nucleation of percolation pathways, as well as a faster growth rate. The time to maximum current will also be dependent upon the thickness of the film because the concentration gradient will remain high until the full pathway is formed across the entire device.

The mathematical equations to describe this process proposed by Aoki et al. have been reviewed by Lyons.[11] p64. The basis is the Butler-Volmer equation for charge transfer. The concentration of charged species propagates linearly through the film with a speed v limited by the charge transfer speed. This yields an equation for the change of charged species "b" with time:

$$\frac{\partial b}{\partial t} = \frac{\partial v}{\partial x}(C_O + C_R)$$

which becomes:

$$\frac{\partial b}{\partial t} = -\lambda \frac{\partial b}{\partial x}$$

where lambda is:

$$\lambda = k_p \exp(\alpha\vartheta)[1 + \exp(-\vartheta)]$$

$$\vartheta = \frac{nF}{RT}(E - E^0)$$

The constants in this equation are remnants of the Butler-Volmer formulation, where E is the applied potential, E_o is the formal potential of the redox couple, F is the Faraday constant, R is the molar gas constant, n is the amount of charge transferred in one oxidation or reduction step, α is the charge transfer constant, and k_p is a new constant related to the rate of propagation of the pathway through the film. This differential equation is different from Fickian diffusion because both distance and time have first order dependencies in this case. This change in the equation is a result of the fact that the driving force for charge movement is no longer dependent upon the concentration but on the applied field instead. The equation can be solved for b, and current is then given by the integration of b over x and the differentiation of the result with respect to time.

Two cases must then be considered: before and after the charge front has reached the outside of the film, at thickness L. These constraints yield two equations for the current, and the crossover point between them is where $t_c = L/\lambda$. Here the current goes through a maximum, and the time to reach this point is described by:

$$\ln t_c = \ln\left(\frac{L}{k_p}\right) - \frac{\alpha nF}{RT}(E - E^0)$$

if we assume we are well above the redox potential of the material.

Current-time plots of the ruthenium complexes in this study are analyzed as a function of voltage according to the equation for the critical time to form a full percolation path. A typical plot is given in Figure 4-6 and is fit to the equation given above. These materials show the characteristic ln(time) dependence of the percolation on the applied voltage. A similar trend is seen if we plot the same data for varying film thickness, another prediction of this theory. From the linear fits, the charge propagation rate and the transfer coefficient can be determined.

These concepts of the formation of separate pathways for the oxidized and reduced couple could serve to explain why the efficiency of the devices often rises quickly at short times. If the nucleation of pathways is slow relative to the growth, a few pathways will quickly cross the film without having a chance to intersect. These conducting paths will contribute to leakage current but will not produce light. As the number of pathways increase, the likelihood that the oxidizing and reduced species will meet increases. Recombination can then take place. This process results in an increase in efficiency as more of the current is transitioned to useful light emission.

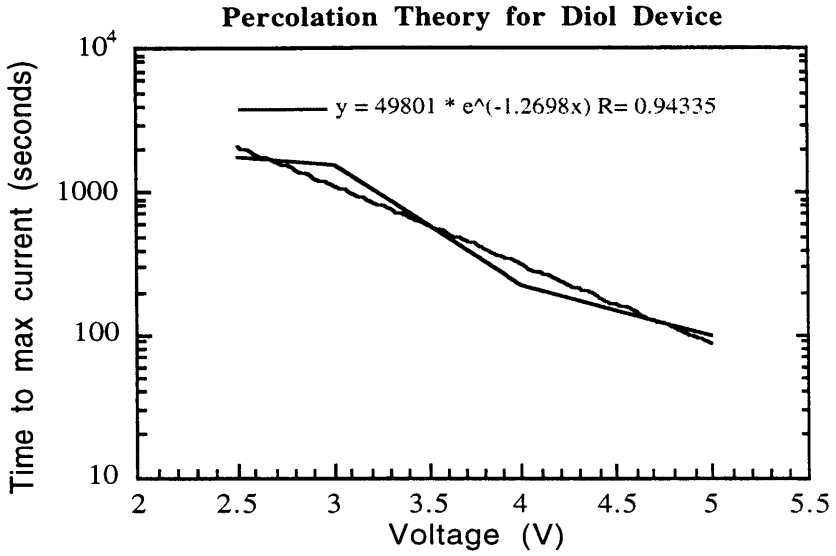

Figure 4-6. Logarithm of the time to reach maximum current versus voltage applied to a diol device. For the redox switching theory due to Aoki, this plot should be linear. Similar analysis has been done on the polyurethane devices.

However, some aspects of our data do not fit this mathematical framework. One major consideration is that the fall in current for most materials after the peak is realized is a much slower decay process than would be predicted by the theory. In addition, studies by Handy that involved charging a device, discharging it, and then charging it again have shown that the current does not reach the same magnitude of the peak current the second time, although the time to reach the maximum is similar. This implies that the slow drop in current has a substantial degradation component and may not be due to the reversible process described by Aoki.

Redox switching theory also predicts that the time required to convert the device to a conductor will depend upon the rate of nucleation of pathways at the electrode interface. Therefore, an increase in the nucleation sites should increase the charging rate. One way to increase nucleation sites is to provide more inhomogeneities in the electric field so that the device will have local "hot spots." This goal can be accomplished by a roughening of the electrode interface or by the addition of particles at the interface to create local regions of high field strength. Samples have been made using ITO etched in hydrochloric acid which

can cause a roughening of the ITO surface. Although these samples had much higher efficiency, they did not show an appreciable difference in charging time. Other explanations for these results need to be examined.

4.3.2 Evolution of the Internal Electric Field

An alternative interpretation of the observed rise in current involves the changing nature of the internal electric field in the device. When the voltage is first applied, the ions at the interface move quickly to reduce the internal field. As the barrier to injection is lowered, redox species at the interface can become oxidized or reduced, partially compensating the mobile ions and causing more ions to move. If the concentration and mobility of the ions is high enough, the internal field can be completely canceled and the voltage will drop only across the interfaces. However, if the concentration of ions is too low or they are slow moving, a remnant electric field will be present in the interior of the device.

From the data presented in Chapter 5, the sweep rate for our current-voltage scans is generally fast enough to preserve an internal electric field. However, for the current-time measurements such as Figure 4-5, the magnitude of the internal field is not well known. The current through the device will be driven by both a concentration gradient and any remaining voltage gradient. If we assume that the change of current is due to a changing electric field, we can describe the way in which the internal field must change. Analysis based upon this premise has also been done by deMello for PPV films.[2]

At the shortest times, an instantaneous current followed by a fast decay is expected. This reflects the charging of the capacitive double layer. This charging must happen very quickly in the ruthenium(II) systems, within approximately one second, because it has not been observed in any of our measurements. The current then begins a rise which is dependent upon the applied voltage as noted above. deMello assigns this increase in current to a decrease in the impedance of the interface as ions continue to move and thin the barrier to injection. The current in this regime is then a combination of voltage-gradient and concentration-gradient driven components because the electric field has not yet been fully nullified. The maximum current should then be limited by the maximum concentration gradient that can be created in the material. Finally, the slow decrease in current would be due to a decrease in the electric field as ions continue to move and reduce the internal field but can no longer contribute to the injection of new charges.

Because the movement of the ions is an activated hopping process, much like the charge transport in this system, the ionic diffusion is exponentially dependent upon the applied voltage. It will also be dependent upon the thickness of the film, because the

driving force on the ions is a function of the voltage gradient, not just the applied voltage. However, this theory does not give any reason that the devices should be non-uniform and does not suggest why the efficiency should increase with time.

Because both this explanation and that of redox switching are dependent upon the motion of ions, they are difficult to distinguish by changing the nature of the ion, the temperature, or the applied bias. They also both predict a changing electric field with time as conducting regions increase and ions move within the sample. However, redox switching predicts a non-uniform growth that is dependent upon nucleation sites. Preliminary attempts to create nucleation sites did not change the growth rate, but observations of devices show very non-uniform charging behavior. More information about the system is necessary before either explanation is completely eliminated.

4.3.3 Double Peak Behavior

Returning to Figure 4-5, two current increases are noted, an initial current peak at short times, followed by a slower rise at longer times. This short time peak could be interpreted as capacitive charging of the device as ionic motion slowly increases the polarization of the material. However, the ionic charging of the interface is expected to be much faster than the characteristic time scale of the first peak, and the total charge calculated by integration under the curve is two orders of magnitude larger than the total quantity of ions in the device. Remembering then that we in fact have both the 3+/2+ and the 2+/1+ redox couples formed at different electrodes, we anticipate that charge transfer from one interface may precede the other, resulting in two populations with different time scales. The first peak may then be assigned to a first wave of charge that forms pathways through the film but does not result in light emission.

The second peak, however, must involve transport of charge through the entire device by both species, because the increase in current is accompanied with a similar increase in light. The double peak has been observed only in low voltage tests, around 2.5 or 3V, before substantial injection of the oxidized species is expected. All of the small molecules show some amount of this short time rise and then decay. Not much data on the polyurethane system is available at these low voltages because of the long charging time it requires; however, the scans that were recorded have some hints of this short time current decay and delay in light onset. At higher voltages, simultaneous injection is expected, and only one peak is seen that is tracked by the light output.

5. Charge Transport in Conditioned Devices

Once ruthenium complex devices have been conditioned to organize the conducting pathways, charge transport becomes limited by the rate of homogeneous charge transfer, or electron hopping between redox centers. As will be demonstrated in this chapter, this charge transfer process can be quite fast, allowing for light emission at higher frequencies than in other organic materials such as PPV. The basic equations that were described in the introduction to describe the flux of carriers through the systems are used to fit the experimental data, and effective diffusion constants and activation energies are determined. These constants can be reliably compared among the four different systems to identify which materials characteristics that have the biggest impact on final device performance.

One caveat in the analysis of the data is the fact that the equations were developed for a single redox couple, i.e. either the 3+/2+ or the 2+/1+ set. In these films, all three valence states must be present to allow for light emission. Therefore, analysis of films in the forward bias under normal conditions will yield materials constants that are a combination of both reactions. However, if the time and temperature dependence of the electroluminescence is of primary interest, as it is in the application of these materials, this combined diffusion constant is the important factor. The remaining caution is that comparison of these values against those in the literature is not completely valid without further experiments to deconvolute the contributions from each redox couple.

A second caveat is that the flux of charge is driven by two forces: the applied voltage gradient, and the concentration gradient set up during the conditioning process. Murray's group has shown that the rate constants for a given material are the same, regardless of whether concentration or voltage gradient driven,[1, 2] so both driving forces must be considered. The separate contributions from each gradient are somewhat easier to deconvolute than the contributions from the multiple redox couples described above. Because the general mode of operation for the most samples is to be driven at large overpotentials, the voltage gradient is generally much larger than the internal concentration gradient. The resulting current can then be analyzed as pure voltage gradient driven transport fairly effectively. These analyses are given in this chapter.

5.1 Theoretical Considerations

5.1.1 Concentration Gradient versus Voltage Gradient driven Transport

The charge transport process is complicated by the effects of two separate driving forces: the concentration gradient of redox species and the externally applied voltage. The

hallmark of concentration-gradient driven current is the appearance of a limiting current, typical of traditional electrochemical solution measurements. In these traditional experiments, the voltage sweep rate is sufficiently slow so that on the time scale of the measurement the counterions have time to redistribute under the applied bias. The electric field within the device remains zero, and the applied bias serves to set up the equilibrium concentration of redox species at each interface. The highest current available under these conditions occurs when the concentration gradient has reached a maximum; higher voltage merely drops across the double layer. The maximum concentration gradient is generally limited by the concentration of redox centers at the interface. However, in the "ion budgeted" case discussed in the next section, the availability of counterions can be the determining factor. The diffusion coefficient can be directly calculated from the limiting current using the previous equation:

$$J = D_{conc}\frac{\partial B}{\partial x} + D_{elec}\left(\frac{AB}{A+B}\right)\left(\frac{\partial \theta}{\partial x}\right)$$

with the voltage gradient equal to zero. Our films, however, do not show any sign of current-limiting behavior until degradation of the material occurs.

For the voltage-gradient driven case, the mixed-valent species are randomly distributed throughout the device. The current then depends solely on the voltage because no concentration gradient is present. Therefore the current does not reach a limit until the material begins to break down under the applied voltage. If the current versus voltage data is fit to a single exponential, the diffusion coefficient for electron hopping can be calculated from the prefactor of this curve. This type of measurement is difficult to do in solution systems because the voltage sweep must be fast in relation to the diffusion time of the ions so the internal electric field can be preserved.

An estimation of more rigorous diffusion constants that can be compared with literature values can be done by making a few assumptions. The carrier flux is a linear superposition of the voltage and concentration gradients. If we assume that half of the voltage drops across either interface, the voltage gradient can be determined. With the same assumption, the equilibrium concentration of oxidized or reduced species can be determined for each interface. The biggest assumption is then that the 3+/2+ and 2+/1+ couples meet in the center of the film where the concentrations of 3+ and 1+ fall to zero. Based on the large conproportionation constant for the 3+/1+ reaction, it is reasonable to assume that the two will annihilate each other whenever they meet. Other arguments based on the limited availability of ions come into play in the assumption that the gradients will meet in the center of the film. These arguments are elaborated in the next section.

5.1.2 Electrochemistry on an "Ion Budget"

Another interesting question for these systems is the role played by the counterions. In a traditional electrochemical cell, local electroneutrality is always preserved so that for every species that is oxidized (or reduced) an anion (or cation) must be present to balance the charge. In most studies found in the literature, the system is made to be mixed valent while in contact with a solution containing an electrolyte of small ions. The film is allowed to equilibrate such that the final film contains an excess (or lack) of ions so the charged species remain charged.

In a few experiments, Jernigan et al. examined a system similar to our case.[3] An electrode was coated with a redox active polymer which was then coated with a porous gold counter-electrode. These devices were submitted to an applied voltage bias in a variety of environments, some of them without the presence of an electrolyte system. The authors found that a standard cyclic voltammogram could be produced with this system, indicating oxidation at one electrode and reduction at the other even in the absence of supporting electrolyte. They note that this dry film differed from the solvent-contacting film in three important ways: an increase in the hysteresis, indicating slower ion movement; an increase in the redox potential required to inject charge; and an increase in the total current injected, indicating faster electron hopping in the dry film. These observations lend support to our findings discussed in this chapter. Additionally, because the only source of ions was the film itself, the system was constrained such that the number of oxidized couples at one electrode was required to be equal to the number of reduced couples at the opposite electrode. Elliot has examined this theoretical case in detail.[4] He has calculated that the recombination zone in the device is constrained to be very close to the center, regardless of the relative hopping rates of the two couples.

These analyses make several important assumptions. The primary assumption is that local neutrality holds everywhere such that the internal electric field in the device is zero. As we have noted earlier, we have sufficient ions in our devices to provide for the conditions of electroneutrality, but we do not sweep the voltage slowly enough to allow for the ions to fully relax the electric field. Elliot states that the attraction of 3+ and 1+ is so great that the conproportionation reaction goes to completion, and the concentrations of charged states fall to zero where the gradients meet. In addition, Elliot assumes that only the first reduction state of the ruthenium molecule is active in the system. As noted above, with the significant overpotential on the currently studied systems, especially in the polyurethane case, it is likely that some Ru^0 is formed. This species would require two anions to preserve electroneutrality and would therefore shift the ion balance.

Another open question is whether we require the motion of ions in our films for device performance. Experiments changing the counterions and the relative ionic conductivity of the matrix greatly affect the rate at which the device charges and the final light output. Therefore, ionic motion must play a large role in optimizing light output.[5] However, performance would follow similar trends if the role of the ions was primarily in charge injection, rather than serving to stabilize species in the bulk of the film. One reasonable interpretation is that the formation of percolation pathways is dependent upon ionic motion as the redox couples are stabilized in the bulk of the film. However, no clear theory is available to describe this process.

If the redox gradients must be coupled to an ionic gradient in the film, then Elliot's analysis applies and the recombination zone must be near the center of the device. However, if this electroneutrality does not hold, the gradients could take on many different forms dependent upon the relative hopping rates of the two couples. Preliminary work has been done in collaboration with Bawendi's group attempting to image the light emission zone in ruthenium films using interdigitated electrodes. These results directly localized the area of recombination within 100 Å of the electrode for a 5 micron film, distinctly not in the center of the device. A representative scan is given in the appendix. Other work described in Chapter 7 on modification to the ITO electrodes is most consistent with a movement of the recombination zone. In addition, the reverse bias charge injection described in the next chapter requires the presence of only one species, in violation of the requirements for charge balance in an "ion budgeted" film. These questions will be further addressed in Chapter 6.

5.2 Data Analysis

5.2.1 Concentration versus Voltage Gradient Driven Transport

Before proceeding to determine diffusion constants, the driving force for charge flux must be determined. Two potential driving forces exist: the concentration gradient and the voltage gradient. If one of the two can be shown to be much larger than the other, the equation and our further analysis can be dramatically simplified. This possibility can be tested by noting the different voltage dependence of the current in the two cases.

In the case of primarily concentration driven hopping, a current limit is expected, such that above a certain voltage the current will no longer increase. Before the maximum concentration gradient is reached, the relative ratios of oxidized and reduced species at each electrode at equilibrium will be governed by the Nernst equation:

$$E = E^0 + \frac{RT}{nF} \ln \frac{C_o^*}{C_R^*}$$

This equation indicates that the concentration at the interface will have an exponential dependence on the applied voltage, or rather the overpotential as given by (E-E°). The current versus voltage curve is then expected to fit to an exponential. In the voltage driven case, however, the gradient and therefore the current will be linear with the applied voltage.

In order to investigate the final dominant driving mechanism, samples must be examined under steady-state conditions so that short- and mid-time injection related effects do not interfere with the analysis. In Figure 5-1, the steady state current for a diol device is plotted versus the driving voltage. The samples were ramped to the indicated voltage and then held until the maximum current value was reached and the current had begun to plateau. As seen from the graph, once the applied bias exceeds the redox gap of the

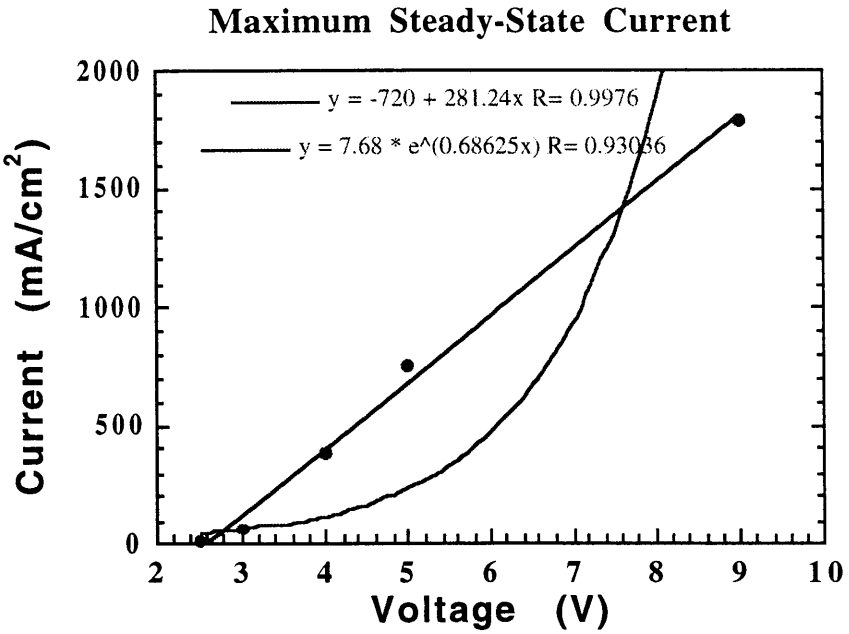

Figure 5-1. Maximum steady state current for a diol device at different voltages. A linear fit shows that the current is primarily voltage-gradient driven. The exponential is given for reference and clearly does not fit well. A different device was used to measure each voltage step. The sample was ramped to the indicated voltage and then held until the current reached its maximum value. Samples at higher voltages either broke down before reaching the maximum voltage or hit the limit of the current meter.

molecule at 2.8V, the current rises linearly. An exponential function fit to the same data is given for reference and clearly does not fit this data well. Further analysis of the films using a voltage-gradient driven model is therefore appropriate.

5.2.2 Determination of Activation Energies

To determine relative diffusion constants and activation energies, the current-voltage (and light-voltage) properties of several small molecule and polymeric ruthenium systems were recorded at temperatures ranging from 80K to 320K. The samples were allowed to equilibrate under voltage at room temperature and then quenched to prevent further motion and to lock-in the established charge transport pathways. Cells were then subjected to a linear voltage sweep from 0V to positive and negative biases at 0.1V/second. These plots were then fit to the theoretical equation proposed by Murray:

$$i = \frac{1}{6}nF(\text{area})dABk_{homo}[\exp(-\frac{\rho nF\vartheta}{2RT}) - \exp(\frac{\rho nF\vartheta}{2RT})]$$

which is the standard Marcus relation for activated electron hopping with an empirical constant, ρ, to account for the slower rise with voltage than expected for the ideal case.

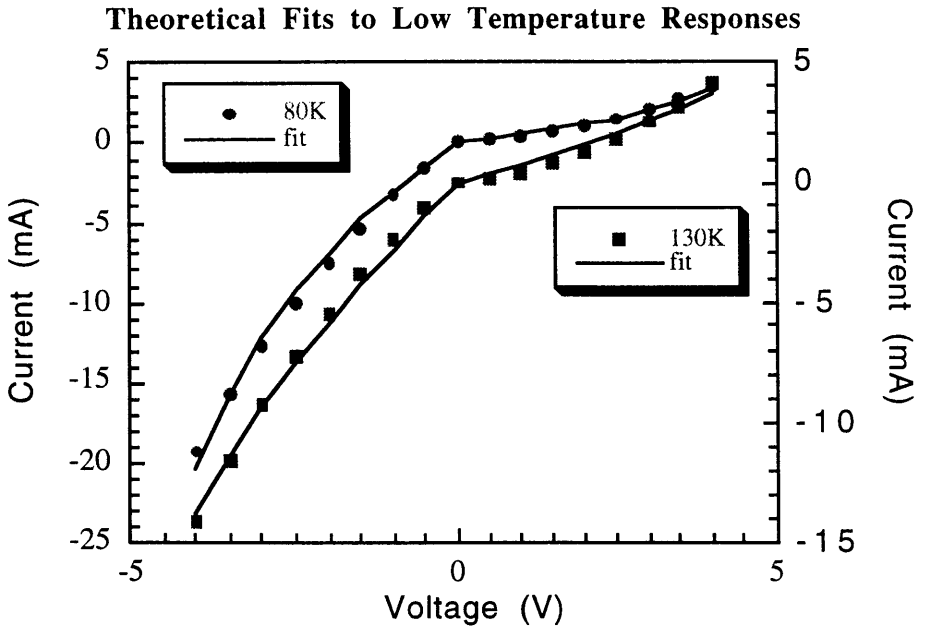

Figure 5-2. Current-voltage curves for the diol taken at 80 and 130K. The sample was ramped to 4V at room temperature and held to allow for the development of conducting pathways. The device was then cooled while the bias was held until the lowest temperature (80K) was reached and the pathways were locked in place. The data is fit to the modified Marcus relation given by the equation above as per Murray.[2]

This equation is appropriate for short-time linear sweep measurements in which the activated nature of the hopping mechanism becomes important. Typical curves for the diol are given in Figure 5-2. The solid points are the experimental data, and the curves are the theoretical fit showing the expected exponential dependence centered at 0V.

The data for a given sample were simultaneously fit at all temperatures to yield one value for ρ which should be device specific and independent of temperature. The prefactor of the exponential, which is the diffusion constant, was allowed to vary for each temperature. Because the diffusion should be an activated process, the individual diffusion constant at each temperature should fit to a general arrhenius plot that applies to all temperatures. This curve fit yields values for the enthalpy and the entropy associated with the hopping process. The equation that describes these curves is:

$$D = \frac{1}{6}nF(\text{area})dAB\upsilon(\exp(\frac{\Delta S}{R}))(\exp(-\frac{\Delta H}{RT}))$$

The plots of the prefactor with temperature for three different systems are given in the following figures:

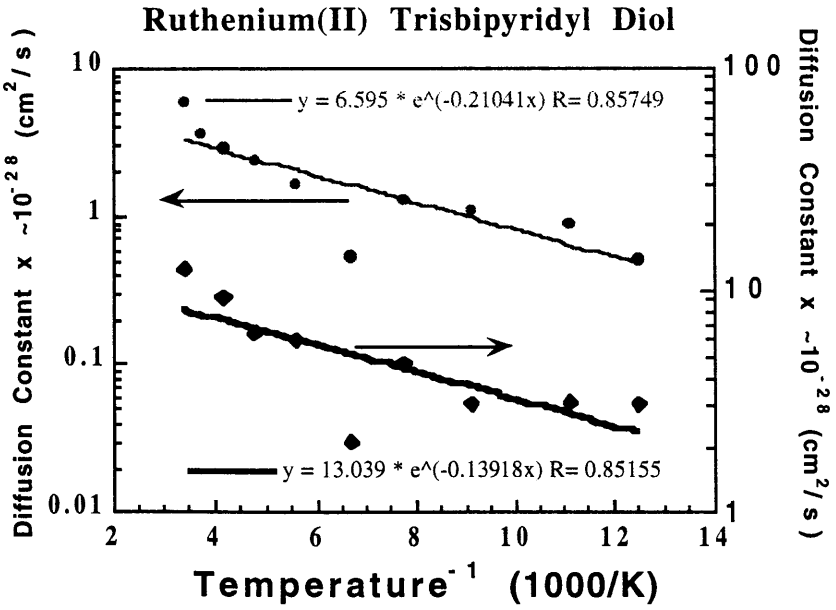

Figure 5-3. Diffusion constants versus temperature for a diol device. Circles indicate forward bias; diamonds indicate reverse bias. The order of magnitude of the constants was estimated using the equations described in the text. The activation energies for this sample are approximately 1.7 kJ/mol in forward bias and 1.1 kJ/mol in reverse bias. The diffusion constants are obtained from the theoretical fits to current-voltage plots from 0 to 4V like those shown in Figure 5-2.

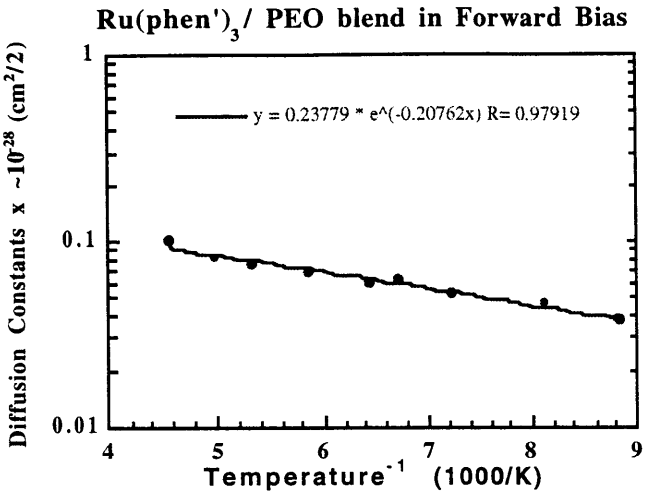

Figure 5-4. Diffusion constants versus temperature for the ruthenium(II) trisphenanthroline blended with PEO, an ion conducting polymer. The activation energy for this system was approximately 2.6 kJ/mol. Constants were calculated from current-voltage curves taken from 0 to 6V at various temperatures.

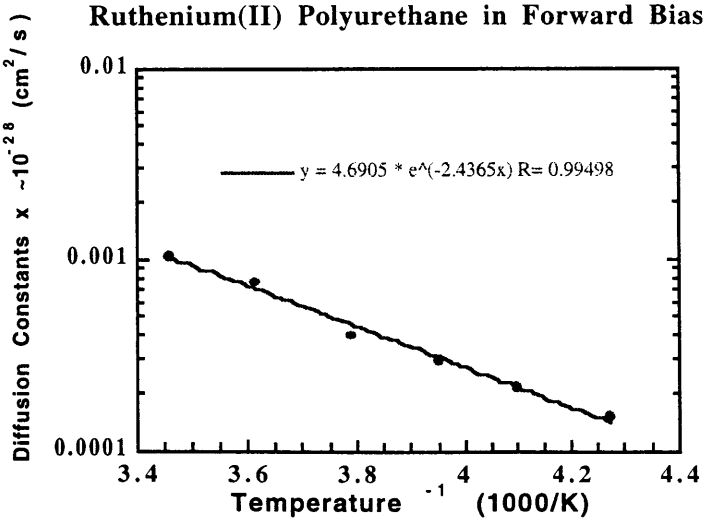

Figure 5-5. Diffusion constants versus temperature for the trisbipyridyl ruthenium(II) polyurethane. The activation energy for this system was approximately 20 kJ/mol. Diffusion constants were calculated from fits to current-voltage curves from 0 to 10V.

From these graphs, the activation energies are 1.7 kJ/mol for the diol, 2.4 kJ/mol for the phenanthroline blended with PEO, and 20 kJ/mol for the polyurethane. The activation energy for the polyurethane is consistent with activation energies quoted in the literature for other redox polymer systems, on the order of 18-80 kJ/mol.[1, 6-8] The activation energies for the small molecule systems follow the trend expected from the knowledge of other parameters of the system. For example, as we increase the size of the molecule by giving it bulkier side groups, such as the sulfonated phenanthroline, or making it polymeric, we expect the mobility of the system to decrease and the barrier to hopping to increase. The addition of poly(ethylene oxide) to the phenanthroline complex does not change the activation energy from samples of the complex alone. This fact may indicate that the phenanthroline complex is phase separating within the blend. However, the variation in activation energies for all of the small molecule systems is fairly insignificant within experimental error.

Typical entropy values have been correlated with different rate-limiting mechanisms in the literature. In our case, because our actual values of A and B are unknown and are likely different for the two separate interfaces, evaluation of the value for the entropy of reaction from this data is not possible. However, using typical values for A and B from the literature, with concentrations around $10^{16}/cm^2$ for each, the entropy for our systems takes on negative values. Negative values for the entropy would be expected for ionic or electron hopping, as opposed to positive values which would indicate polymeric segmental motion.[9] It is interesting to note that the polyurethane still has negative entropy values and therefore does not seem to be limited by segmental motion; presumably the redox centers are close enough that large amounts of motion are not required for hopping.

Also, the relative magnitude of the diffusion coefficient decreases from the diol to the phenanthroline blend to the polyurethane system as shown in the figures above. For example, the room temperature values for each are 6.1, 0.1, 0.001 respectively. The same trend, noted in Chapter 4, is reflected in the ionic conductivity, one representation of the relative mobility of these systems. Recall that these measurements were taken after charging to steady state, so presumably the ionic motion should no longer effect the hopping. However, redox hopping is still dependent upon the mobility of the redox species because the site to site distance can change via thermal or segmental motion. The site to site distance between centers also increases in this series as more organic material is included.

To determine the actual units of the diffusion constants, we must make some assumptions based upon the concentration of oxidized and reduced species in our films. A

value for the charge transfer distance must also be assumed. If the distance is on the order of the spacing between two redox centers, approximately 10Å, and the concentration of species is assumed to be on the order of $10^{16}/cm^3$ as given in the literature, the diffusion constants are on the order of 10^{-28} cm^2/second. This value is extremely low. The most reasonable explanation is that the concentration of species participating in charge transport is much lower in these films than those in the literature that have solvent contact. Even at long times, only a small fraction of the potential pathways can be developed. This observation provides a potential avenue for improvement of these devices. If more of the species could be activated, more current and more light should be possible from these films at the same voltages.

Another fitting parameter which is interesting to examine is the value obtained for the ρ factor included from the equation used to fit the current-voltage data. Murray attributes this factor to inhomogeneities in the films which cause a distributed hopping process to take place. Briefly, the rate of hopping is limited not by hopping from one individual center to another, but by the rate of hopping between redox clusters. ρ is the measure of the relative importance of this secondary rate-limiting step. Therefore, one expects that the most homogeneous films would have the smallest value for ρ, and the films most likely to phase separate to have the highest. In our systems, the highest value for ρ comes in the spin-coated polyurethane system. For this material, the urethane segments should have a high degree of hydrogen bonding, causing a certain amount of segregation between urethane linkages and other portions of the film. In addition, the higher spacer content causes the redox species to be separated from one another, allowing more opportunity for phase separation. It should be noted that all of these values are considerably smaller than those considered by Murray's group, likely because the amount of insulating material is considerably less in our films.

One final note is that similar analysis was performed on the layer-by-layer films of the ruthenium(II) polyester. These films had very low current at room temperature so that after cooling the current was below the resolution of our measurement device. The efficiency was high enough, however, that light curves remained within the sensitivity range of the photodiode. Qualitatively from the light measurements, the behavior of the layer-by-layer films is also an activated process, yielding the expected arrhenius dependence on temperature. However, actual values for the materials constants are difficult to determine due to the additional assumptions involved in using light data for this type of analysis.

5.2.3 Ionic Charging at low Temperatures

A final caveat for this testing protocol is the condition that the voltage sweep be fast on the time scale of ion motion. For the regular room temperature tests, each point is taken after a five second delay to avoid stray capacitive effects. However, for these systems, especially the small molecules, five seconds can be enough time to allow for some ionic movement. This movement was monitored in terms of a change in current (delta current), which was essentially the difference between the first data point taken at the maximum voltage and another point taken five seconds later. The onset of ionic motion was consistently between 180 and 220K for all of the small molecule systems we tested. The plots of change in current for the ruthenium(II) phenanthroline system and for a blend of the complex with an ion-conducting, flexible polymer (PEO) are given in Figure 5-6. The fact that the blend and the Ru(phen') system alone have similar onset temperatures indicates that the charging is not strongly linked to the behavior of the PEO matrix.

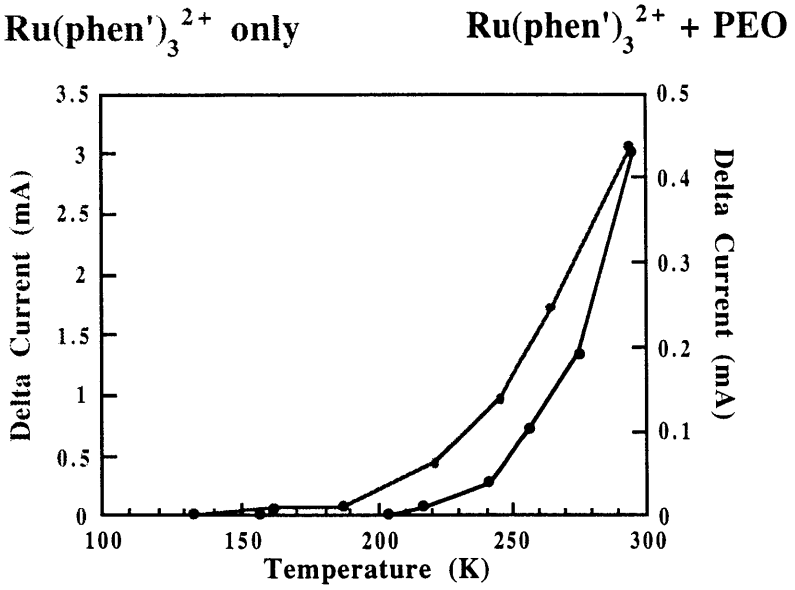

Figure 5-6. The increase in current after a 5 second hold at 4V (delta current) versus temperature for the Ru(phen')$_3$ and the Ru(phen')$_3$/PEO blend systems. This measurement is a probe of the amount of "charging" at each temperature. The onset of charging was consistently between 180-220K.

The low temperature charging effect is likely due to the motion of ions within a monolayer or so of the electrode interface, which would explain the apparent non-dependence of the transition temperature on the material system. However, the steps between temperatures

where data were taken were in some cases quite large, and a subtle variation in this onset temperature would be beyond the resolution of the analysis possible with the current information. The primary utility of this data is in verifying that the voltage sweeps are occurring fast enough at these temperatures to avoid ion movement and complication of the results.

5.2.4 Uncharged Samples

In some respects, the only method to avoid the problems of preset concentration gradients would be to test samples at low temperatures without pre-charging. However, according to the theories asserted to this point, no redox hopping should take place because no ions have moved to stabilize the charge. Under these conditions, the barrier to injection at the interface as well as the barrier to the internal homogeneous charge transfer reaction should be significant. In addition, the percolation pathways for charge transport have not yet been formed so that the material should still be effectively insulating. To probe this behavior, uncharged samples were cooled to low temperatures and the current-voltage characteristics measured as described for the voltage-treated samples above. Although the current was approximately one order of magnitude lower than in the precharged samples, measurable current was obtained in both forward and reverse biases.

From the theoretical fits to the current-voltage data of these samples, diffusion constants were calculated. The diffusion constant activation energy plots for uncharged samples at low temperatures are given in Figure 5-7. The values for the phenanthroline yield an activation energy of 2.7 kJ, which is higher than the precharged value; however, this variation is fairly insignificant within experimental error. If the material were truly insulating as expected under these conditions, the activation energy would be expected to be orders of magnitude higher which is not the case.

When Maness et al. attempted to measure device properties for a sample without the pre-formed mixed valence gradient in their system, they in fact obtained no light, and very little current from their device.[10] Therefore, they conclude that the material is indeed insulating at these temperatures. Based upon the small amount of current, they estimated a rate of 0.5 monolayer of species oxidized per second and ascribed this low level of reaction to the extremely high electric fields present at the interfaces of their 5 micron device. If we apply this rate of reaction to our system, our entire film would be consumed within the time frame of their experiment. The orders of magnitude change in film thickness between their system and ours (from 5 microns to 1000 angstroms) has a large effect on the ability of the system to transport charge. Interestingly, the time required to completely oxidize the film

for their rate constant is fifteen minutes, the same as the time to reach maximum light in our most sluggish polyurethane system.

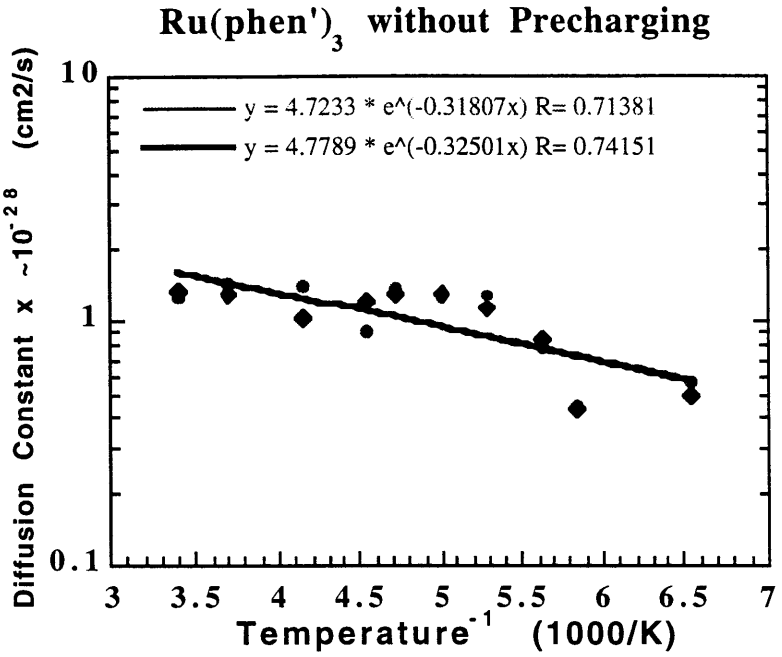

Figure 5-7. Diffusion constants versus temperature for the sulfonated ruthenium(II) trisphenanthroline system measured at low temperatures without precharging at room temperature. The activation energies from this graph are approximately 2.7 kJ for both forward and reverse bias. The energy required for hopping in this system was expected to increase dramatically over the pre-charged case; however, no significant difference was noted.

If Maness' results are applied to the small length scale of our devices, they are consistent with the observations that current will flow in our systems at low temperatures without pre-charging. Even more significantly, current will flow opposite to the presumed pre-set concentration gradient of ions for a pre-charged device. The magnitude of current is approximately the same in reverse bias as in forward bias in both cases, and the activation energies for forward and reverse bias are comparable. These results indicate that the mechanism of charge transport, at least at low temperatures, does not depend on the existence of a mixed-valence gradient or on the position of the ions within the device. Other papers from Murray's group have noted this voltage-gradient driven current that dominates the opposing concentration-gradient driving force.[11, 12] The ion-independent charge transport seen in these films will be examined in greater detail in Chapter 6.

5.3 Charge Transport Limited Behavior

In solution based electrochemical cells, the limiting step at steady state is the mass transport of active species. The characteristic limiting current comes about because the system is dependent upon the diffusion of new molecules to the electrode interface. Therefore, once the voltage has reached a point where the concentration of species at the interface is zero, charge can only continue to be injected at the same rate as new molecules arrive at the interface. In the solid state, that mass transfer limited regime must be where the rate of electron hopping limits the rate of injection, because the only way to bring new molecules to the interface is by having the existing charge on the molecules diffuse away. Interestingly, we never see a current limit in our devices, even for slow scans and steady-state behavior.

It is tempting to assign this feature to the fact that charge transport is never the rate limiting step in these devices. However, as noted in section 4.2, charge transport in these systems can also be dependent on voltage. If electron hopping is described by this equation proposed by Murray:

$$i = \frac{1}{6}nF(\text{area})dABk_{homo}[\exp(-\frac{\rho nF\vartheta}{2RT}) - \exp(\frac{\rho nF\vartheta}{2RT})]$$

the activation energy for the hopping process is given by the voltage gradient between individual redox centers. Therefore, even if the current is diffusion limited at higher voltages or longer times, the rate of diffusion increases at higher voltages so a final limit may not be easily reached.

If charge injection were instead the rate limiting step, then the linear sweep curves and the equilibrium peak currents should fit to the Butler-Volmer injection equation. However, as already noted in section 5.2.1, the equilibrium current is linear with voltage. The short time linear potential sweeps also do not fit injection-limited kinetics because they increase directly from 0V. Butler-Volmer kinetics indicate that current will not flow through the device until the redox potential of the material has been reached. Some method of determining transport limitations must be determined to deconvolute these combined effects.

5.3.1 Space Charge Compensation

As noted in the introduction, the space charge layer at the interface will only remain thin if the injected charges are able to diffuse easily away from the electrode. If the diffusion rate is slow, the redox species will begin to compensate the ions that are present. This combination will cause an increase in the barrier to charge injection, that will be lowered again when the charges are removed. A characteristic decay in the current and

light would be indicative of this change in the barrier and evidence for transport as the rate limiting step in this regime.

One way to probe this behavior is through monitoring the transient response of the device to a square wave pulse. In this case the device is first charged under a low applied bias to allow the ions to migrate to the interfaces and for conducting pathways to form. Once fully charged, the device is subjected to square wave pulses at 8V, separated by rests at 0V. The frequency of this pulse is then changed between 10 Hz and 10^6 Hz. The resulting data for a diol device is given in Figure 5-8. A sharp peak is observed in the light emission at very short times which then relaxes to a steady state plateau. The increase in flux at short times would be assigned to capacitive charging of the cell if we were here monitoring the current. However, this measurement of the light emission indicates that considerably more injection of carriers is allowed at very short times. This high rate of

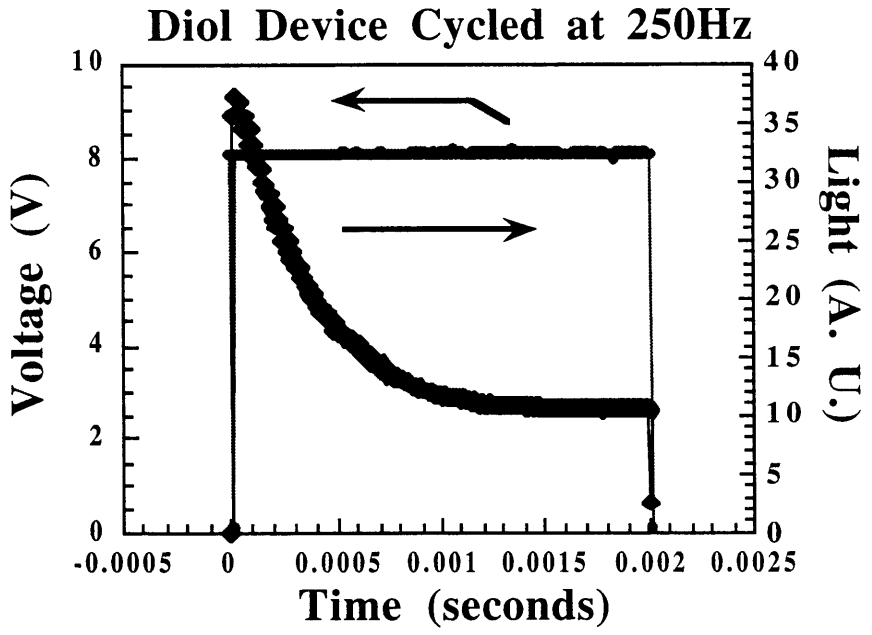

Figure 5-8. Transient luminance response of a diol device cycled at 250 Hz. The device is subjected to a square wave pulse of 0 to 6V. Real time light response is measured by a photomultiplier tube.

injection then slowly decays until the steady state value is reached, approaching the DC light emission as a final plateau.

This behavior is consistent with the hypothesis that charge transport is the rate limiting step after percolation is complete and the device has reached steady state. Under the initial bias, carriers can be injected but some cannot diffuse away. The presence of these additional carriers increases the barrier until the injection rate matches the transport rate at steady state. If the redox species are allowed to relax under zero applied bias, the fast injection process can occur again and the large transient is recovered. However, if injection continues to occur, steady state holds and the light reaches a plateau value. A more extended examination of this behavior is given in a recent paper from our group.[13]

5.3.2 Potential Step Analysis

The transient potential step current has been analyzed by Cottrell and others.[14-16] This theoretical framework was originally developed for charged species moving in solution but can also be applied to redox polymers on electrodes.[17] p124. When the actual constants are calculated, care must be taken to consider the bimolecular hopping nature of the diffusion in the solid state case; however, the general time dependence will be the same as in the original equation. For the transport-limited case, the current is dominated by the diffusion of new species to the electrode to be oxidized or reduced. This diffusion current is described by the Cottrell equation with a characteristic inverse square root of time dependence. Often, data analysis becomes easier when the integrated current, or total charge, is plotted with respect to time according to the equation:

$$Q(t) = \frac{2nFAD_o^{1/2}C_o^* t^{1/2}}{\pi^{1/2}} + Q_{dl} + nFAC_{ad}$$

where Q is the total charge, n is the number of electrons transferred per reaction step (in our case 1), F is the Faraday constant, A is the area of the device, D_o is the diffusion constant of the oxidized species, C_o^* is the concentration of oxidized species in the bulk, t is time, Q_{dl} is the amount of charge necessary to satisfy the capacitance of the double layer at the interface, and C_{ad} is the concentration of species adsorbed directly to the electrode. This graph is linear with the square root of time and the y-axis intercept gives the charge from capacitive charging.

Because current data is not readily available for these systems, the actual values for charge transfer rate, etc. cannot be determined. However, the output of the photomultiplier tube is directly proportional to the number of photons that impinge on the detector. The number of photons emitted by the device will be some fraction of the total current that passes through the sample and will follow the dependence of the slower of the two species if the rate-limiting steps are different. Therefore, some information about the carrier motion

can be obtained by plotting the total number of photons emitted in a given amount of time. Typical plots for the diol devices are given in Figure 5-9.

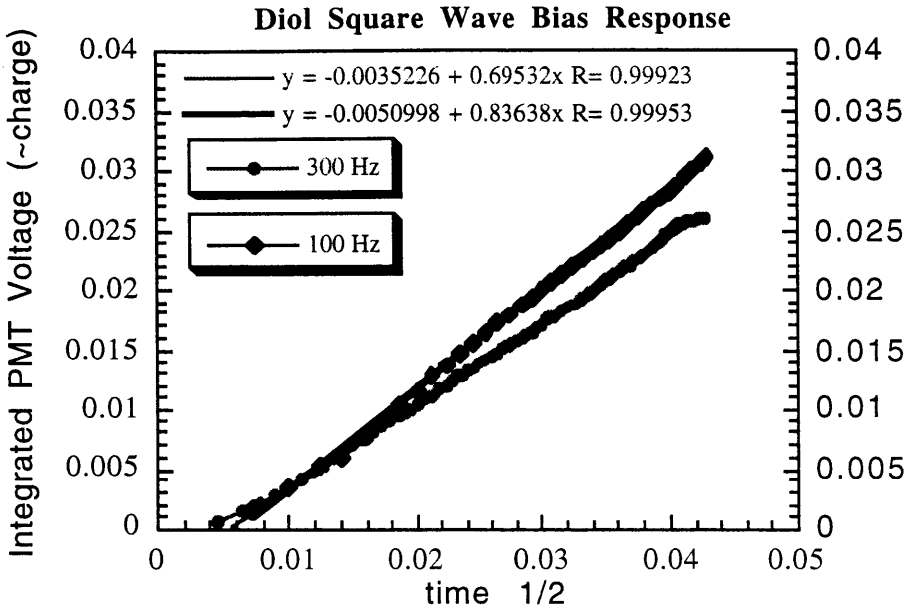

Figure 5-9. Cottrell plot for a diol device. The transient light response of the device to a square wave voltage pulse was measured at different frequencies of the applied voltage. The light decays with a time -1/2 dependence, and the total integrated light gives a linear dependence with the square root of time. This dependence indicates diffusion limited current.

This device response is proportional to the square root of time, as expected for a diffusion limited regime. Therefore, the device must be diffusion limited at long times, rather than continuing to be injection limited.

5.3.3 Alternative Explanations for Transient Behavior

As mentioned above, if this transient were only monitored in the current of the device, it could be explained by capacitive charging effects. In this case, the motion of ions under the applied bias causes a fast polarization of the interface and an accompanying build up of charge on the electrodes. This type of current should not produce light however because it does not indicate injected charge, and only injected charge can meet to recombine. Alternatively, if the applied voltage were an actual AC measurement and switched between positive and negative biases, this type of light transient might be seen depending upon the lifetime of the charges species in the device. For example, if 3+ charges were injected from one electrode and the bias was then switched, the first 1+

species injected would not have to travel through the entire device to encounter a 3+ site. At very short times, 1+ centers could react and give light as fast as they were injected, leading to a dramatic increase in emission. However, because we are operating only in on/off mode and not actually changing biases, only species of the same charge state should be remaining near an electrode.

A final picture that could be used to explain the transient is dependent upon some of the charged states remaining in the device after the bias is switched off. Studies of the stability of the 3+/2+ and 2+/1+ concentration gradients indicate that these gradients will survive in the device for 30 to 60 seconds after the applied bias is removed.[18] Charges near the recombination zone will quickly diffuse together and annihilate each other, so the region of zero charge in the center of the device should expand. In addition, charges near the electrode interface can also relax quickly and give up their charges to the metal sites. Charges near the center of the device however should be stabilized by the counterions present and can remain as long as the ions stay in place to maintain local electroneutrality. If the counterions do not move as quickly as the charges relax, a net negative region will occur at the interface, and an internal electric field will develop, sweeping the charges to the electrodes.

If the bias is turned on again before too many charges relax, the concentration gradient of the remaining species near the center of the device will be much steeper than the steady state value. This increased concentration gradient would cause a higher current and a higher rate of recombination at short times until the steady state profile is regained. This redistribution of species will also be a diffusion process and so is consistent with the Cottrell analysis applied above.

The distinction between this picture and the previous explanation would be the amount of current injected into the device at short times. In the barrier case, the current would be expected to track the light exactly as more carriers are injected upon immediate application of the bias. In the second case, the high light output is primarily due to remaining charge carriers in the device, so the initial charge injection is not as high. Differences may also be seen in the capacitance of the device because the position of the charge in both cases is expected to be quite different. These experiments should clarify which picture is correct.

5.3.4 Applications of the Transient Emission

An interesting side benefit of monitoring this transient process is a net increase in the light under an applied AC field. A typical curve for the diol system is given in Figure 5-10. After conditioning, the samples are cycled from 0 to 8 or 10V AC while a frequency

scan is taken. All of these cells exhibit a maximum in light output around 15 kHz. At this frequency, most of the square wave pulse causes the peak injection of carriers, and the device is cycled off well before the lower plateau is reached. Below this frequency the photodiode detector averages more of the steady state plateau into the measured device response. Above this frequency, the redox species do not have enough time to fully relax before the next voltage pulse, and the transient is not as large. Because of this longer lifetime of the charged states however, these devices will operate under much higher AC fields than typical organic materials such as PPV.

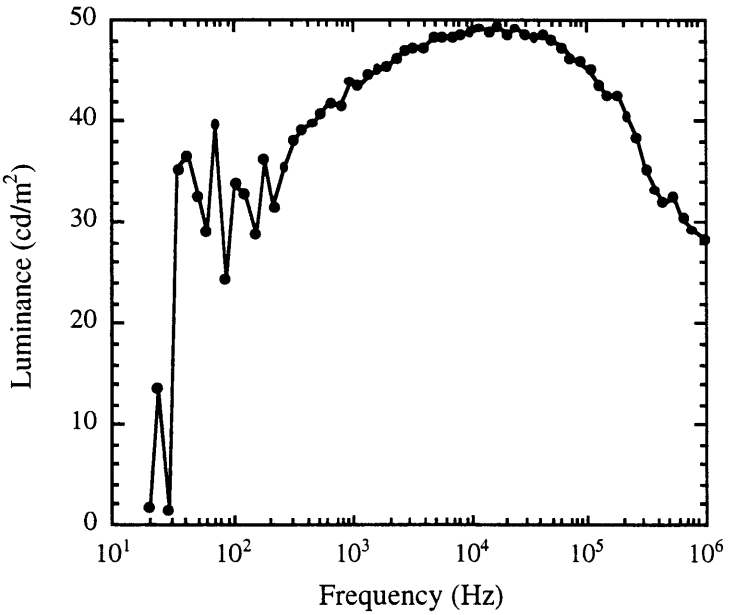

Figure 5-10. Average luminance of a diol device operated under AC bias. The DC offset was adjusted such that the device experienced voltages from 0 to 8V. At low frequencies the light falls off because the photodiode is averaging the "off" times of the AC cycle with the "on" times.

Another benefit of operating under AC bias is the potentially longer lifetime of the devices. Other device observations in our group have pointed to over-reduction of the ruthenium complexes as a likely culprit in the degradation of the light emission.[5] If the injected charges are not allowed to buildup at the interface, the probability is lessened that a 1+ state remains near the electrode to be further reduced to 0 or even 1-. Operation under AC bias helps to limit the amount of time that excess charge can sit at the injection site before it diffuses away.

6. Considerations of High Field Behavior

A very important consideration in the characterization of both charge injection and transport in these sandwich-type structures is the fact that they are only on the order of 1000Å, or 0.1 micron, thick. Most experiments reported in the literature on electrochemically active systems are done with interdigitated electrodes with 2-5 micron spacings. Also, due to the high quality of the films, especially the layer-by-layer samples, biases over 25V in some cases can be applied without reaching breakdown of the material. This combination of thin film and high voltage means that electric fields well in excess of 10^6 V/cm are regularly applied to these devices. Extra energy is therefore available to support non-ideal modes of injection and transport.

One of the results of this excess energy could easily be violation of the assumptions of local electroneutrality in the device. Calculations by Murray's group on the width of the double layer in their samples are sometimes as high as 100 nm.[1] If we truly had 100 nm of interface on each side of our films, more than one-third of our devices could be enveloped by the space charge region. If electroneutrality is not required, it would also be possible to have the injection of only one charge, i.e. rather than balanced oxidation and reduction, only reduction would occur.

Another possible result of the high field is a change in the mechanisms for charge injection and transport. Other metal-center chromophores, such as AlQ_3, transport electrons by delocalization of the charge across the overlapping π^* orbitals of the conjugated ligand groups.[2] It is feasible that similar electron hopping could take place in these ruthenium(II) systems, given high enough overpotential. In fact, an equation describing the excess energy required for this mode of transport has been previously described in the electrochemistry literature. The methodology was developed for a system with tight association between the redox center and its counterion. The result calculated by Peover and Davies is [3]:

$$E = E^0 + \frac{RT}{nF}\ln (K_{cat}K_{an}) + 2\,\frac{RT}{nF}\ln C$$

where K_{cat} and K_{an} are the constants of the ion pairing reaction between the electrolyte and the respective cationic and anionic radical species and C is the concentration of electrolyte. The authors found that with sufficient overpotential (E-Eo), oxidation or reduction could still take place, even when the counterion remained tightly bound to the redox center.

In this chapter, several examples of this type of unusual current and light behavior will be described. Particular attention will be paid to the constraints placed on each system

that do not allow the ions to move out of the way so the lower energy pathway of charge movement can take place.

6.1 Evidence for Single Carrier Injection

One of the challenges in determining charge transfer rates for the systems in this thesis is the fact that the total current is a combination of the rates of two separate species. If a violation of electroneutrality allows the amounts of charge to be independent of each other, the separate contributions of the 3+ and the 1+ states are difficult to deconvolute. However, due to the bimolecular nature of the light emission reaction, the onset and progress of light emission must follow the dependence of the slower of the two species. In contrast, the current will begin first with the injection and transport of the faster species. By comparing the dependence of light and current on voltage and time, some comments can be made about the individual rate constants.

6.1.1 Light and Current versus Voltage

If the rates of 3+ and 1+ injection are independent of each other, the reduction of the ruthenium complex should take place before the oxidation process, because the energy required for reduction is 0.6 eV less. Therefore, if the voltage drops equally across both electrodes, the onset of current should be approximately 2.2V. Conversely, the onset of light should not come until 3.4V. This type of separation of reduction and oxidation does not appear to occur in these devices, because the beginning of light emission is usually between 2.5 and 3V; however, two turn-on events are observed. In general, some current begins to flow upon application of a voltage bias, even before the redox potential is reached. Then at higher voltage, a second increase in current is accompanied by light. This first current could be very low level leakage from minute pinholes in the film, but it is very reproducible. In any event, it does not contribute to the light output. Examples of this two level injection are given for the phenanthroline system in Figure 6-1.

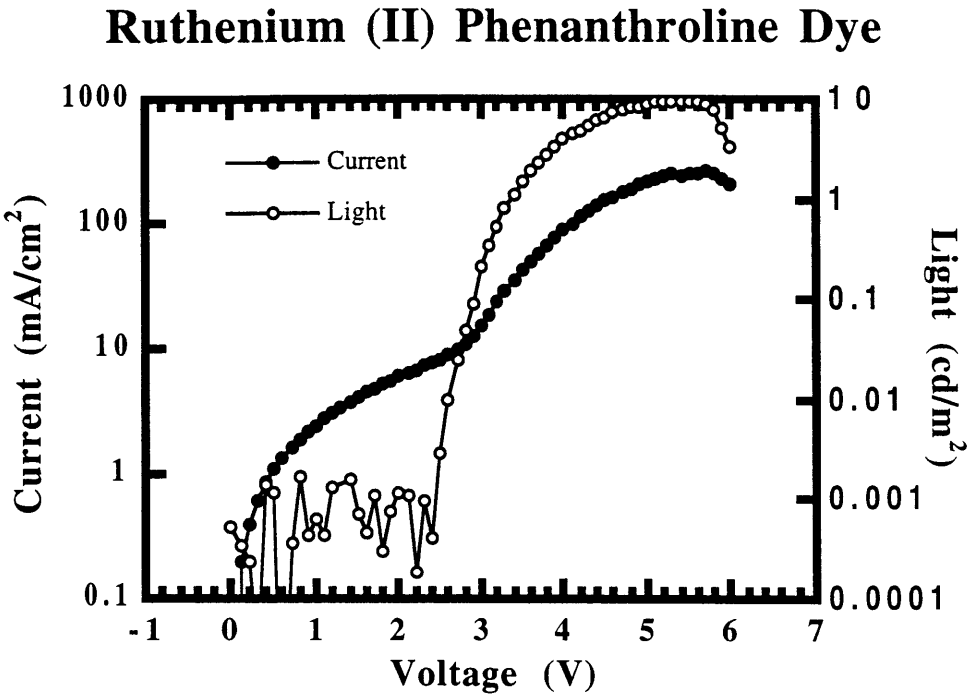

Figure 6-1. Current (closed symbols) and light (open symbols) versus voltage for the trisphenanthroline ruthenium(II) complex. Data are plotted on a logarithmic scale so the turn-on voltage is easier to discern. Note that the current has two turn-on events, one at zero volts and one near 3V when the light begins to rise. The turn-on voltage for light emission is close to 2.5V.

For the layer-by-layer systems, the data indicate that light and current follow each other quite closely. This association implies then that the rates of injection are somewhat linked, so that the voltage does not necessarily drop evenly across both electrodes once charge injection has begun. In addition, the first leakage-type current is no longer evident in these films, consistent with the notion that layer-by-layer processing improves film quality and gives dense, pinhole-free samples. Examples for sequentially adsorbed layers of the ruthenium(II) polyurethane are given in Figure 6-2. The light and current have been plotted on a logarithmic scale so that the turn-on voltage is more readily apparent. This system performed very similarly to the sequentially adsorbed layers of the ruthenium polyester.

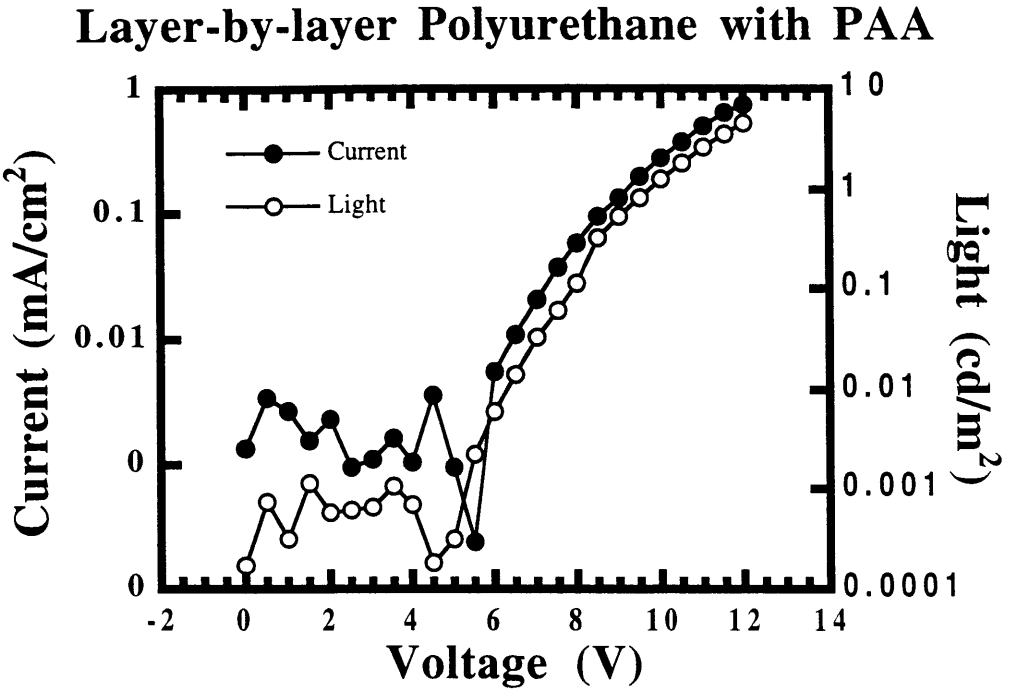

Figure 6-2. Current (closed symbols) and light (open symbols) versus voltage for a layer-by-layer processed film of the trisbipyridyl ruthenium(II) polyester film fabricated using poly (acrylic acid) as the polyanion. Data are plotted on a logarithmic scale to make the turn-on voltage easier to discern. Here both light and current begin at the same voltage, near 6V. The lack of leakage current in these systems compared with the other spincoated films (see Figure 6-1) may partially explain the improvement in device efficiency.

6.1.2 Light and Current versus Time

In general, the light and current track each other quite well in these devices. For the polymeric materials and the small molecules at high voltages (>4V), the light and current appear at the same time without appreciable delay. However, if the efficiency is plotted, which is the relative ratio of light to current, it reaches a maximum well before the maximum of the light emission is observed. This result is consistent with the first appearance of a low level of leakage current at low voltages which becomes a smaller percentage of the total as the second injection process begins to dominate.

In the diol devices held at low voltages (<4V), an interesting trend appears. The light emission does not commence until after the current has reached a local maximum and then decayed, as was shown in Figure 4-5. As noted in Chapter 4 however, this initial current cannot be merely a capacitive charging of the device as the material slowly polarizes

in the field. The magnitude of the total charge injected into the device is much too large to support that explanation. However, if the first peak is interpreted as the injection of only one carrier into the device, light emission would not yet be expected. Because the potential for reduction is lower than that for oxidation, electron injection is most likely preceding hole injection at these voltages. Interestingly, the onset of light emission, and therefore the onset of hole injection, comes at twice the time required for the initial injection to reach a maximum. The plot of this ratio for various samples is given in Figure 6-3:

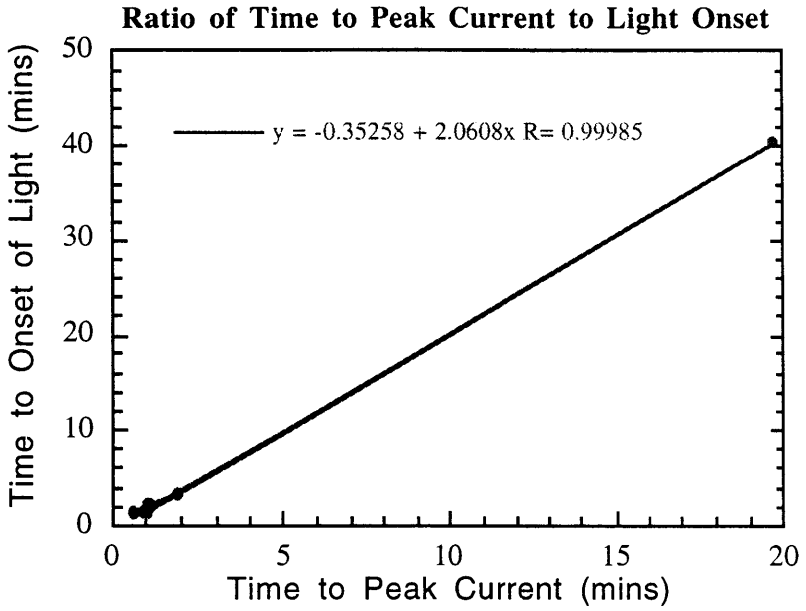

Figure 6-3. Time to the first peak on the current-time graph plotted versus the time to the onset of light emission for various diol devices. The slowest responding device (at 20 and 40 minutes respectively for current and light) is a diol device held at 3V after storage in air. The next longest device was held at 2.5V; all others were held at 3V under nitrogen. The ratio for all cases, however, remains 1 to 2.

Unfortunately, the origin of this ratio is not yet clear. It is likely related to the relative rates of current conduction through the device, but the time scales required are not consistent with any of the diffusion constants calculated thus far.

6.2 Reverse Bias Performance

An interesting question is the lack of reverse bias light for most of these systems since electrochemical cells are expected to give both current and light regardless of the nature of the electrode. As described in the introduction and Chapter 4, all of these ruthenium(II) complexes support plenty of current in reverse bias, excepting only the layer-by-layer film made with SPS. However, only the layer-by-layer film made with PAA showed any light in reverse. Some various explanations have been put forward and will be explored in this section.

One possibility, as noted by a reviewer to a previous paper on this work, is the inability of the aluminum electrode to oxidize the ruthenium at these biases.[4] This explanation is supported by the recovery of light if platinum is used as an inert electrode. Typical curves are shown in Figure 6-4:

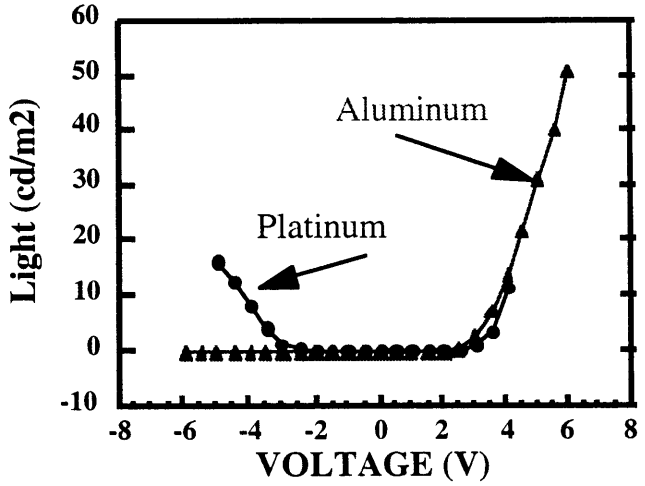

Figure 6-4. Light-voltage curves for a ruthenium bipyridyl diol complex spun onto ITO with aluminum or platinum cathodes. Note that the turn-on voltage is fairly independent of electrode choice, however, reverse bias light emission occurs with platinum and not with aluminum.

Additional credence is given to this explanation by capacitance measurements done in forward and reverse biases, seen in Figure 6-5. Samples were exposed to a square wave DC bias with a small AC field superimposed. The value of the capacitance drops upon application of the higher bias, and often rises slowly as the voltage is held. After the voltage is released, the capacitance returns to its initial value. Detailed studies on the capacitance of these devices is currently in preparation.[5] The interpretation of these measurements dictates that the drop in capacitance upon application of a voltage step is due to oxidation and reduction of the ruthenium centers at the interfaces with the electrodes. In

the reverse bias case, the drop in capacitance is considerably less, consistent with the notion that one of the two processes is not taking place.

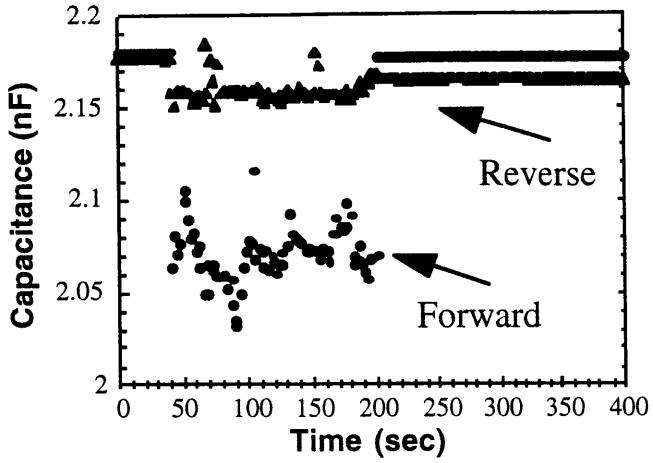

Figure 6-5. A comparison of the capacitance response in forward and reverse bias for a spin coated sample of the ruthenium bipyridyl diol. The drop in capacitance with application of the voltage pulse is related to the amount of reduction or oxidation of the redox centers. The reverse bias pulse clearly injects less charge into the material and is accompanied by an irreversible reaction because the capacitance does not return to the original value.

Another possibility is the imbalance of charge transport rates in these materials which would cause localization of the recombination zone very close to one of the electrodes. If the reduction is faster and happens at lower voltages, then the recombination should occur close to the oxidizing electrode, aluminum in the reverse bias case that would quench more than the ITO. Quenching of excited states is a phenomenon seen for many metals, although the rate of recombination is usually competitive with the quenching rate for most ruthenium/electrode systems.[6, 7]

Quenching arguments do not give an obvious reason that platinum should provide light emission because platinum should also be a quenching electrode. However, when the energy levels for $Ru(bpy)_3$ are considered relative to different metals, the recovery of light with platinum can be explained. As Figure 6-4 shows, reverse bias light output is present in the platinum case, but the amount of light in forward bias has been lowered considerably. If the band model is considered, we note that the use of platinum would cause a significant improvement in the rate of hole injection under reverse bias. This enhancement could balance the charge injection and allow recombination to occur closer to the center of the device. However, there is little evidence from other experiments that device performance has been influenced by the work functions of the electrodes in this way. This possibility of changing the relative rates of charge transport will be discussed in

greater detail in Chapter 7 which describes modifications to the electrodes in an attempt to influence the charge balance.

The outstanding question then becomes the reason that light emission is recovered in the RuP/PAA films discussed in Chapter 4. One hypothesis is that chelation of the carboxylic acid groups of the PAA with the aluminum changes the oxidation potential and allows the oxidation of the ruthenium.[8] However, experiments with adding PAA layers to the top of spincoated ruthenium films did not show substantial improvement. A ruthenium complex containing carboxylic acid groups pendant to the ligands was also tested, yielding results similar to the other small molecules. Therefore, it is difficult to conclude that simple chelation effects are causing this change. Other experiments, described in Chapter 7, which involve modification of only the ITO electrodes, not the aluminum, also give reverse bias light output. These results are difficult to reconcile without inferring some changes in the relative rates of charge injection that can occur when the charges are not forced by electroneutrality to be in a perfect 1 to 1 ratio.

6.3 Low Temperature Device Operation

6.3.1 Electron Transport

Devices have been tested at temperatures varying from room temperature down to 80K, and up to 320K, to determine the diffusion constants reported in Chapter 5. For one type of experiment, the cells were preconditioned at room temperature to set up the conducting pathways in the film. Typical curves are given in Figure 6-6. For the most part, symmetric current-voltage behavior is preserved, although the curve becomes increasingly sigmoidal as temperature decreases. This observation could indicate a decrease in thermal perturbations to the double layer allowing for cleaner injection of charge at lower voltages.[9] p541. The curves also lose their hysteresis at temperatures lower than 180K. This positive hysteresis at room temperature is an indication of the further growth of conductive pathways allowed by the movement of ions in the films; therefore, below 180K motion must be limited. Although the temperature resolution is not very high, most materials investigated showed an onset of charging somewhere between 180 and 220K. The significance of this temperature has not yet been determined.

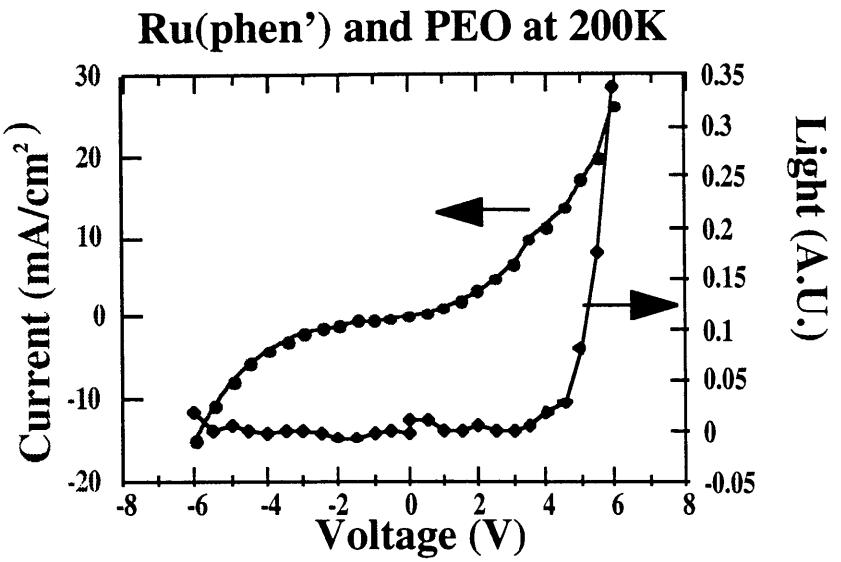

Preconditioned with 4V at Room Temperature.

Figure 6-6. A current-voltage, light-voltage plot taken at 200K after preconditioning with 4V at room temperature. This plot retains the characteristics of the room temperature plot, including reverse bias current even at very low temperatures. This behavior is general to the small molecule systems that have been studied. Light units are arbitrary because the photodiode must be placed far from the device in the low temperature setup, therefore only relative readings are reliable.

In a second type of experiment, the samples were cooled without prior application of voltage. For the small molecule systems, charge injection can occur at very low temperatures, even without the aid of pre-charging of the device at room temperature. A device curve without charging is given in Figure 6-7. In general, the cells seem to behave in an electrochemical fashion, with injection independent of the electrode or the electric field, even at temperatures below those necessary for ion motion to charge the double layer and form conducting pathways in the film. Presumably, the double layer is formed by ions localized near the interface that require very limited mobility to allow for injection.

Layer-by-layer films have also been measured at low temperatures. In general, the room temperature turn-on voltages have been preserved, although the current levels are so low that the analysis becomes more difficult. If the device has not been pre-charged at room temperature however, no light or current is observed. The cause of this loss of current is difficult to deconvolute because both charge injection and transport are be severely limited by loss of ion motion.

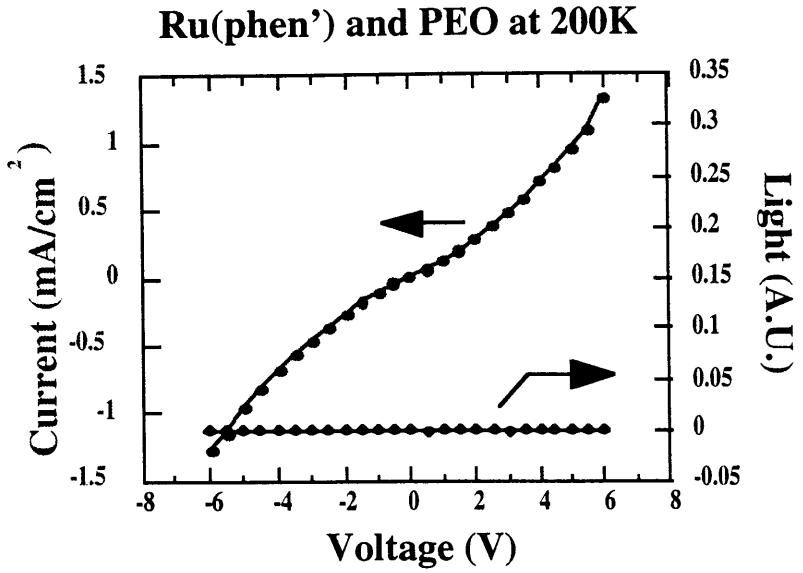

Unconditioned at Room Temperature before cooling.

Figure 6-7. A current-voltage, light-voltage plot taken at 200K without preconditioning at room temperature. Although the current levels are very low, forward and reverse bias is retained at these low temperatures. This behavior is general to the small molecule systems that have been studied.

6.3.2 Light Emission

The previous conclusions are somewhat misleading, because, although we obtain current at low temperatures for uncharged samples, no light is ever observed unless the device has been pre-conditioned at room temperature. As mentioned in the first section, we hypothesize that one of the redox species precedes the other, and perhaps this second species is unable to be formed at low temperatures without the prior presence of a conducting pathway. Because current is also seen in reverse bias, we assume that the missing species is the oxidized 3+ molecule. Recall that the 3+ species is apparently missing from our devices in reverse bias even at room temperature. Therefore, the ruthenium has become an "electron-only" device at low temperature, and local electroneutrality has been violated. Here the ion motion should be extremely limited; however, direct electronic hopping across the ligands may be an alternative to the electrochemical reduction typical at room temperature.

If the ruthenium system is transporting electrons, the addition of a hole transport material should allow for light emission. We have chosen to use poly(para-phenylene vinylene) (PPV) which is the well-known organic semiconducting material with efficient hole transport described previously. If a PPV device is measured at low temperatures,

small amounts of green light are observed. If a ruthenium complex device is measured at low temperatures, no light is observed, as noted above. However, if a device is fabricated with a layer of PPV near the hole-injecting ITO electrode and ruthenium near the electron-injecting aluminum electrode, red light is emitted that is readily detectable by the eye. The comparison plots of the ruthenium only, the PPV only, and the combination heterostructure device are shown in Figure 6-8. Note that the heterostructure yields an order of magnitude more light than the PPV alone, and the color of emission is red, so the light must be coming from the ruthenium layer. The details of the charge transfer at the interface have not yet been determined; however, clearly electrons are traveling across the ruthenium so that recombination can take place.

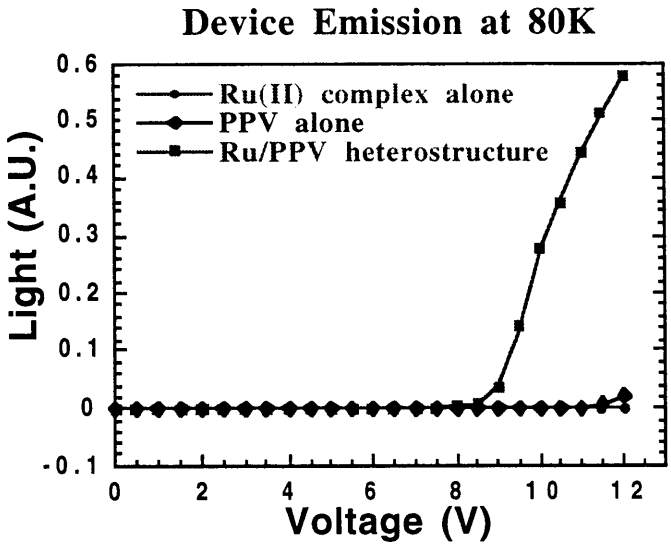

Figure 6-8. Light emission from a PPV/diol device at 80K. Note that the light from the heterostructure is one order of magnitude higher than that from the PPV device, and no light is obtained from the diol structure. Visual observation confirms that the emitted light is red, therefore originating from the diol.

Another test of this electron hopping theory would be the formation of a device with the ligand alone before it has been chelated to the ruthenium center. The conjugated system should be able to support electronic conduction, but is less likely to be redox active. Unfortunately, films of the ligand are difficult to fabricate because they tend to crystallize, and samples of adequate quality could not be made. Addition of the ligand-only material to a PPV heterostructure device, analogous to the experiment described above, might serve to improve the processing of the ligand system and enable the experiment to be conducted.

A final test of the hypothesis of electron transport would be the changing of the metal electrode on the heterostructure device. If the ruthenium is indeed operating in an non-electrochemical mode and supporting only electron hopping, the application of a low work function metal should better match the LUMO level of the ligand and much greater light emission should be possible. This final experiment should show that the device is no longer operating as a purely electrochemical device but some charge transport is possible without supporting ion motion. Preliminary investigations of this proposed dual-mechanism in the heterostructure devices are described in Chapter 7, and a full outline of the proposed experiment is noted in Chapter 8.

6.4 Conclusions

The observations presented in this chapter are consistent with single-carrier injection in these films under certain conditions. Based on the reverse bias results, the missing carrier is the oxidized state. This transport of electrons across the ligands without apparent accompanying oxidation lends support to the notion that electroneutrality may not be required in our films. In the "ion budgeted" system, it would be impossible to reduce species from one side without oxidizing them from the other. The resolution of this issue will have profound effects on the interpretation of current device performance and the approaches to improve efficiency and lifetime. It will also open up methods by which the dual concentration gradients can be potentially deconvoluted to yield meaningful physical constants for the 3+/2+ and 2+/1+ couples in these films. In this case, reverse bias studies would yield an easy way to test a unipolar device with only one of the redox couples present. Once the constants have been determined for one couple, the values for the other can be determined from the combined diffusion constants which are currently available.

7. Modifications of electrodes

In the previous chapters, it has been noted that the source of the slow device response or "charging" effect is likely to be injection limited behavior. However, a faster responding, but higher energy, regime is also evidenced at low temperatures. If the injection can be improved or the energy required for the hopping mechanism can be decreased, device performance should improve dramatically. To this end, the properties of the device interface were studied by the addition of various polymer layers to the ITO before the ruthenium complex was spun on to the substrate. The electrical properties of the layers varied from completely insulating to relatively conducting. A table summarizing the findings of all of these systems is given at the end of section 7.1. Also, heterostructure devices were formed where the thickness of the hole-transporting polymer layer was comparable to the thickness of the ruthenium layer. Through comparing device responses, the effect of the interface modifications can be determined.

7.1 Thin Polymer Modifying Layers

For all of the studies in this section, polymer layers were added to the ITO surface by the layer-by-layer processing technique to improve hole injection into the ruthenium complex. Insulating polymer layers were thought to smooth the ITO interface that is known to have high surface roughness which causes uneven injection of carriers.[1] The ruthenium complex used in these studies was the sulfonated phenanthroline, the first ruthenium compound studied by our group.

Some important things to note about this molecule are related to the sulfonate groups present on the ligand. These groups cause the material to have a net negative charge, whereas all other compounds studied in this thesis are net positively charged due to the 2+ on the ruthenium center. In addition, the sodium ions associated with the sulfonate groups can combine with the chloride ions used to neutralize the ruthenium and be washed away as salt in the purification process.[2] This crystallization results in a material with fewer mobile counterions than the other compounds studied and causes difficulty in forming the conducting pathways described in Chapter 4. In other work with sulfonated materials, the strong acid groups serve to facilitate high current and quenching of light output.[3] Therefore some of the conclusions reached by improving the performance of the sulfonated phenanthroline devices may not be as applicable to the other ruthenium complexes, such as the diol.

7.1.1 Insulating Layers

During this thesis, some work was done by other researchers in the group on the effects of the addition of insulating layers at the ITO and at the aluminum interfaces of films of the layer-by-layer polyester.[4] In general the oxidizing interface seemed the most sensitive; insulating layers at that interface caused current and light to be shut down. For example, insulating layers at the ITO caused a decrease in light in forward bias but an increase in reverse bias. Insulating layers at the aluminum interface caused the opposite effect. The device could be tuned from all forward bias light to all reverse bias light based upon the positioning of the layers.

In this thesis, the only insulating layers that were used were the few layers to promote adhesion for the layer-by-layer films of the ruthenium(II) polyester. Attempts were made to remove those layers for the control experiment, but films of good quality could not be obtained without them. Insulating layers were also placed on top of spun ruthenium films to simulate the effect of the last PAA layer in the layer-by-layer films. These samples were also difficult to fabricate because the ruthenium layer tended to wash off the substrate when it was dipped into the aqueous solution. The devices that were successfully made and tested did not show significant differences in performance from the controls. Some samples were also formed as controls for the heterostructure study with one layer of poly(ethylene imine) (PEI) on the ITO before the ruthenium was spun. This layer did not seem to have much impact on device performance. Unlike the injection into layer-by-layer films studied previously, the injection from ITO into the phenanthroline was not very sensitive to the presence of insulating layers until they became quite thick.

7.1.2 Semiconducting Layers

Many different materials systems in this category were tested. All were hole conductors, either PPV or poly(p-phenylene) (PPP), with various counterions to enable film deposition. A table summarizing the deposition conditions for all of the combinations is given in Chapter 3. The addition of polymer layers to the ITO did not have much effect on the performance of the device in forward bias. Therefore, the oxidation from ITO for the phenanthroline seems to be relatively insensitive to the nature of the intervening material, similar to the results for the purely insulating layers above. The layers formed with insulating PAA or PEI counterions had slightly higher turn-on voltages and slightly lower light output, indicating that oxidation was somewhat more difficult through the insulating layer. However, the layers formed with all conjugated materials, i.e. the PPP/PPP or PPV/PPP combinations, were very similar to the control sample, with only

slightly worse performance. Comparison plots of some of these systems are given in Figure 7-1.

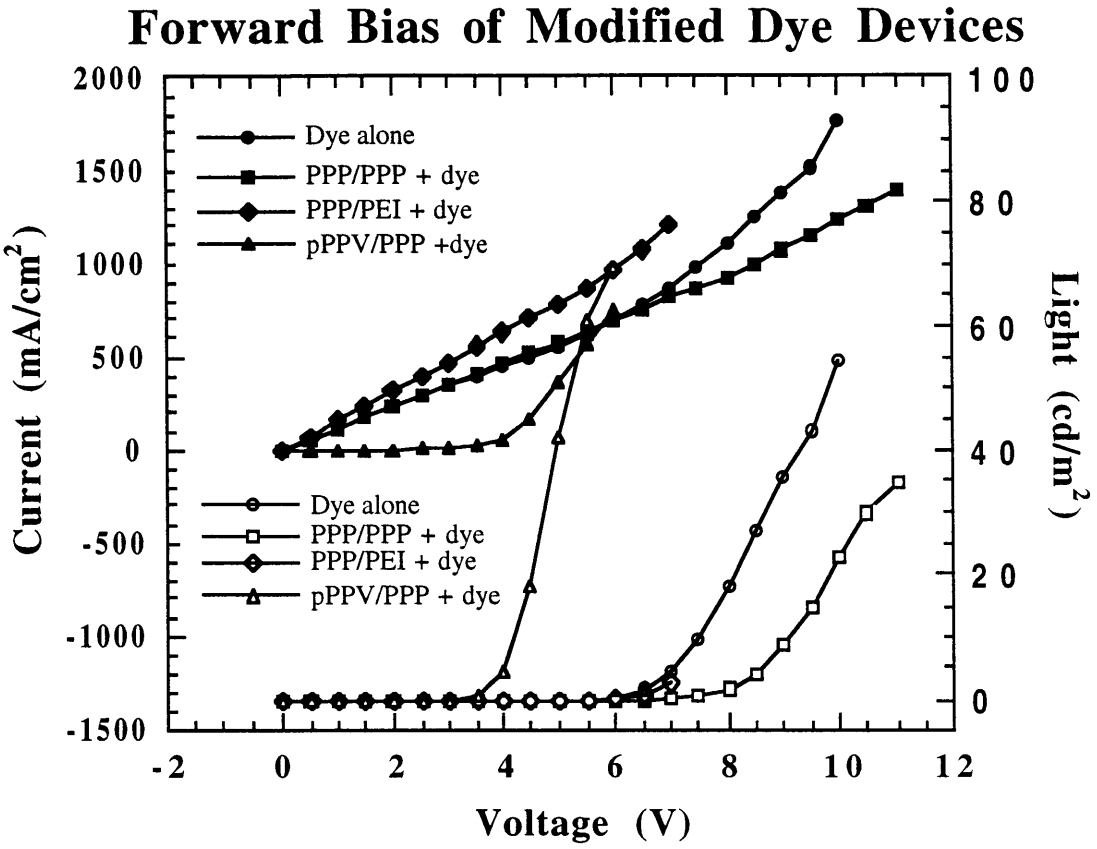

Figure 7-1. Comparison plots for ruthenium(II) phenanthroline devices with various modifying layers at the ITO electrode. Open symbols are light data; closed symbols are current data. Most devices had trouble with leakage current, resulting in poor efficiency.

One system that was noteworthy was the PPP/PPV precursor system. These samples were not thermally converted to the conducting form of PPV but were left with the ionic leaving groups intact. This system actually gave more efficient devices than the control sample alone. One possibility for the improved performance from this system is the higher ionic content near the electrode due to these layers. As noted in the introduction to this section, the phenanthroline complex is likely to have few mobile counterions, causing the barrier to charge injection to remain high. Therefore, any extra ionic material that can contribute to formation of the space charge layer at the interface can improve injection efficiency. The exact nature of the interpenetration of the PPP/PPV system is unknown,

but it may have some ions present that did not participate in the ionic bonding for film formation. In the other systems, the polymer-polymer contact ion pairs could be more numerous, resulting in a matrix that is more rigid and does not contribute as much to device polarization. The PPP/PPP system for example is known to give extremely thin layers indicating a completely intermingled structure.[5] Another possible explanation for the improvement is that the polymer layers were thick enough to block some of the leakage current that plagues the phenanthroline system, but not as thick as the insulating PEI to prevent oxidation. This film processing improvement is not as critical for other ruthenium materials which have better film-forming properties.

7.1.3 Conducting Layers

A side project in this thesis was an attempt to use flexible substrates with patterned poly(pyrrole) lines in place of the standard glass/ITO combination. However, the poly(pyrrole) lines were not as conductive as the ITO, so some attempts were made to increase the conduction by adding conductive modifying layers to the interface with the phenanthroline. For this purpose, layer-by-layer films of poly(aniline) (PAni) were fabricated with SPS as the counter-polymer. Some work has shown that SPS is capable of partially doping the PAni in situ to form a more conducting material.[5] Therefore, 5, 10, and 15 bilayers of the PAni/SPS combination were used without postdoping the material to make it conductive.

In general, the addition of these layers did not change the device properties significantly. The samples with PAni perhaps had a slightly higher turn-on voltage before charging, but did not have substantially different current-voltage curves. Device efficiency was approximately the same, and light output was similar or perhaps a bit lower. These results indicate that the oxidation from the ITO electrodes is either not the limiting factor in the devices or that it is not significantly different from the oxidation from polymer layers. In either case, efficiency does not improve with the modification of the interface.

7.1.4 Reverse Bias Performance

Although forward bias performance does not change much from the performance of the control, the reverse bias performance of these materials is quite complex and a bit controversial. As noted in previous chapters, neat films of ruthenium(II) complexes tend to have sufficient current in reverse bias for light emission, but only support very low light levels. Layer-by-layer films can recover reverse bias performance if the correct proportions of insulating material are present. This phenomenon is somewhat electrode dependent because platinum devices always emit light in reverse bias, although the light from platinum

electrodes is quenched in forward bias relative to aluminum. One hypothesis that has been presented is that the aluminum electrode is easier to oxidize than the ruthenium(II) center, and attempts to oxidize from that electrode fail until much higher voltages are reached. The reverse bias performance from the sequentially adsorbed films could be a result of the PAA outermost layer chelating the aluminum and sufficiently changing its oxidation potential that the barrier is lowered to injection. Unfortunately, attempts to reproduce this effect in spincoated films, either through the addition of PAA layers to the film next to the aluminum electrode as described in the section above, or through the addition of carboxylic acid groups to the ligands themselves, did not allow oxidation from the aluminum to occur.

With this background, the reverse bias results from the ITO electrode modifications are quite surprising. Because the problem seemed to be with the aluminum electrode interface, no change was expected when polymer layers were added to the ITO as the reducing electrode. However, modifications to the ITO electrode served to increase the relative light emission in reverse bias. Interestingly, these layers also decreased the overpotential necessary to see light. Comparison plots are given in Figure 7-2:

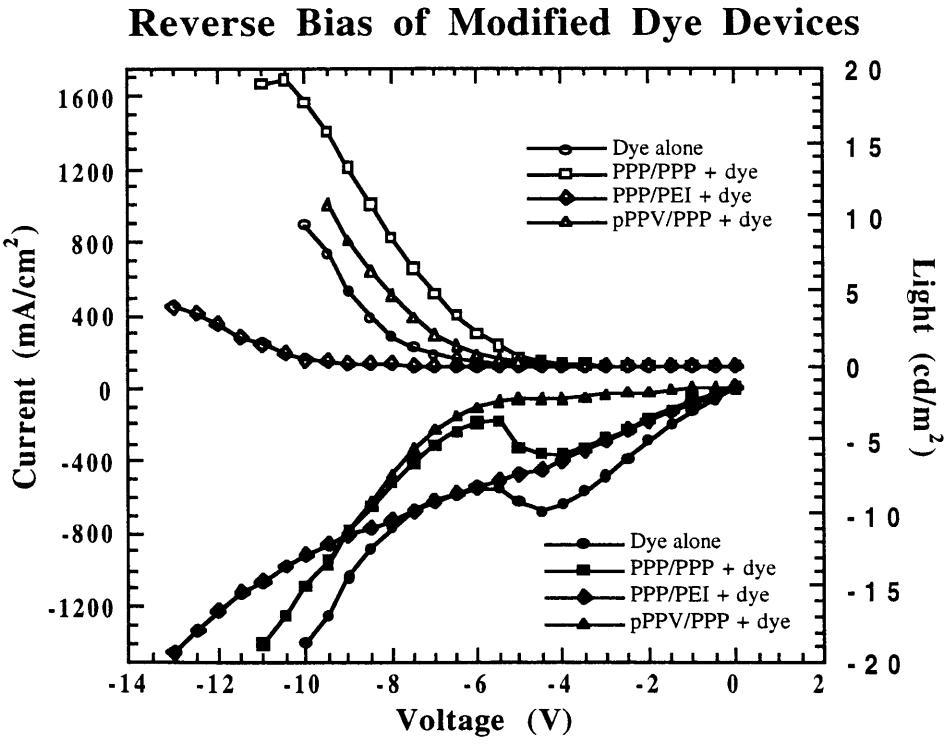

Figure 7-2. Reverse bias performance of the devices shown in Figure 6-1. Open symbols are light data; closed symbols are current data. ITO was biased negative and the aluminum biased positive. The maximum light was about one quarter that in forward bias, but polymer layers at the ITO improve light emission over that of the control sample.

These results seem to imply that the problem with reverse bias light output may not come from oxidation at the aluminum electrode. One possibility is that reduction is normally inhibited by the ITO in reverse bias and the modifying layers increase the reductive capabilities. However, because all of the polymers used in this study were primarily hole-conducting materials, this explanation seems unlikely.

A second hypothesis is that the relative rates of electron and hole injection have now been better balanced so that recombination happens closer to the center of the device where less quenching is likely to occur. In this picture, electron injection and transport would dominate the device. Normal recombination in reverse bias would occur very close to the aluminum electrode and would be largely quenched by proximity to the metal.[6, 7] With addition of the hole-transporting polymer layers at the ITO, the injection of electrons should be slowed, allowing the holes time to diffuse further into the device. This picture is consistent with little change in forward bias performance, as the polymers transport holes sufficiently well. In addition, device efficiency and light output should increase in reverse bias, which is what has been observed.

This concept of balancing charge injection has been contested by Elliot and coworkers. In their theoretical calculations, the rates of oxidation and reduction in these films must necessarily be balanced because of the constraints of electroneutrality. In these arguments, the ions that are required to stabilize charge at one interface must come from the other interface. Therefore, the amount of charge injected each side must be the same and the recombination zone is constrained to be very close to the center of the device.[8] However, this charge balance becomes more complicated than their simple picture if one adds the possibility of over-reduction at one of the electrodes. In addition, these arguments hinge on the requirements of local electroneutrality which may not be necessary in these thin films under high fields as shown in Chapter 6. If electroneutrality is always required in our system, we should not see an electric field within the bulk of the device, because the local environment is always neutral. Determination of the presence of an electric field within our device should help to clarify which picture is correct.

7.1.5 Summary Table

This table provides a summary of the results presented in the previous sections. All notations are comparisons with respect to the phenanthroline sample by itself without modifying layers. If no specific description of the performance is given, the sample behaved similarly to the control in that respect. A few samples were not tested in reverse bias; these devices are noted not available (n/a).

	Forward Bias	Reverse Bias
Insulating layers:		
PAH/PAA	lower light, current	unaffected
PEI	lower light	n/a
Semiconducting layers:		
PPP/PPP	lower light, current higher turn-on voltage	higher light, current lower turn-on voltage
PPP/PEI	lower light, current	lower light, current higher turn-on voltage
pPPV/PPP	higher light, lower current lower turn-on voltage	higher light lower turn-on voltage
PPP/PAA	much lower light, current higher turn-on voltage	n/a
PPV/PPP	lower light, current	lower light, higher current
PPV/PAA	lower light, current higher turn-on voltage	n/a
Conducting layers:		
PAni/SPS	lower light, higher current	lower light, higher current
PPV/SPS	lower light, higher current higher turn-on voltage	higher current

Table 7-1. The results of the polymer modifications to the ITO surface. All comments are with respect to the phenanthroline complex control sample.

7.1.6 Acid Etch

Also of note is the fact that the efficiency of all devices improved dramatically when the ITO electrode was subjected to a one minute HCl etch. Various groups have noted that the work function can be drastically affected by the cleaning procedure, dropping as much as 0.2 eV with a plasma etch.[1] Other possibilities are that residue from the patterning process was still present on the electrodes that the organic solvents alone could not remove. These remnant polymer layers could act like the other modifying polymers to interfere with oxidation at this surface. Extended etching of the surface is also known to increase the roughness and perhaps to aid in nucleation of the percolation pathways through the device. Further study needs to be done to clarify the specific nature of the increase in efficiency with acid etching of the ITO.

7.2 Heterostructures

In general, the formation of a heterostructure device is designed to aid the transport properties of one of the charge carriers in the device. Because the ruthenium complex is known to be easier to reduce than oxidize, it should be better at transporting electrons than holes. In previous sections, the argument has been made that the complex may even, under

certain conditions, switch into an electron transport mode in which electrons are delocalized across the ligands rather than injected as formal charges. For this reason, the addition of a hole transport material should aid in balancing the number of carriers in the device and thereby improve the total device efficiency.

In this thesis we have chosen poly(p-phenylene vinylene) (PPV) as the hole transport material. This material was processed by the layer-by-layer technique of polymer deposition described in the experimental section. This technique allows for very precise control of the PPV layer thickness, important in fine-tuning the efficiency of a heterostructure. The layer-by-layer mode also requires a counter-polymer to allow for the deposition of the PPV. For this purpose, poly(acrylic acid) (PAA) and sulfonated poly(styrene) (SPS) were used as the polyanions. The PPV precursor was then thermally converted to its final conducting form. When PAA was used as the counter-polymer, the PPV control devices showed similar characteristics to normal spun films of the PPV alone. However, when SPS was used in the film, the material appeared to be doped by the strong acid, yielding high currents and showing quenched luminescence.[3] Because the desired properties for an injection layer were unknown, both types of PPV were used in these experiments.

Two basic experiments were undertaken: one testing the effects of the thickness of the PPV films, one testing the effects of using different ruthenium complexes on the total device performance. Basic current-voltage, and current-time tests were done to probe the electrical responses of the films. Finally, high frequency AC testing was done on the samples to gain more information about the time response of the materials.

7.2.1 Varying the Heterostructure Thickness

Early work on heterostructures focused on the best performing PPV device up to that time, which was itself a heterostructure of PPV/SPS and PPV/poly(methacrylic acid) (PMA).[9] Subsequent studies showed the PPV/PMA combination to be less reproducible, so the PMA was replaced with PAA. These layers are slightly thicker than the PPV/PMA layers, but in general have very similar performance to the original devices.[10] The ruthenium complex used was the ruthenium(II) phenanthroline molecule that was the first compound investigated. This chromophore has both positive charges, due to the charged ruthenium core, and negative charges from the sulfonate groups attached to the phenyl rings on the ligands.

The first series done consisted of PPV/SPS and PPV/PMA heterostructures where the thickness of the PPV/SPS layer varied from 0 to 15 bilayers. The PPV/PMA was held constant at 20 bilayers. The thickness of the ruthenium phenanthroline layer was varied by

changing the spin rate of the coating process from 4000 rpm for a thin film, to 2000 rpm for a thicker film. The films made at those spin rates are 700Å and 1000Å thick respectively. The PPV layers were converted prior to spinning the ruthenium complex solution. Attempts to convert the PPV after ruthenium deposition resulted in degradation of the ruthenium layer due to the high temperatures and reactions with the THT leaving group of the PPV precursor. Some attempts were made to fabricate a fully layer-by-layer processed device using the ruthenium polyester with PAA. However, the degradation of the polyester with thermal treatment and the degradation of the converted PPV with exposure to aqueous solution caused all the devices to have poor performance.

Because we did not originally appreciate the implications of the electrochemical nature of the phenanthroline complexes, we thought the addition of a hole-transporting material would improve the performance of the device by eliminating the need for a long charging step and improving hole injection, thereby increasing efficiency and light output. Unfortunately, it did none of these things. For thicker layers of sulfonated phenanthroline, the device performance came closer to that of the control sample, but in general the devices showed quenched luminescence and dramatically higher turn-on voltages than $Ru(phen')_3$ alone without a platform. Interestingly, the thickness of the PPV/SPS layer did not seem to make much difference until 15 bilayers were reached. These layers behaved like a poor extension of the electrode, with little voltage drop supported across the layers, but with less efficient injection than before. Devices still showed the typical charging loop, although the characteristic charging times were similar to $Ru(phen')_3$ devices at lower voltages. For example, all of the PPV/SPS/PPV/PMA/Ru(II) devices at 8V behaved the same as the control device at 6V, except that the heterostructure was additionally quenched.

Because the PPV/PMA film quality became difficult to reproduce, samples of PPV/SPS alone were studied, again varying in thickness from 2 to 30 bilayers. In all cases the PPV/SPS behaved as a sluggishly polarizable electrode. Turn-on voltages were shifted from 2.5 to 3.5 or 4V regardless of device thickness. In addition, devices could withstand higher applied voltage, up to 9V rather than 6V for a neat phenanthroline film. However, the maximum light output, even at these higher voltages, was about half that of the $Ru(phen')_3$ alone. Examples of these runs are given in Figure 7-3. Efficiency values were approximately the same, indicating that the lower light in these samples was due to less efficient charge injection, rather than additional quenching. Some samples showed slightly higher efficiency, but no significant trend was exhibited. These samples also had slightly higher turn-on voltages, so perhaps less of the voltage dropped across the ruthenium in the more efficient devices. This correlation is consistent with the finding that device efficiency

of the ruthenium complexes depends on applied voltage, with lower voltages being more efficient.[11]

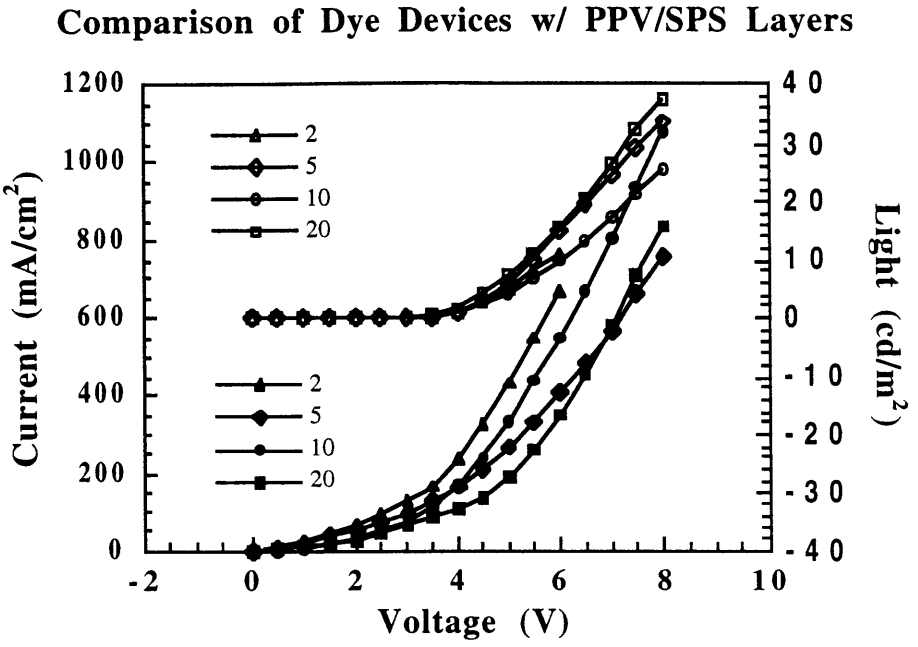

Figure 7-3. Current-voltage (open symbols) and light-voltage (closed symbols) curves for heterostructures of the ruthenium(II) phenanthroline complex on PPV/SPS layers. The thickness of the polymer layers were varied from 2 to 20 bilayers without much difference in device performance. These layers behave primarily as poor extensions of the electrode.

Lifetime studies on the heterostructure samples showed the same trend. Little distinction was made between PPV/SPS layer thickness, even up to 30 bilayers of SPS. Compared to $Ru(phen')_3$ alone, the films were less bright but could withstand higher voltages. From this information, it can be concluded that under normal room temperature DC device operation, polymer layers can oxidize the phenanthroline complex, albeit more slowly than ITO. The total device operates in an electrochemically active mode, with the PPV serving as a sluggishly polarizable electrode.

7.2.2 Varying the Ruthenium(II) Complex

Because the high current PPV/SPS platforms did not result in heterostructures with good device performance, we tried the alternate route with the higher efficiency PPV/PAA platforms. Here samples consisted of many different ruthenium complexes on a standard platform of 20 bilayers of PPV/PAA. Because the platform was extremely hydrophobic, the samples were dipcoated with one layer of poly(ethylene imine) (PEI) after thermal

conversion. This intermediary layer promoted adhesion of the ruthenium compounds which otherwise would bead up and roll off of the PPV films during the spinning process. A secondary effect of the PEI layer was to put a slight positive charge on the substrate. Most of the ruthenium complexes are also positively charged, although the solution also contains counterions to maintain electroneutrality. The slight repulsive forces may have caused some problems with film formation; however all films with the PEI layer were better than those without. The only complex that contained negative charges was the sulphonated phenanthroline, and this compound may have formed better films than the other systems. Evidence for this better film formation is the higher comparative efficiency of the phenanthroline devices as discussed in the conclusions to this section.

In general, the PPV/PAA films served to increase the turn-on voltage of the ruthenium complex and allowed the sample to support a higher voltage in general. When devices were inspected by eye, the heterostructures were universally red-light emitters although the control samples gave the green light characteristic of PPV. Interestingly, the turn-on voltage with the ruthenium complex in place was generally lower than a control sample with only PPV, despite the fact that the total film thickness approximately doubled. Unfortunately, the light output, turn-on voltage, and efficiency of the combinations were worse than in films with only the ruthenium complexes by themselves.

One aspect of device performance did change dramatically with the use of a heterostructure. In almost all cases, these samples did not charge. The only materials that still showed some hysteresis effects were the polymer systems, both the polyester and the polyurethane. The other materials showed only signs of degradation when held at a constant voltage. All samples were also tested with the pulsing protocol where the voltage is stepped directly to the maximum value rather ramped slowly. Even in this "fast pulse" mode, only the polymers showed signs of charging. This lack of charging indicates that the samples equilibrated either very quickly, faster than 5 seconds, or very slowly such that no change occurred during the few minutes of a voltage sweep. Because the polymer systems, which have lower ionic conductivity and generally slower response times, did show some signs of change, the initial light emission from the small molecules must be due to a fast process requiring less than 5 seconds to stabilize. However, because the overall light output is much lower than in a fully charged device, this faster mechanism should be only a small part of the normal operation mode for the ruthenium complexes alone.

A hypothesis that fits these criteria is that, at these short times and high voltages, the complexes support fast electron injection that does not require ion motion. Some evidence of this type of transport was inferred from the low temperature studies described in Chapter 6. Although direct electron hopping across the ligands is a higher energy

pathway than actual reduction stabilized by a counterion, it is an accessible mode of transport if given enough energy.[12, 13] The samples were pulsed to voltages between 20 and 28V, which impose enormous electric fields across devices only 2000Å thick. Initially most of the voltage will drop across the ruthenium layer because it begins as an insulating material. Sufficient energy for direct injection onto the ligands should be easily available in this case.

To probe this fast time response further, high frequency AC voltages were applied to the devices and the light response was measured. An AC bias of 4V for the control and 9V for the heterostructure was superimposed over a similar DC bias so that the total applied bias oscillated from 0 to 8V for the control or 0 to 18V for the heterostructure. In this way the device never experienced a negative bias, but the on/off switching response of the material could be monitored. The frequency of the signal was swept from 10^6 Hz to 20 Hz and then back to 10^6 Hz. In these studies, the light was averaged using a silicon photodiode so the real-time response was not monitored. Examples of the measurement are given in Figure 7-4 for a ruthenium trisbipyridyl heterostructure and control.

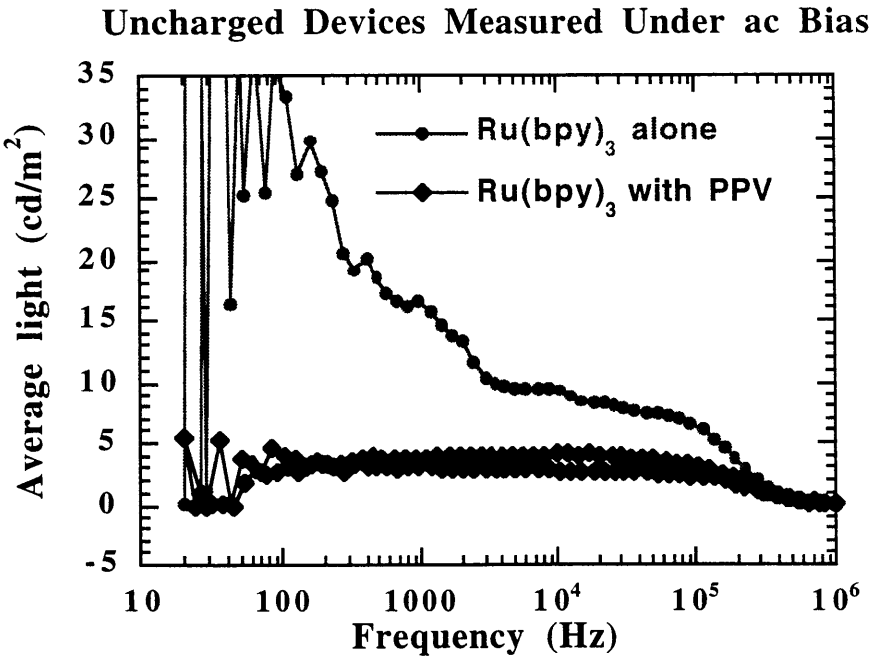

Figure 7-4. Ruthenium trisbipyridyl device tested under 0 to 8V AC bias in comparison with a heterostructure of Ru(bpy) with PPV tested under 0 to 18V AC bias as described in the text. Neither device experienced any voltage bias prior to the measurement. The light output was measured using an averaging silicon photodiode so the on-off nature of the light at low frequencies is reflected as lower values in the diode reading. The ruthenium complex alone gives more light at all frequencies, even before being allowed to charge.

Generally, the first pass at high frequency for the control samples would not allow for light emission of great magnitude because the device could not charge sufficiently under the high frequency signal. Subsequent scans showed significant charging and increased light. With the PPV heterostructure devices, the sample immediately gave the same performance it gave even after being allowed to equilibrate. All of the light was red, indicating charge or energy transfer to and emission from the ruthenium centers. However, although seeming to provide faster response, the level of light from the heterostructure was significantly lower than the control samples, such that more light was obtained from the control immediately even without being allowed to charge.

After having the AC bias applied for a few minutes, the ruthenium samples charged fully and were then able to be run at higher frequencies than either the PPV alone or the heterostructures. The heterostructure response was most likely limited by the need for holes to pass through the PPV layer which could no longer respond at these frequencies. A comparison of the fully charged devices is given in Figure 7-5. These high frequency

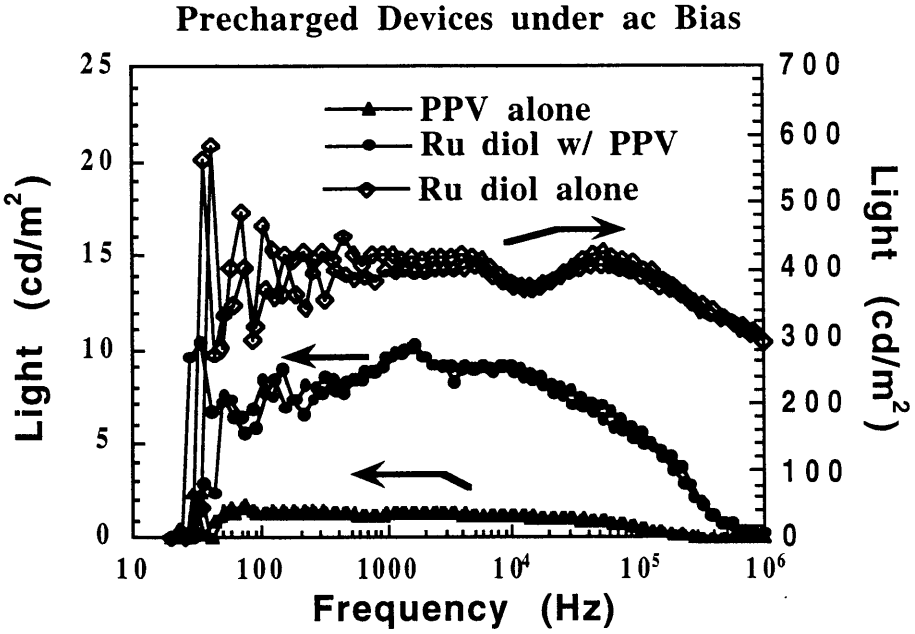

Figure 7-5. Frequency sweeps of heterostructure and control devices measured after samples were allowed to charge under DC bias. The heterostructure and PPV control were run under a 0 to 18V signal; the diol alone was operated from 0 to 8V. The diol device is much brighter than either of the other two devices (note change of scale) and continues to operate at the highest frequency. The heterostructure device is an improvement over PPV alone. Also of note is the apparent peak in light obtained around 10^5 Hz. This peak is discussed in Chapter 5 and is due to increased carrier injection at short times.

results are consistent with the fast time transients described in Chapter 5. However, the appearance of light at these frequencies does not mean that the device is cycling on and off at that rate. At sufficiently high frequencies, the lifetime of the excited states is such that a background DC signal becomes important as carriers that have not yet recombined during one cycle last through the "off" portion of the next cycle.[14]

If the heterostructure samples were held at a constant voltage, some slow charging was eventually observed. The onset voltage for this charging was much higher than the individual controls, and also depended on the thickness of the underlying PPV/PAA layer. For example, 2-bilayer devices behaved similarly to the control, with charging evident at 3V. The 5-bilayer device required 6V, the 10-bilayer required 8V, and the 15-bilayer device did not show significant charging until 10V were reached. This thickness dependence is likely due to varying amounts of the total voltage dropping across the PPV or the ruthenium(II) layer. The charging mechanism must have a certain voltage threshold, likely close to 3V, below which the conducting pathways cannot form. Another possibility is that the charge transfer from the polymer layer is a field-assisted process that requires a certain voltage gradient to allow significant injection. This type of voltage-gradient driven hopping was described in Chapter 5.

7.2.3 Conclusions

At first, the heterostructures appeared to improve the response time of the devices over the performance of the ruthenium(II) complexes alone. The addition of PPV as a hole-transporting material did highlight the fact that some initial transport of electrons is taking place in these ruthenium systems. This transport is likely the same as the initial current shown in Chapter 6 before the electrochemical injection process begins. In this respect, these heterostructures were important to lend further support to a picture of two modes of charge transport: first single carrier injection, then the traditional two-carrier oxidation and reduction.

However, the PPV layers were not very efficient at oxidizing the ruthenium so that very little of the potential of the ruthenium emitting layer was realized. At much higher voltages and longer times, the heterostructure device was able to charge somewhat in spite of the polymer platform, but the platform certainly did not aid in the process. The total light output of the heterostructure was always quenched with respect to the control samples, even at short times and high frequencies before the control was allowed to charge. Therefore, harvesting this fast-responding, single-carrier mechanism of charge transport will not lead to improvements in overall device performance under normal operating conditions.

One hindering factor may well have been the insulating PEI layer between the PPV and the ruthenium materials. PEI is known to have a fairly branched structure, and one layer may have been quite thick in some places. In addition, the slight positive charge may have forced ruthenium complexes slightly away from the interface. Support for this repulsion of the chromophores is the fact that the most efficient heterostructure was the one containing the negatively charged sulfonated phenanthroline complex which would be better attracted to the interface. The resulting device may have had more efficient charge injection into the ruthenium(II) layer even though the phenanthroline material as a whole is less efficient. Some improvement may be seen for the other materials if a negatively charged polymer such as PAA were used in place of the PEI. However, the heterostructure as a whole was primarily detrimental to the performance of the samples. Therefore, other methods of device improvement should be more profitable areas of research. Some suggestions for this improvement are given at the end of Chapter 8.

8. Conclusions and Future Work

Charge injection and transport has been investigated in many trischelated ruthenium(II) systems, and the data on four of them has been presented. In addition, some attempts have been made to improve device performance based on early concepts of the device mechanism. This chapter aims to summarize these findings generally for all systems, with the specific details for each complex enumerated at the end. Finally, some methods are described by which more information can be obtained from this existing data and some device improvement may be made.

8.1 Device Behavior in the Standard Mode

The evolution of the standard device at room temperature is as follows. For a fresh cell, the ions are distributed evenly throughout the device. A small space charge exists at the interfaces due to the equilibration of the two working electrodes. As long as the ionic content in the device is high (on the order of 10^{20} /cm^3), the space charge layer will be compensated by ions at the interface. The width of this layer can be calculated based on assumptions but is approximately the width of one monolayer of ions at the interface, or 10Å to 20Å thick. One interesting note is that this ionic layer at equilibrium will actually be of inverse charge to the one formed under applied bias, i.e. anions near the cathode, cations near the anode. This small space charge must be erased and then reversed when the bias is applied.

When the voltage is first applied, ions in the bulk have not yet had time to migrate through the device. This allows a large electric field to be distributed across the film. Charge injection at this point will be limited primarily to the interfaces because the ions necessary to stabilize homogeneous charge transfer according to Marcus theory have not yet redistributed themselves into a concentration gradient. Nucleation sites form where the necessary ionic motion is available, and percolation pathways of conducting sites grow through the film. Once they reach the opposite side of the sample, the pathways grow in diameter and begin to coalesce into larger-scale gradients of mixed valent states.

After the device is fully "charged" and all ion motion is complete, the current transport properties become diffusion limited. Charge transport then happens via homogeneous charge transport driven mainly by the voltage gradient imposed by voltage sweep rates faster than can be neutralized by the movement of the ions. These voltage-gradient driven curves can be fit to a modified Marcus transport equation, and the resulting diffusion constants are reported in the next sections. After charging, samples can be run under a square wave bias with instantaneous on/off switching up to 20 kHz. Above this

frequency, the lifetime of the excited states is longer than the voltage cycle so that a background DC signal is always present. In addition, the injection mechanism appears to be space charge assisted. The sample has high light output for the first milliseconds, followed by a fast decay to a steady state value. We explain this via partial compensation of the space charge by injected carriers that are slow to traverse the device. We assume that light emission occurs via the standard annihilation reaction of 3+ and 1+ species. All of our data is consistent with this mechanism of light emission.

8.2 Device Behavior under High Field, Limited Ion Movement

Generally, the low energy pathway for charge transport is through electrochemical oxidation and reduction to form mixed valence couples stabilized by counterion motion towards or away from the charged center. The highest light output has been obtained in devices under this mode of operation. However, when the electric field or potential gradient becomes high enough, charge carriers can be transported at temperatures and times where little ion motion is expected. The fastest device response has been measured in this fashion because no charging time is required to get maximum light emission.

During this high field response, we assume that the charges transported are only electrons on the ligand groups, because the ligand transport is most facile. Our hypothesis is supported by the fact that this current does not emit light. In addition, the use of a hole transport material allows for light emission in the absence of significant ion motion. The assumption then becomes that electrochemical behavior is the lowest energy pathway, although higher energy modes of direct electron hopping are accessible.

Additional support for this two phase model comes from heterostructure devices. At low biases, the device behavior has little hysteresis, similar to that from a PPV device alone. At higher biases however, the voltage drop across the ruthenium(II) layer is high enough to begin some ionic movement and charging of the device. This cross-over voltage changes with device thickness, as would be expected.

8.3 Total Device History

For each of the systems evaluated in this project, the same basic processes must occur, as outlined in the sections above. The major difference between the systems is that, dependent upon the ionic conductivity in the film (both concentration and mobility of the available ions), the time or voltage required to transition from one stage to another will change. This section aims to summarize the findings for each device system, including the characteristic device constants where available.

8.3.1 The Trisbipyridyl Ruthenium(II) Diol

The diol is our most idealized system. Ionic conductivity is high relative to the other systems (around 10^{-8} S/cm) and therefore the space charge layer forms within the five seconds of delay in our measurement procedure. However, the formation of the mixed valence states within the film is a significant barrier to charge injection and overall device performance. The time required to reach maximum current in the film has an exponential voltage dependence typical of the nucleation and growth of percolation pathways. Once the pathways are set, they will remain viable for about a minute after the applied voltage is removed. This characteristic is shown in the slow decay of capacitance after a voltage pulse is applied to the film.[1] The species responsible for the characteristic time to form these conducting pathways is likely a very slow moving population of ions in the bulk of the film. Once injection has occurred and the device is fully "charged," device response is very rapid, with operation possible above 100 kHz. The final diffusion constant is the highest of any of the systems, with the lowest activation energy at 1.7 kJ/mol. Examination of transient peaks show that this fast response is now charge transport limited.

If operated at low temperatures to quench the ionic mobility, the characteristic time constants for the diol will change dramatically. In this regime, around 180K, the injection process takes 20 minutes rather than 3 minutes when held at 4V. If cooled further, the ionic conductivity is so low that only very low currents are possible unless conducting paths have been formed at room temperature. No light is possible in this regime. Therefore, only one species, likely the reduced complex, is present in the film. The mode of transport has shifted to delocalized electron hopping across the ligands, and the current is always injection limited.

8.3.2 The Sulfonated Ruthenium(II) Trisphenanthroline

Although this system has not been as fully characterized as the diol, the available data is fully consistent with the proposed outline of device evolution. The "charging" time is approximately 3 minutes, similar to the diol, likely because the mobility of both systems are comparable. After charging, the diffusion constants are slightly lower and the activation energy is slightly higher, at 3.2 kJ/mol, than for the diol system. This decrease in electron mobility is due to the increased separation between redox sites from the bulkier phenyl rings on the dye ligand in comparison with the bipyridyl diol. The increased conductivity of the "charged" state relaxes within several minutes, but if voltage is continually applied, the high frequency response is similar to the diol. The low temperature behavior also follows that of the diol, with current in both forward and reverse bias down

to 80K. No light is emitted without the prior conditioning at room temperature, until some charging begins around 180-220K.

Blends of this complex with PEO, a flexible ion-conducting polymer, do not significantly effect either the charging time or the activation energy for electron-hopping. In addition, the temperature at which charging begins does not change much. One possibility is that the blend is somewhat phase-separated so that the higher mobility of the polymer does not have much influence on the more tightly packed regions of the phenanthroline complex. The dense areas would be expected to have faster electron hopping and would therefore dominate the final device performance. This inhomogeneity is demonstrated in a higher value of ρ (the non-ideal dispersive current factor) than for the diol.

Although the photoluminescent quantum efficiency of this molecule is higher than the diol in solution, the electroluminescence was an order of magnitude less efficient, around 0.1% external quantum efficiency. Very recent solution work on related molecules indicates that the phenyl rings may twist to be coplanar with the phenanthroline group in the excited state, but relax to the transverse in the ground state.[2] This required rotation may hinder device performance when mobility is limited in the solid state. The bulky nature of the phenyl rings may also contribute to the relatively poor film quality that was seen in pure films of this complex.

Ambiguity about the nature and concentration of ions made conclusions about ionic conductivity difficult. Recall that we have evidence that some of the small sodium and chlorine ions complex together and are washed away, complicating estimations of ionic concentration. Presumably sufficient ions remained to form the double layer because the addition of small ions did not change the turn-on voltage. However, inclusion of the molecule in a PEO blend also raises questions about phase separation as noted above. The phenanthroline and associated salts could be clustering into clumps throughout the film rather than forming a homogeneous mixture. In general, this system ended up being our most complicated system to understand.

8.3.3 The Spin-cast Polyurethane

Following the trend of the previous two materials, the polyurethane seems to have little trouble forming a space charge layer, and in the "charged" state it becomes transport limited. The diffusion constants are the lowest measured, with the highest activation energy, at 20 kJ/mol. However, all values are not greatly different from those of the small molecules, especially considering the increase in redox site separation due to the addition of carbon spacers in the polymer. The large change in this system relative to the others is the

time required for the transition to the conducting state. At voltages near the redox potential, 3-4V, charging is exceptionally slow with almost no current able to cross the film. Even at voltages well above the energy gap, 8-10V, the percolation pathways require approximately 20 minutes to form. The ionic conductivity is lower in the polyurethane than in the small molecules, around 10^{-9}, however the characteristic diffusion required for motion on the timescale of 20 minutes would be near 10^{-18}. This diffusion constant is on the order of what could be expected for the movement of polymer segments through the film. Perhaps the formation of conductive areas in the film actually requires motion of the redox sites themselves into specific regions, similar to a phase separation process, rather than merely the migration of the small ions.

Due to other trends of differences in materials constants between surface properties and properties of the bulk, it is reasonable to consider two populations of ions in the polymer films: one with high mobility at the interface, and one with lower mobility within the material. These two populations could account for the apparently fast charging of the double layer at the interface, as compared with the very long development of conduction in the bulk.

8.3.4 Sequentially Adsorbed Polyester Films

Because these films are fabricated by the use of polymeric (or at least oligimeric) electrolytes with ionic crosslinks between the layers, they are expected to have both the lowest concentration and lowest mobility for ions of any of the systems studied. The ionic conductivity is commensurately low, at 10^{-12} S/cm. Even this level of conductivity should allow for enough ions to form a suitable space charge layer, and the films made with PAA show the symmetric behavior characteristic of being independent of the nature of the electrode. Here, some limited protonic conduction may take place across the remnant carboxylic acid groups that were not used in the sequential adsorption process. However, for the films deposited using the strong acid SPS, the space charge layer does not seem to form. The strong acid nature of the SPS could result in tight association between the sulfonic acid groups and the ruthenium centers, allowing for very little rotational freedom and very few free ions to contribute to ionic conduction. These films are completely rectifying until much higher voltages, which could be due to a dependence of injection on the work function of the electrode. The lack of mobile ions in the SPS films causes any space charge layer that does form to be distributed over a thicker region of the film and is therefore less effective in reducing the barrier to injection.

The primary issue with these films is the transition between insulating and conducting material. The films formed with the weak poly(acrylic acid) could potentially

have enough protonic conduction to facilitate the formation of percolation regions. However, the redox sites are even further separated than in the polyurethane case, and the mixed valence states are even more difficult to stabilize in this matrix. The samples with less than 50% polymer are particularly dilute, but even the devices with 70 or 80% polyester contain more insulating material than the small molecule systems. Due to these restrictions, these films are likely to remain injection limited until very high overpotentials are reached. This observation is consistent with the high turn-on voltages (8-10V) necessary for current and light in these films. Most of the device performance is likely limited to high energy activated hopping between small clusters of species that coincidentally happen to be in close proximity within the sample.

This device picture should lead to very low diffusion constants with much higher activation energies than any of the previous materials. These factors also lead to such low levels of current that the materials constants can not be reliably obtained with the current sensitivity of our equipment. Because such high potentials are required to run the device, many percolation pathways are likely to be nucleated simultaneously. This high nucleation rate allows for a more uniform progression of charge through the film, causing light emission more evenly through the area of the device. This condition also makes it more likely for the two concentration gradients to intersect rather than bypassing each other and causing leakage current through the film. The fact that the highest efficiency devices are in this system could be partially attributable to this more uniform injection path.

A secondary effect should be considered in the increased efficiency for the sequentially adsorbed layers. The carbon spacers between ruthenium centers in these systems could allow a better balance between the two rates of transport. This distance effect has been seen by Jernigan et al. in the study of solvated and dried films of redox active osmium polymers. The diffusion rates of the reduced species increase upon drying and compaction of the film, whereas the diffusion rates of the oxidized species decrease. The authors attribute this difference to the physical separation of the complexes; in the dried state the ligand-centered reduction transition is easier because of the closer proximity of neighboring carbon rings, but the metal center has lost the mobility needed to allow for thermal excitations that decrease the jump distance for oxidative hopping.[3] As the species are separated, the two rates become more equal, improving the efficiency of the device.

Also of note is the single turn-on observed in these films. The very low levels of leakage current in the small molecule systems have been effectively eliminated through the superior film quality produced by the layer-by-layer process. Finally we note that the photoluminescence of the sequentially adsorbed films is also enhanced relative to the

spincoated version of the same material. The dilution may serve to reduce self-quenching between ruthenium centers and improve light emission by that mechanism as well.

8.4 Suggestions for Future Study

Much of this thesis has been devoted to the sketching of a basic picture of the process of charge injection and transport in these devices resulting in light emission. A good framework has been set for the design of new experiments to fill in some of the details. Some of these experiments will require new equipment or testing procedures; however, many of the suggestions need minimal modifications to the existing setup to provide crucial data.

8.4.1 Current Transients

An important piece of information currently lacking in this data set is the current behavior at short times. The light response to the square wave pulse provides the general time dependence of the injection and transport, but to derive measurable constants we require the actual values of the current. In addition, current information at very short times will give information about capacitive charging of the interface. In theory, the formation of the space charge layer should be accompanied by an immediate capacitive current. However, the available resolution of our time measurements is not sufficient to catch this fast decay. The function generator is capable of generating very high frequency pulses, but we require a circuit to transform the resulting current to a voltage so we can monitor it on the oscilloscope.

8.4.2 Internal Electric Field Determination

A key question remaining in these samples is the degree of electric field remaining in the sample in the steady state. Knowledge of the magnitude of the field and the way it changes over time will yield important information to enable better analysis of the current-time behavior in these samples. If the field goes to zero within the film, the current must be analyzed in terms of concentration gradient driven transport at long times. The concentration of ions should be sufficient to allow for this counterbalance to occur, but the characteristic current limit indicating concentration-gradient driven diffusion has not been observed.

One possible method to monitor this decay has been described by Jernigan.[4] The experiment involves placing three identical samples in series, applying a voltage across the external leads and monitoring the resulting voltage across the internal leads. When the voltage drops across the entire series evenly, approximately one third of the applied bias

will be measured across the middle device. However, when the ions are able to balance the field, only a small fraction of the applied voltage is found to fall across the center. If three samples of the ruthenium system are linked in this way, we may be able to determine if most of the voltage in the center of the device is balanced by ion movement, and if so, how long it takes for the field to decay to zero.

Another idea to monitor the progression of ion movement in the device is to monitor the capacitance over the lifetime of a sample. If the decay in current is due to a slow decay in a remnant electric field that is slowly balanced by the movement of ions in the bulk, the capacitance of the device should show a similar steady increase. This increase should result from the excess charge that can be supported on the electrodes as the additional ions migrate to the interface.

8.4.3 Ligand-based Transport

Several explanations for the lack of light in reverse bias and at low temperatures have been suggested. The most controversial is the violation of local electroneutrality to allow for electron-only transport under these situations. One method to probe this theory would be the monitoring of the electric field within the device, because with local electroneutrality the field should drop to zero.

An additional measurement to probe the existence of reduced species in the device is the technique of spectroelectrochemistry. This measurement consists of monitoring the absorption characteristics of a sample while the electrochemical reactions are taking place. The oxidized and reduced species have distinctive absorption bands, and their relative ratio can be determined from the magnitude of the peaks.[5] p577. If the metal cathode is made quite thin, this type of measurement could likely be made on the equipment already in use by our group. Care must be taken to protect the detector from the higher intensity light given off by the electroluminescence of the ruthenium systems. However, because the emission and absorption bands are separated by 200 nm or so, the emission should not interfere with the spectroelectrochemical signal. We can then monitor the device for the presence of 3+ species as we attempt oxidation from the aluminum electrode. The results can be verified by using platinum as the electrode which would normally allow for light emission in reverse bias.

8.4.4 Unipolar Devices

One of the critical difficulties encountered in the analysis of the data from these devices was the presence of two sets of charge carriers contributing to the light and the current. Because the resulting data is a combination of the two, specific materials constants

relating to the individual transport cannot be calculated. In addition, little concrete evidence can be provided for the relative rates between electron and hole hopping in these specific materials under these conditions. If a device can be fabricated that allows for the transport of only electrons or only holes, the individual heterogeneous and homogeneous charge transfer rates can be calculated. Then the values for the other carrier can be calculated from the combined data.

If the lack of light in reverse bias at room temperature is in fact due to preferential oxidation of the aluminum electrode, reverse bias studies may serve as a method for calculating electron-only materials parameters. These samples must be carefully prepared to exclude moisture because water will react at the aluminum interface to form an insulating oxide. Other, more stable, materials systems would be a better choice for these investigations, but for preliminary results, reverse bias measurements would be an easy extension of the current work.

8.4.5 Percolation Theory Predictions

Little concrete proof has been offered for the existence of percolation networks in our samples. The device behavior does follow the voltage and thickness dependencies stipulated by redox switching theory, and the light emission does appear to be speckled. However, other explanations could account for these characteristics. Experiments should be designed to systematically probe the mechanisms of formation and growth of these pathways to show that they exist.

One approach would be to increase the number of nucleation sites at the interface. The etching of the ITO substrate in acid supports the idea that a more rough surface will provide more nucleation sites. The resulting increase in efficiency would then be due to a more even progression of charge through the film, rather than isolated pathways that could miss each other and contribute to leakage current. The intentional addition of heterogeneous nucleation sites, such as metallic particles to increase the local electric field, would be expected to have similar effects on the efficiency.

Another test of this theory would be the monitoring of the device under the microscope over time. The speckling apparent by eye should be able to be more readily quantified. In addition, if percolation is required every time the device is charged, the emission should always begin in sections and then grow to fill the entire cell. If later runs on the device show the same charging time dependence but light emission is more uniform, some other mechanism must be the rate limit in this case.

8.4.6 Injection Limited Behavior

At very short times, the device should be injection limited and so Butler-Volmer kinetics should apply. However, the transition from insulating to conducting material interferes with the clear measurement of this process. The transient square wave pulse should provide important information about the injection process at short times, without the charging limitations. If the square wave pulse is applied at different biases, the value of the current at the peak of the transient should fit to the Butler-Volmer theory. The data available at the moment is from a sine wave, so the fast time transient due to the immediately applied high bias is lost. Once current can be monitored during this transient, the data to test this theory should be easy to measure.

8.4.7 Heterogeneous Charge Transfer

The rate constant for heterogeneous charge transfer from the electrode to the ruthenium complex should be readily available from impedance spectroscopy. If the data is analyzed as a Cole-Cole plot, the charge transfer resistance is given by the diameter of the curve corresponding to the interface, and the frequency of the maximum of that curve will yield the rate of charge transfer. A good review of this procedure is given in the reference by Lyons.[6] p466.

8.4.8 Device Response Time Improvement

The rest of these suggestions have been primarily aimed at increasing the scientific knowledge base about these materials, but part of the goal of this thesis was to improve the engineering performance of these devices as well. To that end, I attempted to use the fast response mode of the ruthenium(II) complexes as electron transporters in a heterostructure with PPV as the hole transport agent. Unfortunately, as discussed in Chapter 7, this fast transport mode does not provide the high light output or efficiency of the devices in the more traditional electrochemical mode. Therefore, increasing the rate of the insulator/conductor transition seems to be the most promising avenue of research.

One approach to this problem is to increase the surface area of the oxidizing electrode to provide more sites from which to start conducting paths through the sample. A method of accomplishing this could be the addition of conducting polymer, such as PAni, to the ITO interface. However, as noted in Chapter 7, if the layer is coherent, it will interfere with the charge transfer from the ITO. Therefore, we propose a loose network of conducting polymer molecules, backfilled with the active ruthenium(II) species. If the network is loose enough, contact can still be made from the ITO. The main purpose of the polymer would then be to attract ions in the bulk of the film to provide a concentration of

ions in a pathway that would then support easier formation of the mixed valence states. This designed inhomogeneity may speed up the perceived charging time of the device.

Appendix A

In order to monitor the position of the recombination zone, some work was done using interdigitated electrodes rather than our previous sandwich device structure. The electrodes were gold separated by 5 micron gaps on a silicon substrate. A 4 wt% solution of the ruthenium(II) phenanthroline complex was spun from 2-methoxyethanol to coat the electrode array. The sample was then annealed in the vacuum oven and observed under an optical microscope to verify that a thin film of the ruthenium(II) material covered the entire gap to avoid shorting or open circuits. The samples were then tested in the equipment setup used by the Bawendi group at MIT in collaboration with Stephen Empedocoles.

To align the sample, the material was illuminated with white light and the photoluminescence from the ruthenium centers was collected by a CCD camera so that spatial resolution could be obtained. This PL spectrum is the top graph on the following page. Because the ruthenium(II) complex was deposited both on top of and in between the electrodes, PL is emitted from the entire sample. However, PL from electrode regions is brighter, because light that would be lost to absorption by the substrate will be reflected by the metal surface, and more of the emitted light will reach the detector. The electrode edges can then be spatially located by this variation in the PL spectrum. Note that in this cross-section two full and two partial electrodes can be seen. Because they are interdigitated, the strips will carry alternating polarity under voltage bias, and the electric field will be applied along the x-direction of this graph.

After the sample was satisfactorily aligned, a voltage was applied across the electrodes and the electroluminescence was monitored. The EL spectrum is the bottom graph on the following page, with the regions of highest brightness marked with vertical lines to guide the eye. The light is close to the edges of every other electrode, therefore, the recombination zone occurs closer to one polarity than the other. Based on the wiring of the electrodes, this electrode appears to be the cathode. This result is consistent with the idea that the reduction happens faster and travels farther through the film to recombine near the oxidizing electrode. The light was fairly unstable because the sample was run in air, so a new sample had to be made to check each measurement. Therefore these results are not conclusive, however, they are consistent with a possible violation of the conditions of electroneutrality in these films.

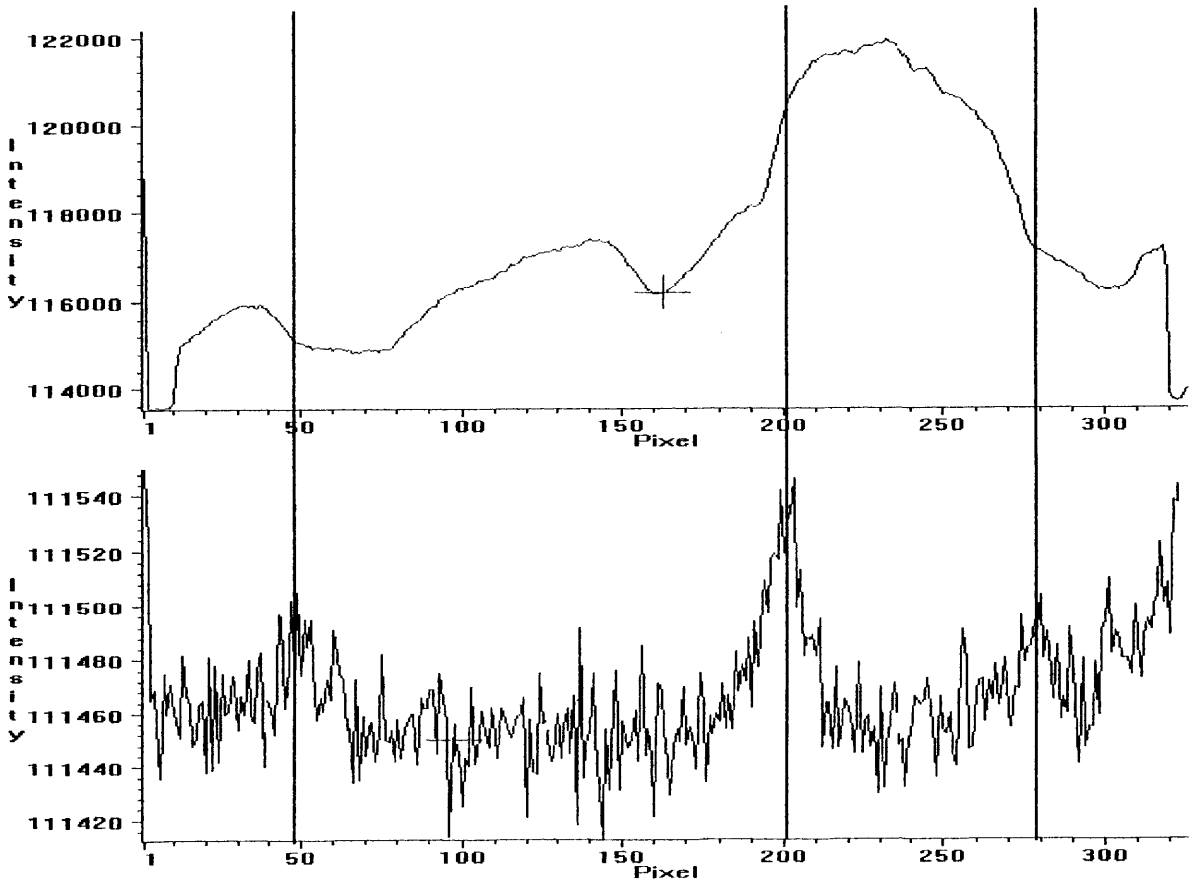
122000
120000
118000
116000
114000
Intensity
1
50
100
150
200
250
300
Pixel
111540
111520
111500
111480
111460
111440
111420
Intensity
1
50
100
150
200
250
300
Pixel

9. References

Chapter One

1. N. E. Tokel and A. Bard, Journal of the American Chemical Society, 1972. **94**, 2862.
2. C. W. Tang and S. A. VanSlyke, Applied Physics Letters, 1987. **51**, 913.
3. J. H. Burroughes, Nature, 1990. **347**, 539.
4. C. Hosokawa, IS&T's 49th Annual Conference Proceedings, 1994, 388.
5. K. Pichler, IS&T's 49th Annual Conference Proceedings, 1994, 404.
6. C. Zhang, Synthetic Metals, 1994. **62**, 35.
7. D. D. C. Bradley, Synthetic Metals, 1993. **54**, 401.
8. I. D. Parker, Journal of Applied Physics, 1994. **75**(3), 1656.
9. R. H. Friend, Journal of Physics D: Applied Physics, 1987. **20**, 1367.
10. D. Neher, J. Gurner, V. Cimrova, W. Schmidt, R. Rulkens and U. Lauter, Polymers for Advanced Technologies, 1998. **9**, 461.
11. N. C. Greenham, R. H. Friend and D. D. C. Bradley, Advanced Materials, 1994. **6**, 491.
12. Q. Pei, G. Yu, C. Zhang, Y. Yang and A. J. Heeger, Science, 1995. **269**, 1089.
13. A. J. Bard and L. R. Faulkner, *Electrochemical Methods: Fundamentals and Applications*. 1980, New York: John Wiley and Sons.
14. Y. Cao, G. Yu, A. J. Heeger and C. Y. Yang, Applied Physics Letters, 1996. **68**(23), 3218.
15. Q. Pei, Y. Yang, G. Yu, C. Zhang and A. J. Heeger, Journal of the American Chemical Society, 1996. **118**, 3922.
16. J. C. deMello, N. Tessler, S. C. Graham and R. H. Friend, Physical Review B, 1998. **57**(20), 12.
17. D. L. Smith, Journal of Applied Physics, 1997. **81**(6), 2869.
18. M. E. G. Lyons. *Fundamentals*. Electroactive Polymer Electrochemistry, ed. M. E. G. Lyons. Vol. 1. 1994, Plenum Press: New York.
19. D. M. Roundhill, *Photochemistry and Photophysics of Metal Complexes*. Modern Inorganic Chemistry, ed. Jr. Fackler, John P. 1994, New York: Plenum Press.
20. E. F. Dalton, J. C. Surridge, J. C. Jernigan, K. O. Wilbourn, J. S. Facci and R. W. Murray, Chemical Physics, 1990. **141**, 143.
21. K. M. Maness, R. H. Terrill, T. J. Meyer, R. W. Murray and R. M. Wightman, Journal of the American Chemical Society, 1996. **118**, 10609.
22. R. H. Terrill, J. E. Hutchison and R. W. Murray, Journal of Physical Chemistry B, 1997. **101**, 1535.
23. C. S. Sosnoff, M. Sullivan and R. W. Murray, Journal of Physical Chemistry, 1994. **98**, 13643.
24. M. G. Sullivan and R. W. Murray, Journal of Physical Chemistry, 1994. **98**, 4343.
25. H. Scher and E. W. Montroll, Physical Review B, 1975. **12**(6), 2455.
26. G. Pfister, Physical Review B, 1977. **16**(8), 3676.
27. D. Yoo, J.-K. Lee, E. S. Handy and M. F. Rubner, Applied Physics Letters, 1996. **69**, 1.
28. C. H. Lyons, E. D. Abbas, J.-K. Lee and M. F. Rubner, Journal of the American Chemical Society, 1998. **120**(46), 12100.

29. E. S. Handy, A. J. Pal and M. F. Rubner, Journal of the American Chemical Society, 1999. **121**(14), 3525.
30. J.-K. Lee, D. Yoo and M. F. Rubner, Chemistry of Materials, 1997. **9**, 1710.
31. E. S. Handy, *Structural Design of Tris(bipyridyl)ruthenium(II) Derivatives for High-Performance Solid-State Light-Emitting Devices,* Chemistry, MIT, Cambridge, 1999.
32. M. E. Williams, private communication, 1998.
33. A. Wu, J.-K. Lee and M. F. Rubner, Thin Solid Films, 1998.
34. A. Wu, D. Yoo, J.-K. Lee and M. F. Rubner, Journal of the American Chemical Society, in submission.

Chapter Two

1. N. E. Tokel and A. Bard, Journal of the American Chemical Society, 1972. **94**, 2862.
2. W. L. Wallace and A. J. Bard, J. Phys. Chem., 1979. **83**, 1350.
3. P. McCord and A. J. Bard, Journal of Electroanalytical Chemistry, 1991. **318**, 91.
4. A. Kapturkiewicz, Chemical Physics Letters, 1995. **236**, 389.
5. J. C. Jernigan and R. W. Murray, Journal of the American Chemical Society, 1987. **109**, 1738.
6. D. M. Kelly and J. G. Vos, *Osmium and Ruthenium Poly(pyridyl) Redox Polymers as Electrode Coatings*, in *Electroactive Polymer Electrochemistry: Part 2 Methods and Applications*, Michael E. G. Lyons, Editor. 1996, Plenum Press: London. p. 173.
7. R. Jiang and F. C. Anson, Journal of Physical Chemistry, 1991. **95**, 5701.
8. M. J. Cook, A. P. Lewis, G. S. G. McAuliffe, V. Skarda and A. J. Thomson, Journal of the Chemical Society Perkins Transactions 2, 1984. **8**, 1293.
9. D. Laser and A. Bard, J. Electrochem. Soc., 1975. **122**(5), 632.
10. L. R. Faulkner and A. J. Bard, in *Electroanalytical Chemistry*, A. J. Bard, Editor. 1977, Dekker: New York.
11. G. H. Brilmyer and A. J. Bard, J. Electrochem. Soc., 1980. **127**(1), 104.
12. H. Schaper, J. Electroanal. Chem., 1981. **129**, 335.
13. E. Hill, E. Humphreys and D. J. Malcome-Lawes, J. of Chromatography, 1986. **370**, 427.
14. H. Schaper and E. Schnedler, J. Phys. Chem, 1982. **86**, 4380.
15. I. Rubinstein and A. J. Bard, Journal of the American Chemical Society, 1980. **102**, 6641.
16. I. Rubinstein and A. J. Bard, Journal of the American Chemical Society, 1981. **103**, 5007.
17. D. A. Buttry and F. D. Anson, Journal of the American Chemical Society, 1982. **104**, 4824.
18. E. F. Dalton, J. C. Surridge, J. C. Jernigan, K. O. Wilbourn, J. S. Facci and R. W. Murray, Chemical Physics, 1990. **141**, 143.
19. P. Daum and R. W. Murray, Journal of Physical Chemistry, 1981. **85**, 389.
20. J. C. Jernigan, C. E. D. Chidsey and R. W. Murray, Journal of the American Chemical Society, 1985. **107**, 2824.
21. K. M. Maness, R. H. Terrill, T. J. Meyer, R. W. Murray and R. M. Wightman, Journal of the American Chemical Society, 1996. **118**, 10609.
22. N. A. Surridge, M. E. Zvanut, F. R. Keene, C. S. Sosnoff, M. Silver and R. W. Murray, Journal of Physical Chemistry, 1992. **96**, 962.

23. C. E. D. Chidsey and R. W. Murray, Journal of Physical Chemistry, 1986. **90**, 1479.
24. J. M. Saveant, Journal of Electroanalytical Chemistry, 1986. **201**, 211.
25. R. J. Forster, A. J. Kelly, J. G. Vos and M. E. G. Lyons, Journal of Electroanalytical Chemistry, 1989. **270**, 365.
26. P. J. Peerce and A. J. Bard, Journal of Electronanalytical Chemistry, 1980. **114**, 89.
27. R. J. Forster, J. G. Vos and M. E. G. Lyons, Journal of the Chemical Society Faraday Transactions, 1991. **87**(23), 3769.
28. J. S. Facci, R. H. Schmehl and R. W. Murray, Journal of the American Chemical Society, 1982. **104**, 4959.
29. R. J. Forster and J. G. Vos, Journal of the Electrochemical Society, 1992. **139**(6), 1503.
30. X. Zhang and A. J. Bard, Journal of Physical Chemistry, 1988. **92**, 5566.
31. Y. S. Obeng and A. J. Bard, Langmuir, 1991. **7**(1), 195.
32. R.-J. Lin, T. Onikubo, K. Nagai and M. Kaneko, Journal of Electroanalytical Chemistry, 1993. **348**, 189.
33. C. S. Sosnoff, M. Sullivan and R. W. Murray, Journal of Physical Chemistry, 1994. **98**, 13643.
34. R. H. Terrill, J. E. Hutchison and R. W. Murray, Journal of Physical Chemistry B, 1997. **101**, 1535.
35. R. A. Denny and M. V. Sangaranarayanan, Journal of Physical Chemistry B, 1998. **102**, 2131.
36. H. D. Abruna, T. J. Meyer and R. W. Murray, Inorganic Chemistry, 1979. **18**, 3233.
37. X.-H. Xu and A. J. Bard, Langmuir, 1994. **10**, 2409.
38. M. G. Sullivan and R. W. Murray, Journal of Physical Chemistry, 1994. **98**, 4343.
39. J. C. Jernigan and R. W. Murray, Journal of Physical Chemistry, 1987. **91**, 2030.
40. C. P. Andrieux and J. M. Saveant, Journal of Physical Chemistry, 1988. **92**, 6761.
41. J. M. Saveant, Journal of Electroanalytical Chemistry, 1988. **242**, 1.
42. G. Pfister, Physical Review B, 1977. **16**(8), 3676.
43. H. Scher and E. W. Montroll, Physical Review B, 1975. **12**(6), 2455.
44. K. M. Maness, H. Masui, R. M. Wightman and R. W. Murray, Journal of the American Chemical Society, 1997. **119**, 3987.
45. F. Pichot, C. J. Bloom, L. S. Rider and C. M. Elliott, Journal of Physical Chemistry B, 1998. **102**, 3523.
46. M. M. Richter, F.-R. F. Fan, F. Klavetter, A. J. Heeger and A. J. Bard, Chemical Physics Letters, 1994. **226**, 115.
47. J. C. deMello, N. Tessler, S. C. Graham and R. H. Friend, Physical Review B, 1998. **57**(20), 12.
48. D. L. Smith, Journal of Applied Physics, 1997. **81**(6), 2869.
49. G. Yu, Y. Cao, M. Andersson, J. Gao and A. Heeger, Advanced Materials, 1998. **10**(5), 385.
50. Q. Pei, Y. Yang, G. Yu, C. Zhang and A. J. Heeger, Journal of the American Chemical Society, 1996. **118**, 3922.
51. Q. Pei, G. Yu, C. Zhang, Y. Yang and A. J. Heeger, Science, 1995. **269**, 1089.
52. D. J. Dick, A. J. Heeger, Y. Yang and Q. Pei, Advanced Materials, 1996. **8**(12), 985.
53. I. Riess and D. Cahen, Journal of Applied Physics, 1997. **82**(6), 3147.

54. I. Riess, Journal of the Physical Chemistry of Solids, 1986. **47**(2), 129.
55. I. Riess, Physical Review B, 1987. **35**(11), 5740.
56. I. Riess, Solid State Ionics, 1994. **69**, 43.

Chapter Three

1. E. S. Handy, *Structural Design of Tris(bipyridyl)ruthenium(II) Derivatives for High-Performance Solid-State Light-Emitting Devices,* Chemistry, MIT, Cambridge, 1999.
2. E. S. Handy, A. J. Pal and M. F. Rubner, Journal of the American Chemical Society, 1999. **121**(14), 3525.
3. J.-K. Lee, D. Yoo and M. F. Rubner, Chemistry of Materials, 1997. **9**, 1710.
4. D. Yoo, J.-K. Lee, E. S. Handy and M. F. Rubner, Applied Physics Letters, 1996. **69**, 1.
5. G. Decher and J.-D. Hong, Makromol. Chem., 1991. **46**, 321.
6. G. Decher and J. D. Hong, Ber. Bunsenges. Phys. Chem., 1991. **95**, 1430.
7. G. Decher, J. D. Hong and J. Schmitt, Thin Solid Films, 1992. **210/211**, 831.
8. A. Wu, J.-K. Lee and M. F. Rubner, Thin Solid Films, 1998.
9. A. Wu, D. Yoo, J.-K. Lee and M. F. Rubner, Journal of the American Chemical Society, in submission.
10. A. C. Fou, O. Onitsuka, M. Ferreira and M. F. Rubner, Journal of Applied Physics, 1996. **79**(10), 7501.
11. M. F. Durstock, *Light Emitting Characteristics and Dielectric Properties of Polyelectrolyte Multilayer Thin Films,* Materials Science and Engineering, MIT, Cambridge, 1999.
12. J. Baur, *Fabrication and Structural Studies of Sequentially Adsorbed Polyelectrolyte Multilayers,* Materials Science and Engineering, MIT, Cambridge, MA, 1997.
13. D. Yoo, A. Wu, J.-K. Lee and M. F. Rubner, Synthetic Metals, 1997. **85**, 1425.
14. N. C. Greenham, R. H. Friend and D. D. C. Bradley, Advanced Materials, 1994. **6**, 491.

Chapter Four

1. I. Riess, Solid State Ionics, 1994. **69**, 43.
2. J. C. deMello, N. Tessler, S. C. Graham and R. H. Friend, Physical Review B, 1998. **57**(20), 12.
3. D. L. Smith, Journal of Applied Physics, 1997. **81**(6), 2869.
4. J. Schmitt, T. Grunewald, G. Decher, P. S. Pershan, K. Kjaer and M. Losche, Macromolecules, 1993. **26**(25), 7058.
5. M. F. Daniel, B. Desbat and J. C. Lassegues, Solid State Ionics, 1988. **28-30**, 632.
6. M. F. Durstock, *Light Emitting Characteristics and Dielectric Properties of Polyelectrolyte Multilayer Thin Films,* Materials Science and Engineering, MIT, Cambridge, 1999.
7. D. Neher, J. Gurner, V. Cimrova, W. Schmidt, R. Rulkens and U. Lauter, Polymers for Advanced Technologies, 1998. **9**, 461.
8. A. J. Bard and L. R. Faulkner, *Electrochemical Methods: Fundamentals and Applications.* 1980, New York: John Wiley and Sons.
9. Y. Tezuka and K. Aoki, Journal of Electroanalytical Chemistry, 1989. **273**, 161.
10. K. Aoki and Y. Tezuka, Journal of Electroanalytical Chemistry, 1989. **267**, 55.

11. M. E. G. Lyons. *Fundamentals*. Electroactive Polymer Electrochemistry, ed. M. E. G. Lyons. Vol. 1. 1994, Plenum Press: New York.

Chapter Five

1. E. F. Dalton, J. C. Surridge, J. C. Jernigan, K. O. Wilbourn, J. S. Facci and R. W. Murray, Chemical Physics, 1990. **141**, 143.
2. J. C. Jernigan, N. A. Surridge, M. E. Zvanut, M. Silver and R. W. Murray, Journal of Physical Chemistry, 1989. **93**, 4620.
3. J. C. Jernigan, C. E. D. Chidsey and R. W. Murray, Journal of the American Chemical Society, 1985. **107**, 2824.
4. F. Pichot, C. J. Bloom, L. S. Rider and C. M. Elliott, Journal of Physical Chemistry B, 1998. **102**, 3523.
5. E. S. Handy, *Structural Design of Tris(bipyridyl)ruthenium(II) Derivatives for High-Performance Solid-State Light-Emitting Devices,* Chemistry, MIT, Cambridge, 1999.
6. R. J. Forster and J. G. Vos, Journal of the Electrochemical Society, 1992. **139**(6), 1503.
7. P. G. Pickup, W. Kutner, C. R. Leidner and R. W. Murray, Journal of the American Chemical Society, 1984. **106**, 1991.
8. S.-M. Oh and L. R. Faulkner, Journal of Electroanalytical Chemistry, 1989. **269**, 77.
9. R. J. Forster, J. G. Vos and M. E. G. Lyons, Journal of the Chemical Society Faraday Transactions, 1991. **87**(23), 3769.
10. K. M. Maness, H. Masui, R. M. Wightman and R. W. Murray, Journal of the American Chemical Society, 1997. **119**, 3987.
11. R. H. Terrill, J. E. Hutchison and R. W. Murray, Journal of Physical Chemistry B, 1997. **101**, 1535.
12. J. C. Jernigan and R. W. Murray, Journal of Physical Chemistry, 1987. **91**, 2030.
13. A. J. Pal, E. D. Abbas, E. S. Handy and M. F. Rubner, to be submitted, 1999.
14. H. A. Laitinen, Transactions of the Electrochemical Society, 1942. **82**, 289.
15. H. A. Laitinen and I. M. Kolthoff, Journal of the American Chemical Society, 1939. **61**, 3344.
16. F. G. Cottrell, Zeitschrift fur Physikalische Chemie, 1902. **42**, 385.
17. M. E. G. Lyons. *Fundamentals*. Electroactive Polymer Electrochemistry, ed. M. E. G. Lyons. Vol. 1. 1994, Plenum Press: New York.
18. K. M. Maness, R. H. Terrill, T. J. Meyer, R. W. Murray and R. M. Wightman, Journal of the American Chemical Society, 1996. **118**, 10609.

Chapter Six

1. R. H. Terrill, J. E. Hutchison and R. W. Murray, Journal of Physical Chemistry B, 1997. **101**, 1535.
2. C. H. Chen, J. Shi and C. W. Tang, Macromol. Symp., 1997. **125**, 1.
3. M. E. Peover and J. D. Davies, Journal of Electroanalytical Chemistry, 1963. **6**, 46.
4. C. H. Lyons, E. D. Abbas, J.-K. Lee and M. F. Rubner, Journal of the American Chemical Society, 1998. **120**(46), 12100.
5. A. J. Pal, E. S. Handy, E. D. Abbas and M. F. Rubner, to be submitted to Journal of Applied Physics, 1999.
6. X. Zhang and A. J. Bard, Journal of Physical Chemistry, 1988. **92**, 5566.

7. X.-H. Xu and A. J. Bard, Langmuir, 1994. **10**, 2409.
8. A. E. Martell and M. Calvin. *Chemistry of the Metal Chelate Compounds.* . 1952, Prentice-Hall: Englewood Cliffs, NJ.
9. A. J. Bard and L. R. Faulkner, *Electrochemical Methods: Fundamentals and Applications*. 1980, New York: John Wiley and Sons.

Chapter Seven

1. J. S. Kim, M. Granstrom, R. H. Friend, N. Johansson, W. R. Salaneck, R. Daik, W. J. Feast and F. Cacialli, Journal of Applied Physics, 1998. **84**(12), 6859.
2. M. E. Williams, private communication, 1998.
3. A. C. Fou, O. Onitsuka, M. Ferreira and M. F. Rubner, Journal of Applied Physics, 1996. **79**(10), 7501.
4. A. Wu, D. Yoo, J.-K. Lee and M. F. Rubner, Journal of the American Chemical Society, in submission.
5. J. Baur, *Fabrication and Structural Studies of Sequentially Adsorbed Polyelectrolyte Multilayers,* Materials Science and Engineering, MIT, Cambridge, MA, 1997.
6. X.-H. Xu and A. J. Bard, Langmuir, 1994. **10**, 2409.
7. X. Zhang and A. J. Bard, Journal of Physical Chemistry, 1988. **92**, 5566.
8. F. Pichot, C. J. Bloom, L. S. Rider and C. M. Elliott, Journal of Physical Chemistry B, 1998. **102**, 3523.
9. D. Yoo, J.-K. Lee, E. S. Handy and M. F. Rubner, Applied Physics Letters, 1996. **69**, 1.
10. M. F. Durstock, *Light Emitting Characteristics and Dielectric Properties of Polyelectrolyte Multilayer Thin Films,* Materials Science and Engineering, MIT, Cambridge, 1999.
11. E. S. Handy, *Structural Design of Tris(bipyridyl)ruthenium(II) Derivatives for High-Performance Solid-State Light-Emitting Devices,* Chemistry, MIT, Cambridge, 1999.
12. M. E. Peover and J. D. Davies, Journal of Electroanalytical Chemistry, 1963. **6**, 46.
13. J. D. Anderson, E. M. McDonald, P. A. Lee, M. L. Anderson, E. L. Ritchie, H. K. Hall, T. Hopkins, E. A. Mash, J. Wang, A. Padias, S. Thayumanavan, S. Barlow, S. R. Marder, G. E. Jabbour, S. Shaheen, B. Kippelen, N. Peyghambarian, R. M. Wightman and N. R. Armstrong, Journal of the American Chemical Society, 1998. **120**, 9646.
14. A. J. Pal, E. D. Abbas, E. S. Handy and M. F. Rubner, to be submitted, 1999.

Chapter Eight

1. A. J. Pal, E. S. Handy, E. D. Abbas and M. F. Rubner, to be submitted to Journal of Applied Physics, 1999.
2. N. H. Damrauer, T. R. Boussie, M. Devenney and J. K. McCusker, Journal of the American Chemical Society, 1997. **119**(35), 8253.
3. J. C. Jernigan and R. W. Murray, Journal of Physical Chemistry, 1987. **91**, 2030.
4. J. C. Jernigan and R. W. Murray, Journal of the American Chemical Society, 1987. **109**, 1738.
5. A. J. Bard and L. R. Faulkner, *Electrochemical Methods: Fundamentals and Applications*. 1980, New York: John Wiley and Sons.
6. M. E. G. Lyons. *Fundamentals*. Electroactive Polymer Electrochemistry, ed. M. E. G. Lyons. Vol. 1. 1994, Plenum Press: New York.